Ten Lectures on Spatially localized structures

Edgar Knobloch

Department of Physics
University of California, Berkeley, CA 94720, USA
http://tardis.berkeley.edu

Imperial College, 23-27 May 2016

Lecture outline

- Lecture 1: Spatially localized structures and the Swift-Hohenberg equation: derivation
- Lecture 2: Spatially localized structures and the Swift-Hohenberg equation: basic properties
- Lecture 3: The Swift-Hohenberg equation in one dimension
- Lecture 4: The Swift-Hohenberg equation in two dimensions
- Lecture 5: Oscillons
- Lecture 6: Spatially localized states in fluid mechanics: convectons
- Lecture 7: Colliding convectons
- Lecture 8: Binary convection in porous media
- Lecture 9: The conserved Swift-Hohenberg equation and crystallization
- Lecture 10: Localized states in systems with a conserved quantity

Patterns in nature

Stripes

Ferro-fluids

Labyrinths

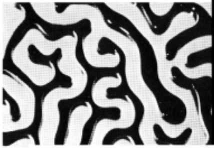

- **Self Organization**
- **Spontaneous (!) Symmetry Breaking**
- **Universality**

Spiral Waves

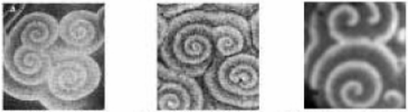

1) BZ reaction 2) Dictyostellium 3) Intracellular Ca2+

Buckling of a cylinder

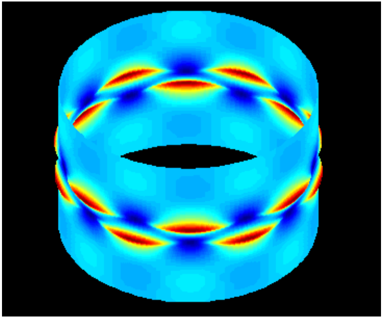

Right panel: courtesy G. Lord

Buckling of a cylinder

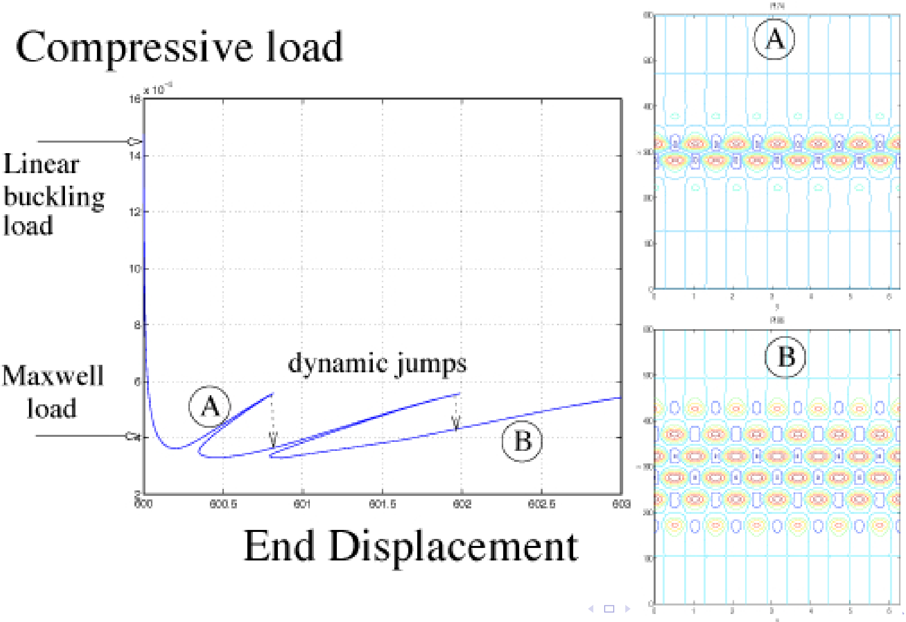

Ferrofluid in a magnetic field

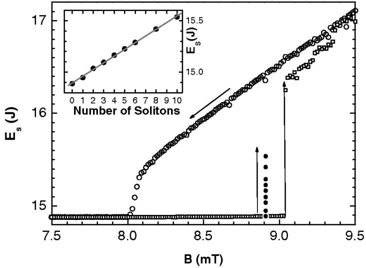

Stationary peaks in a ferrofluid experiment: Richter and Barashenkov, PRL **94**, 1 (2005)

Oscillons

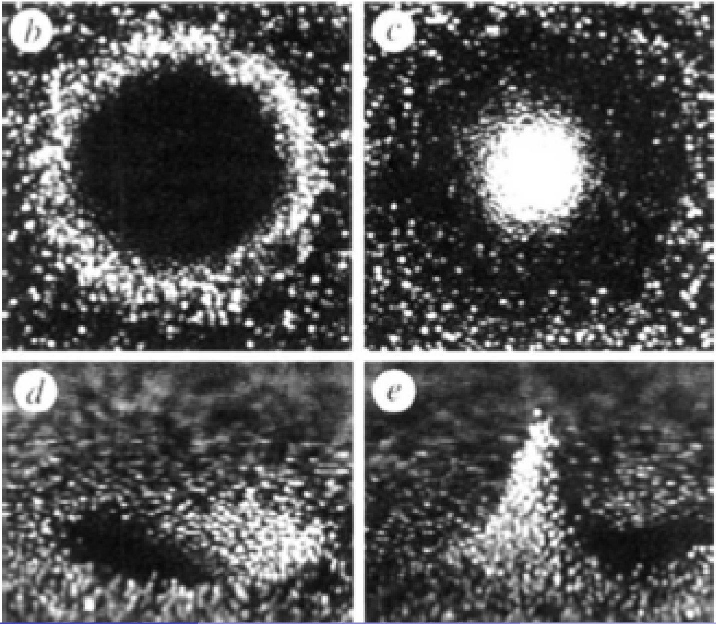

Oscillons

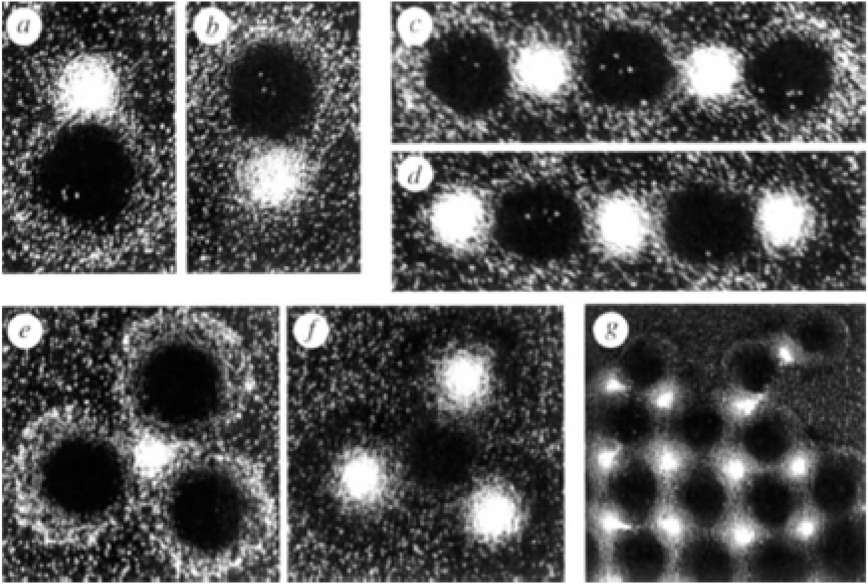

Bound state of oscillons

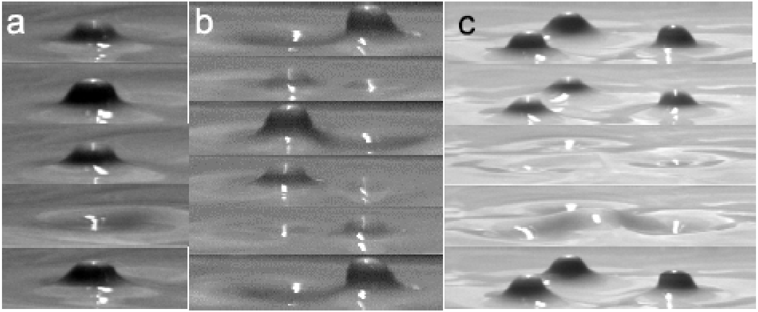

Faraday resonance in a colloidal suspension: Lioubashevski et al., PRL **83**, 3190 (1999)

Photonics: Cavity solitons

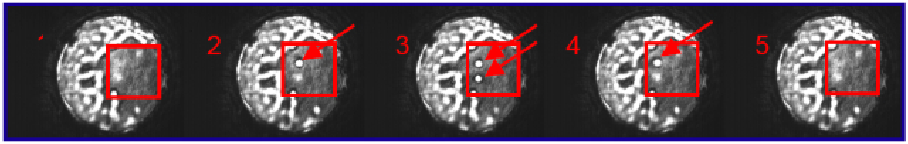

Writing and erasing of cavity solitons in a broad area VCSEL. See Fundamentals, Functionalities, and Applications of Cavity Solitons: www.funfacs.org

Photonics: liquid crystal light valve with feedback

Solitary localized structures 5

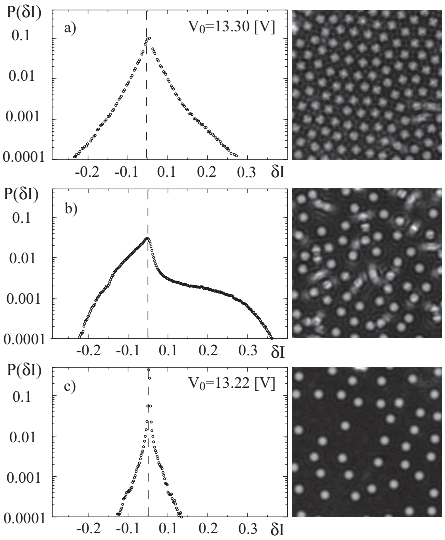

Figure 2. Experimental PDF (left) and instantaneous snapshots (right) showing the

Photonics: Bortolozzo et al., NJP **11**, 093037 (2009)

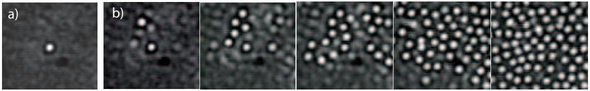

Figure 4. Experimental snapshots showing the transition from the SLS (state 1) to the HEX pattern (state 2); a) $V_0 = 13.22\ V$, b) $V_0 = 13.30\ V$: successive frames correspond to successive instant times with a time step of 0.4 s; $I_{in} = 0.45\ mW/cm^2$.

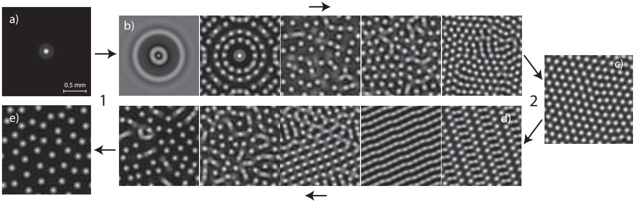

Figure 5. Numerical snapshots showing the evolution of the liquid crystal tilt angle $\theta(x, y, t)$ during the transition $1 \to 2 \to 1$. The spatial scales are identical in all panels. a) $V_0 = 13.22\ V$ with a single localized structure (state 1); b) $V_0 = 13.22\ V$: successive frames correspond to successive instant times with a time step of 0.4 s; $I_{in} = 0.45\ mW/cm^2$; c) final HEX pattern (state 2); d) $V_0 = 13.22\ V$: successive

Convectons

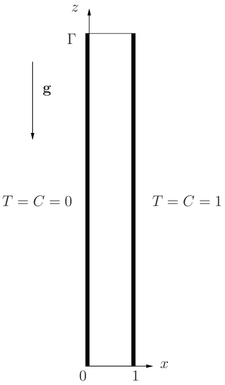

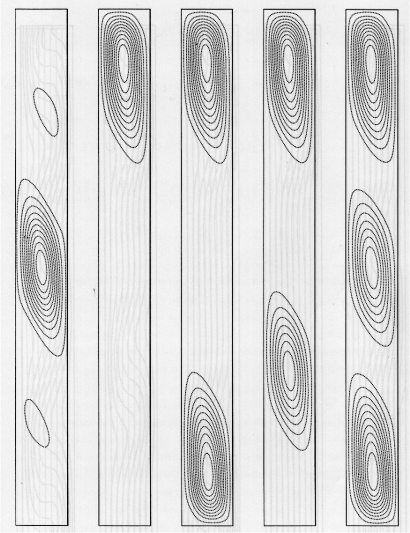

Ghorayeb & Mojtabi, Phys. Fluids **9**, 2339 (1997); Ghorayeb, PhD Thesis, Toulouse, 1997

Convectons in magnetoconvection

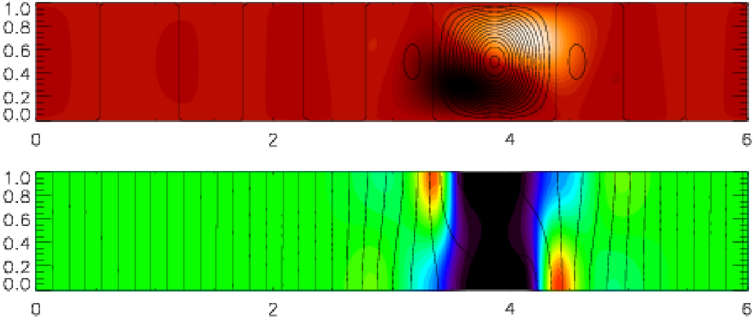

Blanchflower, Phys. Lett. A **261**, 74 (1999)

Convectons in binary fluid convection

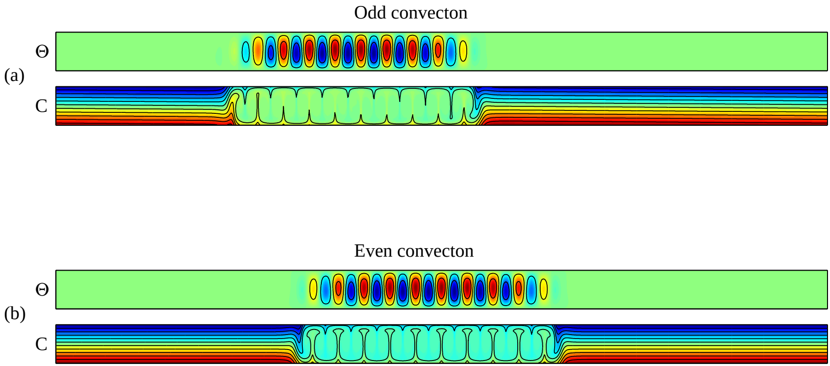

Batiste et al., J. Fluid Mech. **560**, 149 (2006)

Vortices in rotating convection

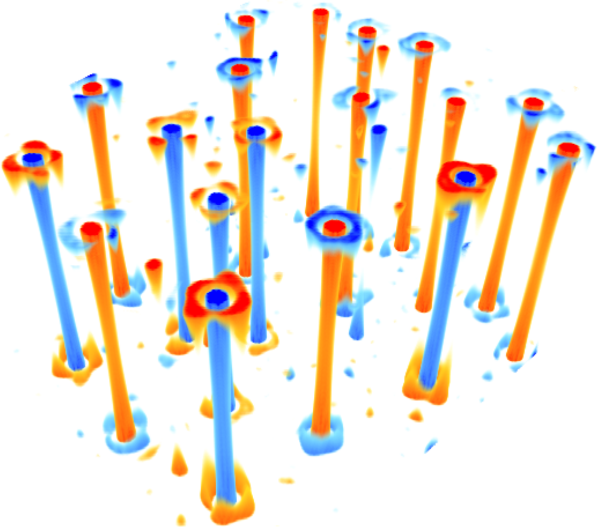

Sprague et al., J. Fluid Mech. **551**, 141 (2006)

Hurricane Katrina, 28 August 2005

The Swift-Hohenberg equation

$$u_t = -(1+\nabla^2)^2 u + ru + f(u)$$

competition between localised patterns:

(a) hexagons & targets preferred for $f(u) = su^2 - u^3$

(b) stripes & targets preferred for $f(u) = su^3 - u^5$

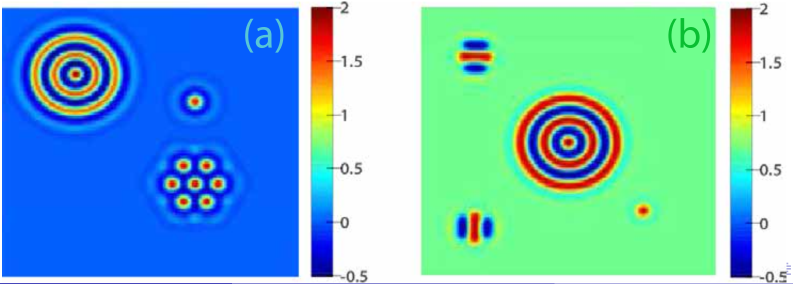

Spatially localized states

Spatially localized states (LS) are common in fluid flows and are present in convection, shear flows, and as vortices in both rotating and nonrotating flows. They are also of great importance outside of fluid dynamics: nonlinear optics, reaction-diffusion systems arising in chemistry, structural mechanics, and increasingly in ecology.

- LS exist in one, two and three spatial dimensions, and may be stationary or propagate in the form of traveling pulses
- LS are usually created by finite amplitude perturbation and are therefore strongly nonlinear
- Instability may lead to splitting, decay and disappearance, propagation or complex dynamics
- LS may form bound structures or a gas-like state

Question: What do these systems have in common? Is there a universal description of LS?

Remark: Although LS are sometimes called dissipative solitons they are NOT solitons in the classical sense. So interactions between moving LS are generally inelastic.

Swift-Hohenberg equation: a derivation

Inviscid long water waves:

$$\phi_{xx} + \phi_{yy} = 0 \quad \text{in} \quad -H < y < \zeta(x,t) \tag{1}$$

with

$$\phi_y = 0 \quad \text{on} \quad y = -H \tag{2}$$

and

$$\zeta_t + \phi_x\zeta_x - \phi_y = 0 \quad \text{on} \quad y = \zeta(x,t) \tag{3}$$

and

$$\phi_t + \frac{1}{2}(\phi_x^2 + \phi_y^2) + g\zeta - \frac{\kappa\zeta_{xx}}{(1+\zeta_x^2)^{3/2}} = 0 \quad \text{on} \quad y = \zeta(x,t). \tag{4}$$

Here $\phi(x,y,t)$ is the velocity potential ($u = \phi_x$, $v = \phi_y$), the flow is assumed to be two-dimensional, and κ is the surface tension.

Linear theory

The problem (1)–(4) has the trivial solution $\phi \equiv 0$, $\zeta \equiv 0$. An infinitesimal perturbation of the free surface of the form $\zeta = \zeta_0 \sin(kx - \omega t)$, where k is the perturbation wavenumber and ω is its frequency, represents a periodic wave traveling to the right with phase speed $c = \omega/k$. Associated with this disturbance is a velocity disturbance given by $\phi = \phi_0(y)\cos(kx - \omega t)$, where the function $\phi_0(y)$ captures the decrease of the velocity with depth. With this Ansatz Eq. (1) yields

$$\phi_{0yy} - k^2\phi_0 = 0. \tag{5}$$

The boundary condition (2) implies that $\phi_{0y} = 0$ at $y = -H$ and hence that

$$\phi_0 = A\cosh\left[k(y+H)\right], \tag{6}$$

where A is an arbitrary constant. The perturbed velocity potential then reads

$$\phi = A\cosh\left[k(y+H)\right]\cos(kx - \omega t). \tag{7}$$

Linear theory

Equation (3), linearized about $y = 0$, now yields

$$\zeta_0 \omega = -Ak \sinh(kH), \tag{8}$$

while Eq. (4) yields

$$-\omega A \cosh(kH) + g\zeta_0 + \kappa k^2 \zeta_0 = 0. \tag{9}$$

Elimination of the arbitrary amplitude A yields finally the dispersion relation for infinitesimal gravity-capillary waves:

$$\omega^2 = (g + \kappa k^2) k \tanh(kH). \tag{10}$$

We will be interested in long waves, i.e., waves for which $kH \ll 1$. Since $\tanh(kH) = kH(1 - k^2H^2/3) + \mathcal{O}(k^5H^5)$ the relation (10) becomes

$$\omega^2 = gk^2H + gk^4H^3(\mathrm{Bo} - 1/3) + \mathcal{O}(k^6), \tag{11}$$

where $\mathrm{Bo} \equiv \kappa/gH^2$ is the Bond number. Thus long waves are nondispersive at leading order but with a dispersive correction at higher order as described by the second term provided $\mathrm{Bo} \neq 1/3$. In the following we study the weakly nonlinear regime near the special value $\mathrm{Bo} = 1/3$.

Swift-Hohenberg equation: a derivation

We first write the equations in a frame traveling with phase speed c to the right:

$$\phi_{\xi\xi} + \phi_{yy} = 0 \quad \text{in} \quad -H < y < \zeta(\xi, t) \tag{12}$$

with

$$\phi_y = 0 \quad \text{on} \quad y = -H \tag{13}$$

and

$$\zeta_t + c\zeta_\xi + \phi_\xi \zeta_\xi - \phi_y = 0 \quad \text{on} \quad y = \zeta(\xi, t) \tag{14}$$

and

$$\phi_t + c\phi_\xi + \frac{1}{2}(\phi_\xi^2 + \phi_y^2) + g\zeta - \frac{\kappa \zeta_{\xi\xi}}{(1+\zeta_\xi^2)^{3/2}} = 0 \quad \text{on} \quad y = \zeta(\xi, t). \tag{15}$$

Here $\xi \equiv x - ct$.

Swift-Hohenberg equation: a derivation

We look at long waves with wavelength of order $\epsilon^{-1} \gg 1$: we introduce the large spatial scale $X = \epsilon\xi$ and anticipate the need for a slow time $T \equiv \epsilon^5 t$ (in the moving frame). We also pick $\kappa = \kappa_0 + \kappa_2\epsilon^2$, where κ_0 is determined by the requirements of the theory: $\kappa_0 \equiv \frac{1}{3}gH^2$ (see below). Finally we let $(\phi, \zeta) \to (\epsilon^3\phi, \epsilon^4\zeta)$:

$$\epsilon^2\phi_{XX} + \phi_{yy} = 0 \quad \text{in} \quad -H < y < \epsilon^4\zeta(X, T) \tag{16}$$

with

$$\phi_y = 0 \quad \text{on} \quad y = -H \tag{17}$$

and

$$\epsilon^6\zeta_T + c\epsilon^2\zeta_X + \epsilon^6\phi_X\zeta_X - \phi_y = 0 \quad \text{on} \quad y = \epsilon^4\zeta(X, T) \tag{18}$$

and

$$\epsilon^4\phi_T + c\phi_X + \frac{1}{2}\epsilon^2(\epsilon^2\phi_X^2 + \phi_y^2) + g\zeta - \epsilon^2(\kappa_0 + \kappa_2\epsilon^2)\zeta_{XX} = O(\epsilon^{12}) \tag{19}$$

on $y = \epsilon^4\zeta(X, T)$.

Swift-Hohenberg equation: a derivation

We now write $\phi = \phi_0 + \epsilon^2\phi_2 + \ldots$, and $\zeta = \zeta_0 + \epsilon^2\zeta_2 + \ldots$.
At leading order Eq. (16) yields

$$\phi_{0yy} = 0 \tag{20}$$

subject to $\phi_{0y} = 0$ on $y = -H$. Thus $\phi_0 = f_0(X, T)$, where $f_0(X, T)$ is unknown. At $O(\epsilon^2)$ we obtain

$$\phi_{2yy} = -f_{0XX} \tag{21}$$

subject to $\phi_{2y} = 0$ on $y = -H$. Thus

$$\phi_2 = -\frac{1}{2}(y + H)^2 f_{0XX} + f_2(X, T), \tag{22}$$

where $f_2(X, T)$ is unknown.

Swift-Hohenberg equation: a derivation

It follows that on $y = \epsilon^4 \zeta(X, T)$

$$\phi_y = \phi_{0y} + \epsilon^2 \phi_{2y} + O(\epsilon^4) = -\epsilon^2 H f_{0XX} + O(\epsilon^4). \tag{23}$$

Thus Eq. (18) becomes, at leading order,

$$c\zeta_{0X} = -H f_{0XX} \tag{24}$$

or, integrating once,

$$c\zeta_0 = -H f_{0X}. \tag{25}$$

Eq. (19) becomes, at leading order,

$$c f_{0X} + g\zeta_0 = 0, \tag{26}$$

implying the usual dispersion relation for long waves: $c^2 = gH$.

Swift-Hohenberg equation: a derivation

We now proceed to next order. Eq. (16) yields

$$\phi_{4yy} = -\phi_{2XX} = \frac{1}{2}(y+H)^2 f_{0XXXX} - f_{2XX}, \tag{27}$$

and so

$$\phi_4 = \frac{1}{24}(y+H)^4 f_{0XXXX} - \frac{1}{2}(y+H)^2 f_{2XX} + f_4(X,T). \tag{28}$$

Likewise

$$\phi_{6yy} = -\phi_{4XX} = -\frac{1}{24}(y+H)^4 f_{0XXXXXX} + \frac{1}{2}(y+H)^2 f_{2XXXX} - f_{4XX}, \tag{29}$$

and so

$$\phi_{6y} = -\frac{1}{120}(y+H)^5 f_{0XXXXXX} + \frac{1}{6}(y+H)^3 f_{2XXXX} - (y+H) f_{4XX}. \tag{30}$$

Swift-Hohenberg equation: a derivation

We now need to impose the surface boundary conditions. Eq. (18) yields at $O(\epsilon^4)$

$$c\zeta_{2X} = \phi_{4y} = \frac{1}{6}H^3 f_{0XXXX} - Hf_{2XX}, \tag{31}$$

or

$$c\zeta_2 = \frac{1}{6}H^3 f_{0XXX} - Hf_{2X}, \tag{32}$$

Eq. (19) yields at $O(\epsilon^2)$

$$c\phi_{2X} + g\zeta_2 - \kappa_0\zeta_{0XX} = 0, \tag{33}$$

or equivalently,

$$c(-\frac{1}{2}H^2 f_{0XXX} + f_{2X}) + g\zeta_2 + \frac{c\kappa_0}{g} f_{0XXX} = 0. \tag{34}$$

Equations (32) and (34) are identical provided

$$\kappa_0 = \frac{1}{3}gH^2, \qquad \text{i.e.,} \quad \mathrm{Bo} = 1/3. \tag{35}$$

Swift-Hohenberg equation: a derivation

We proceed next to $O(\epsilon^6)$ in Eq. (18):

$$\zeta_{0T} + c\zeta_{4X} + f_{0X}\zeta_{0X} = -\frac{1}{120}H^5 f_{0XXXXXX} + \frac{1}{6}H^3 f_{2XXXX} - Hf_{4XX} - \zeta_0 f_{0XX}. \tag{36}$$

The last term in this equation arises from the ζ contribution to ϕ_{2y}. We also have from Eq. (19) at $O(\epsilon^4)$

$$\phi_{0T} + c\phi_{4X} + \frac{1}{2}(f_{0X})^2 + g\zeta_4 - \kappa_0\zeta_{2XX} - \kappa_2\zeta_{0XX} = 0, \tag{37}$$

where ϕ_4 is to be evaluated at $y = 0$ (to this order) using Eq. (28). Eliminating f_4 and ζ_4 from the resulting equations we obtain a solvability condition which can in turn be simplified by eliminating f_0 in favor of ζ_0. We obtain

$$\frac{2c}{H}\zeta_{0T} - \frac{3g}{H}\zeta_0\zeta_{0X} + \kappa_2\zeta_{0XXX} + \frac{1}{30}gH^4\zeta_{0XXXXX} = -\kappa_0\zeta_{2XXX} - \frac{1}{3}cH^2 f_{2XXXX}. \tag{38}$$

Swift-Hohenberg equation: a derivation

The right hand side of this equation can be evaluated in terms of ζ_0 with the help of Eqs. (34) and (35) leading finally to an evolution equation satisfied by ζ_0:

$$\frac{2c}{H}\zeta_T - \frac{3g}{H}\zeta\zeta_X + \kappa_2\zeta_{XXX} - \frac{1}{45}gH^4\zeta_{XXXXX} = 0. \tag{39}$$

This is a generalization of the Korteweg-de Vries equation.

Solitary waves: Solitary waves traveling to the right with speed V may now be obtained by writing $z = X - VT$. After one integration such waves are found to satisfy the ordinary differential equation

$$\frac{1}{45}gH^4\zeta'''' - \kappa_2\zeta'' + \frac{2cV}{H}\zeta + \frac{3g}{2H}\zeta^2 = 0, \tag{40}$$

where the prime denotes a derivative with respect to z. This is the simplest case of the **Swift-Hohenberg equation**. This SH20 equation was studied by Buffoni, Champneys, Toland ...

The Korteweg-de Vries equation

When $\kappa - \kappa_0 = \mathcal{O}(1)$ the (scaled) equation for the surface elevation is the KdV equation

$$\zeta_\tau + \zeta\zeta_X \pm \zeta_{XXX} = 0, \tag{41}$$

depending on $\mathrm{sgn}(\mathrm{Bo} - 1/3)$. Writing $z = X - V\tau$, we integrate twice, obtaining

$$\pm\frac{1}{2}\zeta_z^2 + U(\zeta) = E, \tag{42}$$

where E is a constant and $U(\zeta) \equiv \frac{1}{6}\zeta^3 - \frac{1}{2}V\zeta^2$.

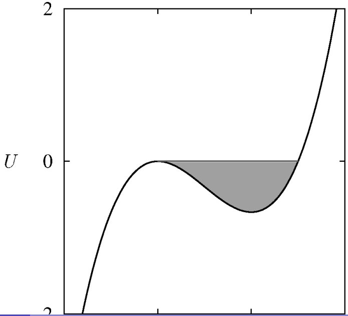

The Korteweg-de Vries equation

Thus sinusoidal oscillations are present around the local minimum of the potential provided $E + 2V^2/3 \ll 1$. As E increases the oscillations become more and more nonlinear and their (spatial) period increases. When $E = 0$ the solutions have infinite period, i.e., they are solitary waves. For $\kappa < \kappa_0$ these form a one parameter family,

$$\frac{\zeta}{H} = a\,\mathrm{sech}^2 \frac{a}{2\sqrt{3}H}[x - \sqrt{gH}(1 + \frac{a}{3})t], \tag{43}$$

with $a > 0$ (solitary waves of elevation: bright solitons). Thus all finite amplitude solitons travel faster than $\sqrt{gH}$ and larger solitons travel faster than smaller solitons. Greene, Kruskal and Zabusky discovered that these solutions interact in a particle-like manner: this makes them into **solitons**. This is a consequence of complete integrability of the KdV equation as an infinite-dimensional Hamiltonian system.

Remark: If $\kappa > \kappa_0$ we have solitary waves of depression: dark solitons

The Korteweg-de Vries equation

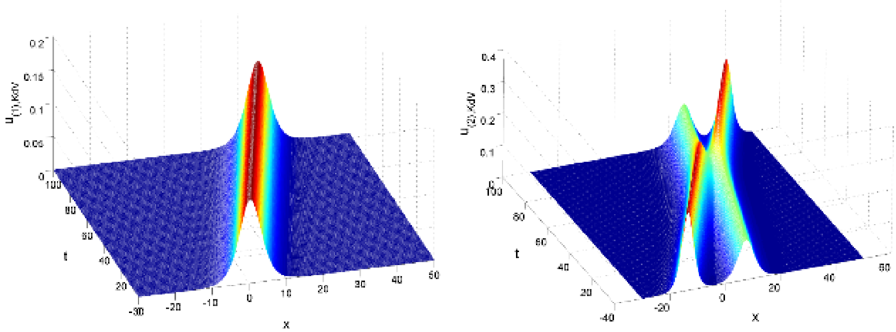

Collision of two KdV solitons

Swift-Hohenberg equation in one spatial dimension

The Swift-Hohenberg equation

$$u_t = ru - \left(q_c^2 + \partial_x^2\right)^2 u + f(u)$$

is very simple but has very remarkable properties. These are a consequence of the following:

- Fourth order in space
- Intrinsic length scale $2\pi/q_c$
- Bistability due to competing nonlinear terms
- Spatial reversibility: $x \to -x$, $u \to \pm u$
- Variational dynamics

  $$u_t = -\frac{\delta F}{\delta u},$$

  where

  $$F = \int_{-\infty}^{\infty} dx \left\{ -\frac{1}{2} r u^2 + \frac{1}{2}\left[(q_c^2 + \partial_x^2)u\right]^2 - \int_0^u f(v)\, dv \right\}$$

  In the following we think of $F[u]$ as the (free) energy of the system

Localized solutions of the Swift-Hohenberg equation SH23

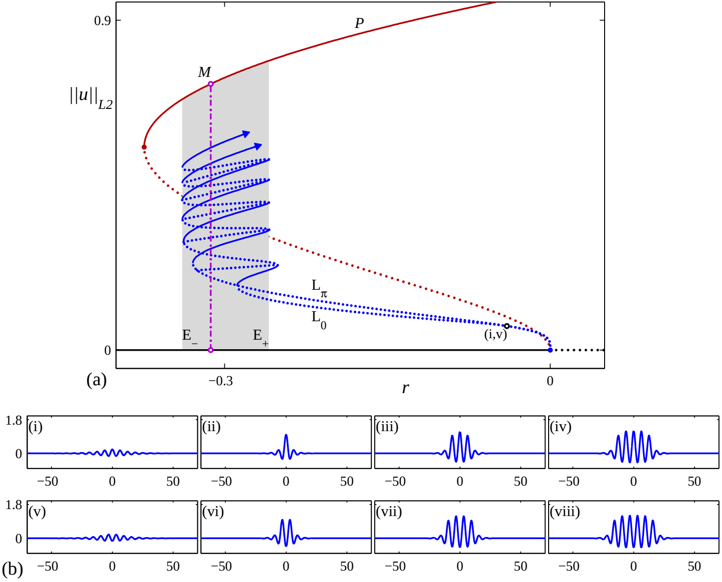

Temporal vs spatial dynamics: Kirchgässner (1982)

The linearized problem around $u = 0$ is

$$u_t = ru - \left(q_c^2 + \partial_x^2\right)^2 u.$$

Thus $u(x,t) \propto \exp(\sigma t + iqx)$ grows in time if $\sigma(q) > 0$. So steady solutions are present when $\sigma = 0$, i.e., at $q = q^{\pm}$, and these **collide** at $(r,q) = (r_c, q_c)$. Thus $r = r_c = 0$ is a reversible Hopf bifurcation in *space* with 1:1 resonance: for $r < 0$ the spatial growth rate $\lambda \equiv \pm\lambda_r \pm i\lambda_i$, $\lambda_r \neq 0$, thereby allowing both growth and decay **in space**:

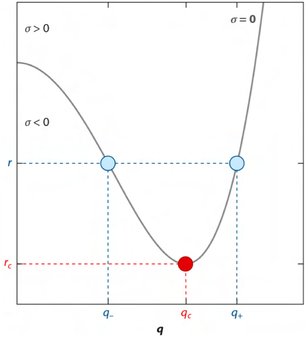

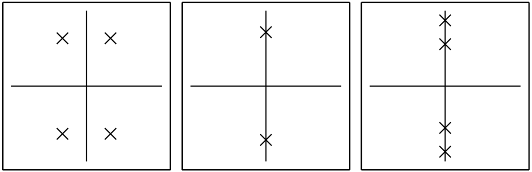

(a) $r < 0$ (b) $r = 0$ (c) $r > 0$

Spatial dynamics and homoclinics

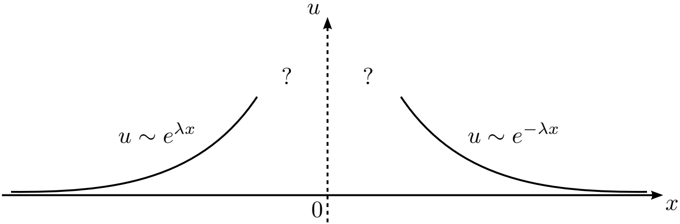

We can establish the presence of homoclinic orbits near $r = 0$ by setting $r \equiv \mu = -\epsilon^2 \mu_2$ and using a multiple scale expansion with spatial scales x and $X \equiv \epsilon x$,

$$u_\ell(x) = \epsilon u_1(x, X) + \epsilon^2 u_2(x, X) + \dots ,$$

where

$$u_1(x, X) = Z(X; \epsilon) e^{iq_c x} + c.c. \tag{44}$$

We start by computing Z at $r = 0$.

Weakly nonlinear theory: SH35

Multiple scale expansion at $r = 0$ with spatial scales x and $X \equiv \epsilon x$,

$$u_\ell(x) = \epsilon u_1(x, X) + \epsilon^2 u_2(x, X) + \dots ,$$

yields

$$\mathcal{O}(\epsilon): \quad \left(\partial_x^2 + q_c^2\right)^2 u_1 = 0 \tag{45}$$

$$\mathcal{O}(\epsilon^2): \quad \left(\partial_x^2 + q_c^2\right)^2 u_2 = -4\partial_{xX}\left(\partial_x^2 + q_c^2\right) u_1 \tag{46}$$

$$\begin{aligned} \mathcal{O}(\epsilon^3): \quad \left(\partial_x^2 + q_c^2\right)^2 u_3 = {} & -4\partial_{xX}\left(\partial_x^2 + q_c^2\right) u_2 - 4\partial_{xxXX} u_1 \\ & - 2\partial_{XX}\left(\partial_x^2 + q_c^2\right) u_1 + b_3 u_1^3 \end{aligned} \tag{47}$$

$$\begin{aligned} \mathcal{O}(\epsilon^4): \quad \left(\partial_x^2 + q_c^2\right)^2 u_4 = {} & -4\partial_{xX}\left(\partial_x^2 + q_c^2\right) u_3 - 4\partial_{xxXX} u_2 \\ & - 2\partial_{XX}\left(\partial_x^2 + q_c^2\right) u_2 - 4\partial_{xXXX} u_1 + 3b_3 u_1^2 u_2 \end{aligned} \tag{48}$$

$$\begin{aligned} \mathcal{O}(\epsilon^5): \quad \left(\partial_x^2 + q_c^2\right)^2 u_5 = {} & -4\partial_{xX}\left(\partial_x^2 + q_c^2\right) u_4 - 4\partial_{xxXX} u_3 \\ & - 2\partial_{XX}\left(\partial_x^2 + q_c^2\right) u_3 - 4\partial_{xXXX} u_2 - \partial_X^4 u_1 \\ & + 3b_3\left(u_1 u_2^2 + u_1^2 u_3\right) - b_5 u_1^5 . \end{aligned} \tag{49}$$

Weakly nonlinear theory: SH35

The $\mathcal{O}(\epsilon, \epsilon^2)$ equations are solved by

$$u_1(x,X) = A_1(X)e^{iq_cx} + c.c.\,, \qquad u_2(x,X) = A_2(X)e^{iq_cx} + c.c.\,, \quad (50)$$

where $A_{1,2}(X)$ are as yet undetermined and $c.c.$ denotes a complex conjugate. The Ansatz

$$u_3(x,X) = A_3(X)e^{iq_cx} + C_3(X)e^{3iq_cx} + c.c. \quad (51)$$

in the $\mathcal{O}(\epsilon^3)$ equation leads to the two results

$$4q_c^2A_1'' = -3b_3A_1|A_1|^2\,, \qquad C_3 = \frac{b_3}{64q_c^4}A_1^3\,, \quad (52)$$

with A_3 arbitrary. The Ansatz

$$u_4(x,X) = A_4(X)e^{iq_cx} + C_4(X)e^{3iq_cx} + c.c. \quad (53)$$

in the $\mathcal{O}(\epsilon^4)$ equation likewise leads to

$$4q_c^2A_2'' = 4iq_cA_1''' - 3b_3\left(2|A_1|^2A_2 + A_1^2\bar{A}_2\right)\,; \quad (54)$$

the expression for C_4 in terms of $A_{1,2}$ is not needed in what follows.

Weakly nonlinear theory: SH35

Finally, the $\mathcal{O}(\epsilon^5)$ equation with the Ansatz

$$u_5(x,X) = A_5(X)e^{iq_c x} + C_5(X)e^{3iq_c x} + E_5(X)e^{5iq_c x} + c.c. \tag{55}$$

yields

$$4q_c^2 A_3'' = 4iq_c A_2''' + A_1'''' - 3b_3\left(2A_1|A_2|^2 + \bar{A}_1 A_2^2 + 2|A_1|^2 A_3 + A_1^2\bar{A}_3\right) + \left(-\frac{3b_3^2}{64q_c^4} + 10b_5\right) A_1|A_1|^4 \tag{56}$$

after elimination of C_3. Eqs. (52), (54) and (56) can now be assembled into a *single* equation for $Z(X,\epsilon) \equiv A_1(X) + \epsilon A_2(X) + \epsilon^2 A_3(X) + \ldots$:

$$4q_c^2 Z'' = -3b_3 Z|Z|^2 + 4iq_c\epsilon Z''' + \epsilon^2\left[Z'''' + \left(-\frac{3b_3^2}{64q_c^4} + 10b_5\right) Z|Z|^4\right] + \mathcal{O}(\epsilon^3)$$

or

$$4q_c^2 Z'' = -3b_3 Z|Z|^2 - \frac{3i\epsilon b_3}{q_c}(2Z'|Z|^2 + Z^2\bar{Z}') + \epsilon^2\left[\frac{9b_3}{2q_c^2}\left(2Z|Z'|^2 + (Z')^2\bar{Z}\right) + \left(-\frac{327b_3^2}{64q_c^4} + 10b_5\right) Z|Z|^4\right] + \mathcal{O}(\epsilon^3) \tag{57}$$

Normal form theory: Iooss and Pérouème (1993)

The normal form for the reversible Hopf bifurcation with 1:1 resonance is

$$\begin{aligned} \dot{A} &= iq_c A + B + iA\,P(\mu; y, w) \\ \dot{B} &= iq_c B + iB\,P(\mu; y, w) + A\,Q(\mu; y, w)\ , \end{aligned} \tag{58}$$

where $y \equiv |A|^2$, $w \equiv \frac{i}{2}(A\bar{B} - \bar{A}B)$, μ is an unfolding parameter analogous to r, and P and Q are polynomials with real coefficients:

$$\begin{aligned} P(\mu; y, w) &= p_1\mu + p_2 y + p_3 w + p_4 y^2 + p_5 wy + p_6 w^2 + \cdots \\ Q(\mu; y, w) &= -q_1\mu + q_2 y + q_3 w + q_4 y^2 + q_5 wy + q_6 w^2 + \cdots\ . \end{aligned}$$

To compute the coefficients in this normal form we set $\mu = 0$ and write $(A, B) = (\epsilon\tilde{A}(X), \epsilon^2\tilde{B}(X))e^{iq_c x}$, obtaining

$$\epsilon^2 A' = \epsilon^2 B + i\epsilon A\left[\epsilon^2 p_2|A|^2 + \epsilon^3 p_3\frac{i}{2}(A\bar{B} - \bar{A}B)\right] + \mathcal{O}(\epsilon^5) \tag{59}$$

$$\begin{aligned} \epsilon^3 B' = {} & i\epsilon^2 B\left[\epsilon^2 p_2|A|^2 + \epsilon^3 p_3\frac{i}{2}(A\bar{B} - \bar{A}B)\right] \\ & + \epsilon A\left[\epsilon^2 q_2|A|^2 + \epsilon^3 q_3\frac{i}{2}(A\bar{B} - \bar{A}B) + \epsilon^4 q_4|A|^4\right] + \mathcal{O}(\epsilon^6) \end{aligned} \tag{60}$$

Coefficients in the normal form

Eq. (59) yields a power series expansion for B in terms of A,

$$B = A' - i\epsilon p_2 A|A|^2 + \epsilon^2 \frac{p_3}{2} A(A\bar{A}' - \bar{A}A') + \mathcal{O}(\epsilon^3), \tag{61}$$

and this equation can be used to eliminate B from Eq. (60):

$$\begin{aligned} A'' = q_2 A|A|^2 + i\epsilon \left[\left(3p_2 - \frac{1}{2}q_3\right) A'|A|^2 + \left(p_2 + \frac{1}{2}q_3\right) A^2\bar{A}' \right] \\ + \epsilon^2 \left[p_3((A')^2\bar{A} - AA'\bar{A}') + (q_4 - q_3 p_2 + p_2^2)A|A|^4 \right] + \mathcal{O}(\epsilon^3)\,. \end{aligned} \tag{62}$$

Finally, writing $Z = A + \epsilon^2 \rho A|A|^2 + \mathcal{O}(\epsilon^4)$ allows one to deduce the normal coefficients:

$$\rho = \frac{9b_3}{16q_c^4}\,, \quad p_2 = -\frac{9b_3}{16q_c^3}\,, \quad q_2 = -\frac{3b_3}{4q_c^2}\,, \quad p_3 = 0\,, \quad q_3 = -\frac{3b_3}{8q_c^3}\,,$$

$$q_4 = -\frac{177b_3^2}{128q_c^6} + \frac{5b_5}{2q_c^2}\,.$$

Unfolding of the normal form

The remaining coefficients p_1 and q_1 are determined as part of the unfolding. We write $r \equiv \mu = -\epsilon^2 \mu_2$, where μ_2 is $\mathcal{O}(1)$. The unfolded versions of Eqs. (57) and (62) through $\mathcal{O}(\epsilon)$ are

$$4q_c^2 Z'' = \mu_2 Z - 3b_3 Z|Z|^2 + \frac{i\epsilon}{q_c}\left[\mu_2 Z' - 3b_3(2Z'|Z|^2 + Z^2 \bar{Z}')\right] + \mathcal{O}(\epsilon^2)$$

$$A'' = q_1 \mu_2 A + q_2 A|A|^2 + i\epsilon\left[-2p_1\mu_2 A' + \left(3p_2 - \frac{1}{2}q_3\right)A'|A|^2 + \left(p_2 + \frac{1}{2}q_3\right)A^2\bar{A}'\right] + \mathcal{O}(\epsilon^2)$$

Matching terms through this order gives

$$p_1 = -\frac{1}{8q_c^3}, \qquad q_1 = \frac{1}{4q_c^2}. \tag{63}$$

Properties of the normal form

We transformed SH35 to normal form near $r = 0$ because the properties of this normal form are already analyzed. Specifically, the normal form is completely integrable, with integrals

$$K \equiv \frac{1}{2}(A\bar{B} - \bar{A}B), \qquad H \equiv |B|^2 - \int_0^{|A|^2} Q(\mu, s, K)\, ds. \tag{64}$$

Orbits homoclinic to $(0,0)$ lie in the surface $H = K = 0$. In this case the equation for $a \equiv |A|^2 > 0$ takes the form

$$\frac{1}{2}\left(\frac{da}{dX}\right)^2 + V(a) = 0, \tag{65}$$

where

$$V(a) = 2q_1\mu a^2 - q_2 a^3 - \frac{2}{3} q_4 a^4. \tag{66}$$

Homoclinics and heteroclinics

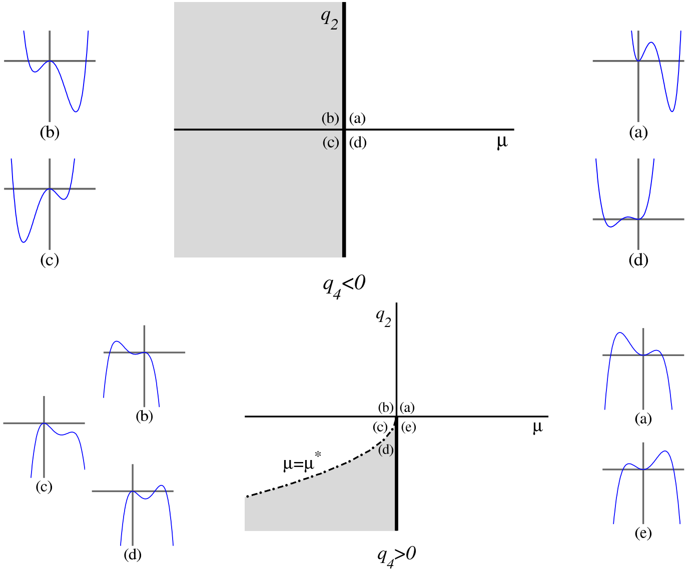

Homoclinics

The leading order amplitude equation

$$4q_c^2 Z'' = \mu_2 Z + 4q_c^2 q_2 Z|Z|^2 + \mathcal{O}(\epsilon),$$

has two types of solution when $q_2 < 0$, $\mu_2 > 0$:

- periodic: $Z(X) = \left(\frac{-\mu_2}{4q_c^2 q_2}\right)^{1/2} e^{i\phi} + \mathcal{O}(\epsilon)$
- corresponding to: $u(x) = \left(\frac{r}{4q_c^2 q_2}\right)^{1/2} \cos(q_c x + \phi) + \mathcal{O}(r)$

and

- localized: $Z(X) = \left(\frac{-\mu_2}{2q_c^2 q_2}\right)^{1/2} \operatorname{sech}\left(\frac{X\sqrt{\mu_2}}{2q_c}\right) e^{i\phi} + \mathcal{O}(\epsilon)$
- corresponding to:
  $u(x) = 2\left(\frac{r}{2q_c^2 q_2}\right)^{1/2} \operatorname{sech}\left(\frac{x\sqrt{-r}}{2q_c}\right) \cos(q_c x + \phi) + \mathcal{O}(r)$

For the periodic states ϕ is arbitrary; this is not so for the localized states!

Beyond all orders effects

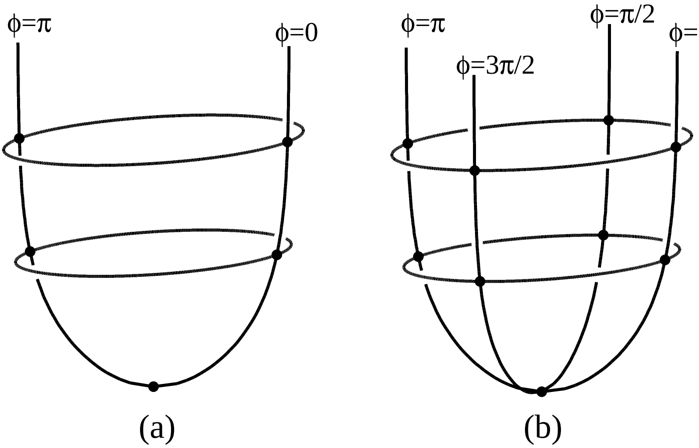

See G. Kozyreff and S.J. Chapman, PRL **97**, 044502 (2006); Physica D **238**, 319 (2009); A. Dean et al., Nonlinearity **24**, 3323 (2011)

Example: Natural doubly diffusive convection

Linear analysis about the conduction state in an infinite slot:
$(u, w, T, C) = (\tilde{u}, \tilde{w}, \tilde{T}, \tilde{C})(x)\ \exp(\lambda z)$ with $\lambda = q_r + iq_i$ shows that $q_r = 0$, $q_i = \pm q_c$ at $Gr_c = 650.9034$. Moreover $q_c = 2.5318$ and

- $Gr < Gr_c$: $\lambda = \pm iq_c \pm \mathcal{O}(\sqrt{Gr_c - Gr})$
- $Gr > Gr_c$: $\lambda = \pm iq_c \pm i\mathcal{O}(\sqrt{Gr - Gr_c})$

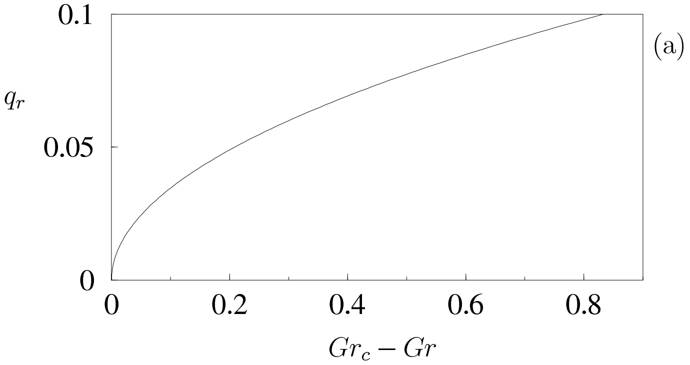

Snakes-and-ladders structure of the pinning region: SH23

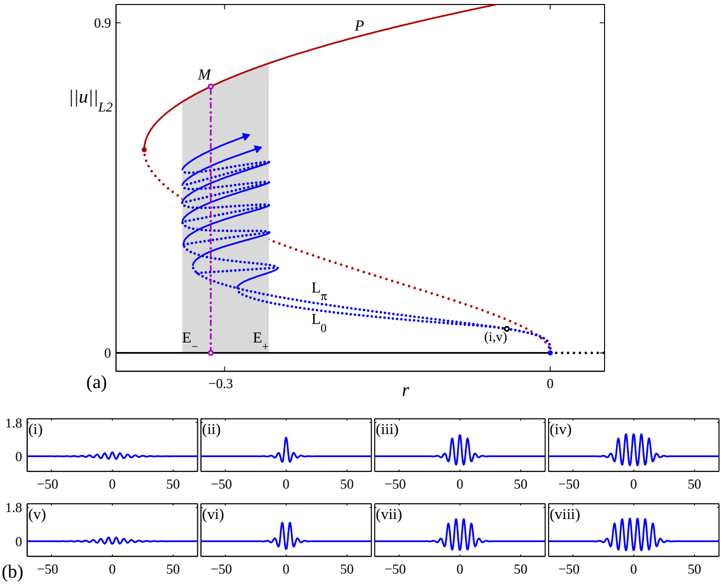

Snakes-and-ladders structure of the pinning region: SH23

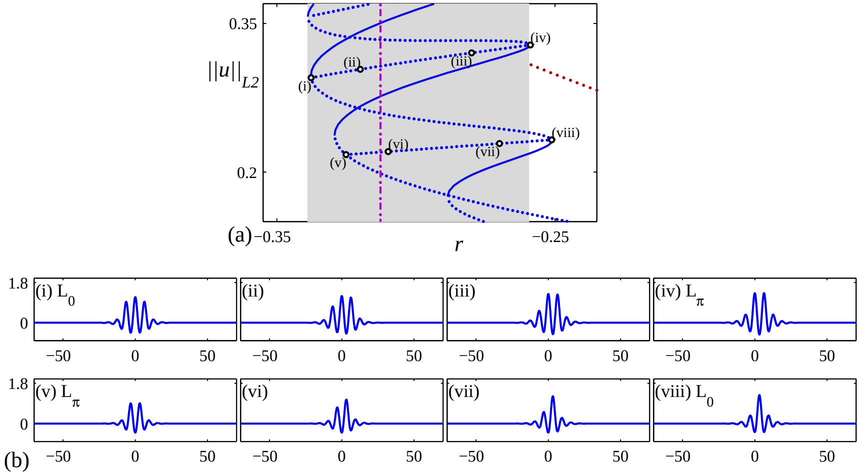

Stability

The location of the pitchfork bifurcations is determined by linearizing SH23 about a localized solution $u = u_0(x)$ and solving the eigenvalue problem

$$\mathcal{L}[u_0(x)]\,\tilde{U} \equiv \{r - (q_c^2 + d_x^2)^2 + 2b_2\,u_0 - 3u_0^2\}\tilde{U} = \sigma\,\tilde{U} \qquad (67)$$

for the eigenvalues σ and for the corresponding eigenfunctions $\tilde{U}$. This problem has to be solved numerically; if the domain used is much larger than the length of the localized structure the resulting eigenvalues will be independent of the boundary conditions imposed at the boundary. The eigenvalues comprise the spectrum of the linear operator $\mathcal{L}[u_0(x)]$ and this spectrum consists of two components depending on the symmetry of the eigenfunctions. Even eigenfunctions share the symmetry of $u_0(x)$ and correspond to *amplitude* modes. These modes are neutrally stable ($\sigma = 0$) at saddle-node bifurcations.

Stability

Odd eigenfunctions will be called phase modes. There is always one neutrally stable phase mode, the Goldstone mode. To see this consider two stationary solutions of SH23, $u_0(x+d)$ and $u_0(x)$, i.e., a pair of solutions related by translation. Now subtract the equations satisfied by these solutions, divide by d and take the limit $d \to 0$. The result is

$$\mathcal{L}[u_0(x)]\, u_0' = 0, \tag{68}$$

implying that u_0' is a neutrally stable eigenfunction of $\mathcal{L}[u_0(x)]$ for **all** parameter values. This is a consequence of the translation invariance of the system. In addition, there is a discrete set of neutrally stable phase modes associated with symmetry-breaking bifurcations of $u_0(x)$, i.e., the creation of the rung states. The next figure shows these eigenfunctions for a relatively long localized state high up the snakes-and-ladders structure. We make two important observations: the amplitude and phase modes are localized in the vicinity of the fronts bounding $u_0(x)$; by adding and subtracting these modes we construct eigenfunctions localized at one or other front. This observation implies that both the saddle-nodes and the pitchfork bifurcations are associated with instabilities of **individual fronts**.

Stability

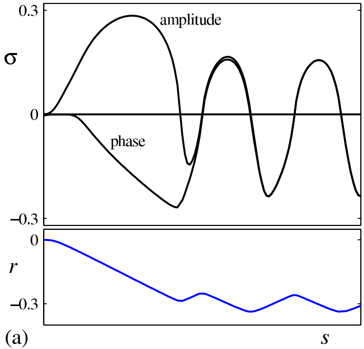

Growth rates of symmetric and antisymmetric perturbations along the (a) L_0 and (b) L_π branches

Marginal modes

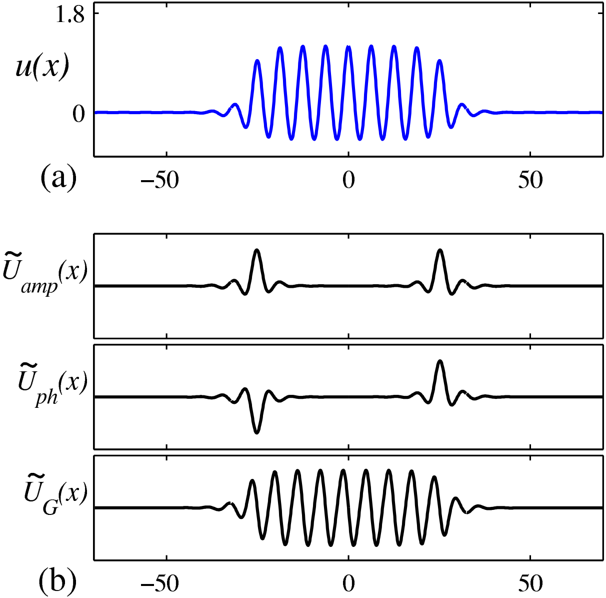

Snakes-and-ladders structure of the pinning region: SH23

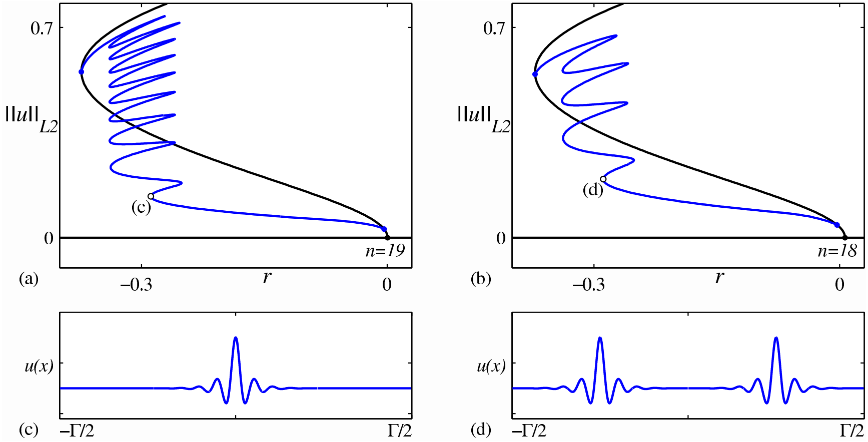

One and two pulse states occupy the same pinning region

Snakes-and-ladders structure of the pinning region: SH23

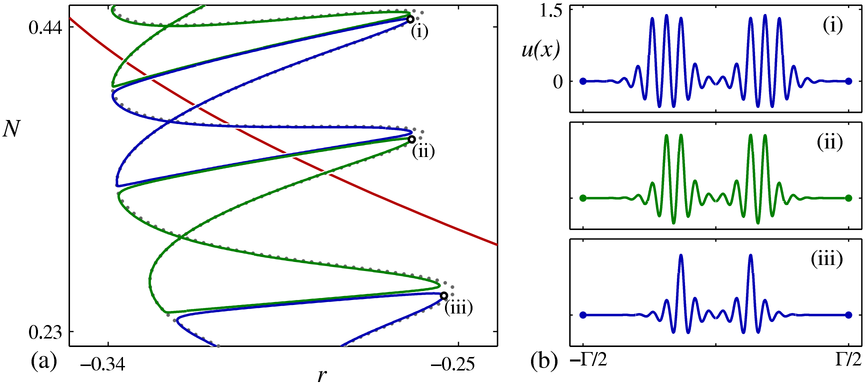

Other two-pulse states fall on a stack of isolas

Snakes-and-ladders structure of the pinning region: SH23

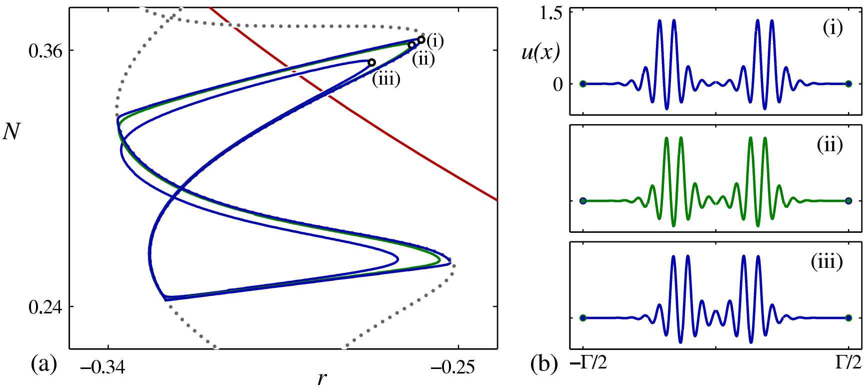

Other two-pulse states fall on a stack of isolas

Warning!

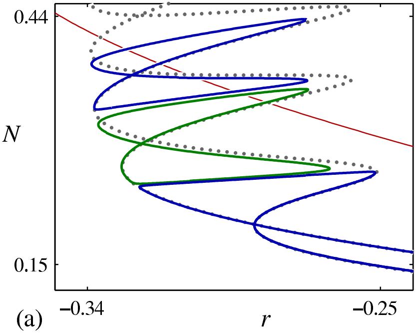

Insufficient accuracy results in branch jumping

Snakes-and-ladders structure of the pinning region: SH23

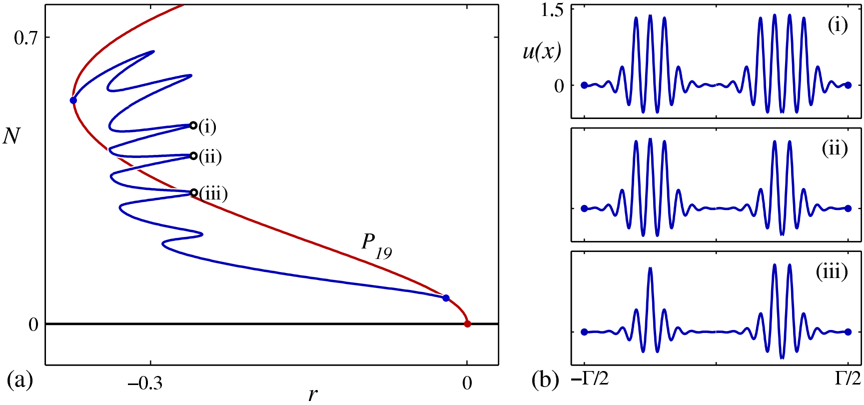

Snaking of dissimilar pulses

Dynamical systems interpretation: Beck et al (2009)

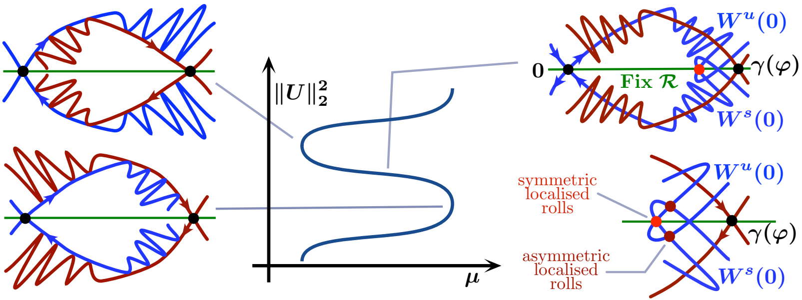

Horseshoe dynamics near the Maxwell point

Energetics: Maxwell point

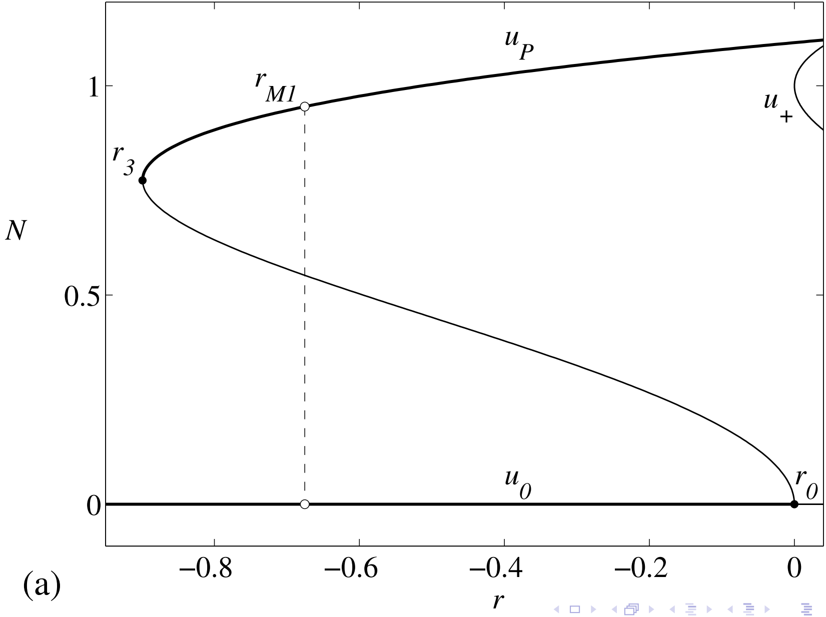

First order phase transition in terms of the free energy

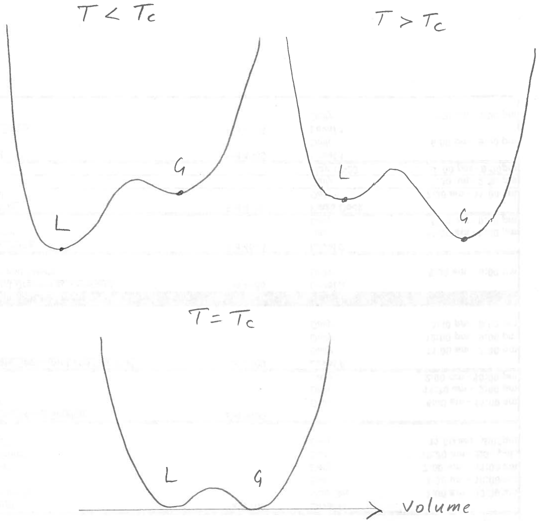

First order phase transition in a van der Waals fluid

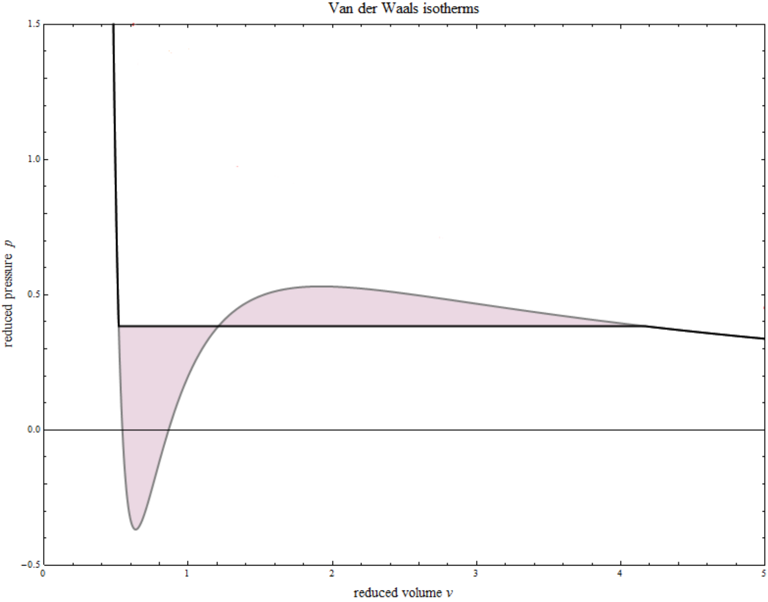

Front pinning: Pomeau (1984)

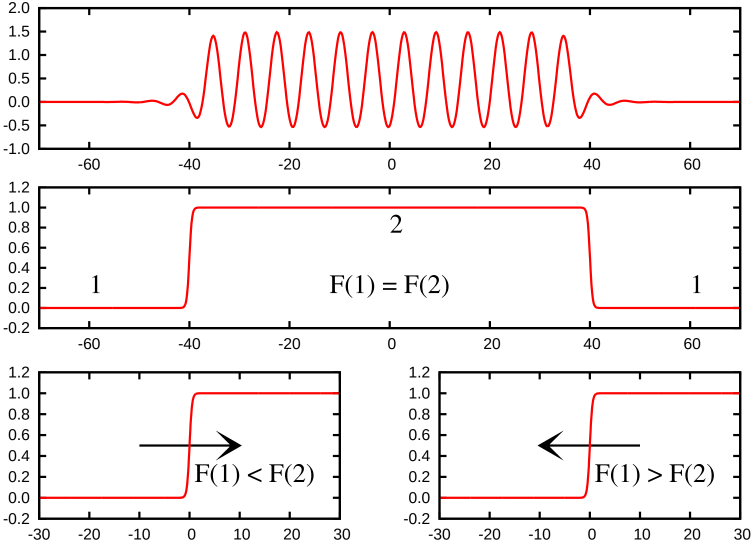

The fronts may pin to the heterogeneity within the localized state

Front pinning: SH23

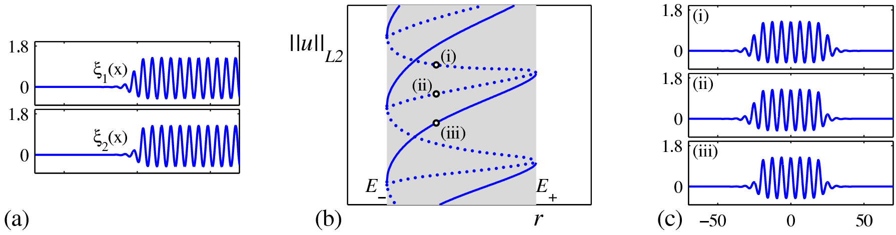

The two different front types may be combined to produce three different localized states

Wavelength selection: SH23

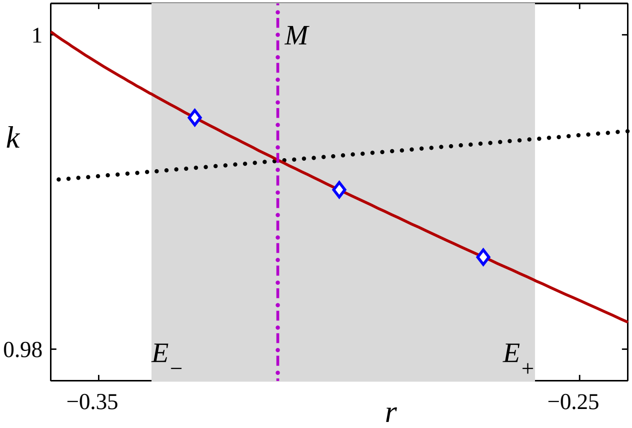

Wavelength $L \equiv 2\pi/k$ of the pattern varies across the pinning region, and is determined by the condition $H = 0$, where

$$H = -\frac{1}{2}\left(r - q_c^4\right)u^2 + q_c^2 u_x^2 - \frac{1}{2}u_{xx}^2 + u_x u_{xxx} - \int_0^u f(v)dv.$$

Pinning region: SH23

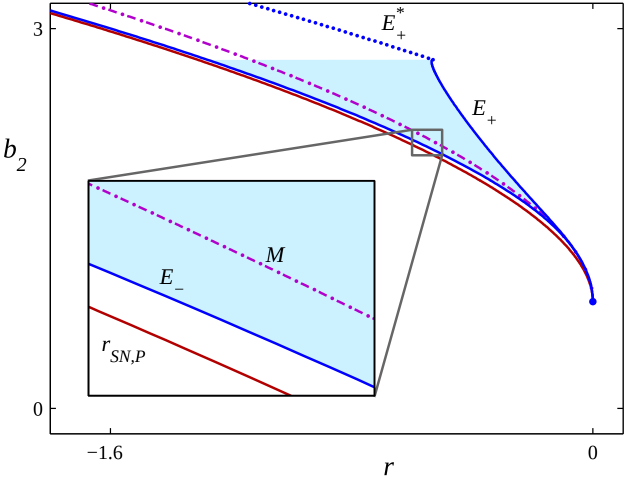

Pinning region opens out from the codimension-two point $(0, q_c^2\sqrt{27/38})$ and is of width $\epsilon^{-4}\exp(-\pi/\epsilon^2)$ when $r = \mathcal{O}(\epsilon^4)$ and $|b_2 - q_0^2\sqrt{27/38}| = \mathcal{O}(\epsilon^2)$, $\epsilon \ll 1$ (Kozyreff and Chapman, PRL (2006); Physica D (2009))

Pinning region: SH35

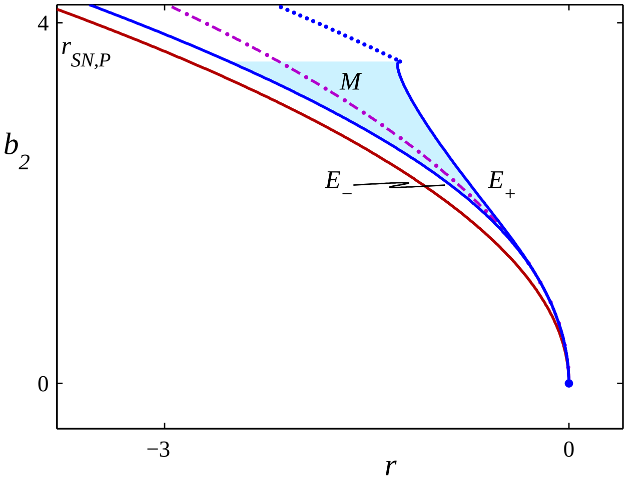

Pinning region opens out from the codimension-two point $(0, 0)$ and is of width $|r - r_M| \leq \frac{10240\pi}{9b_3} \exp(-8\sqrt{30}\pi/b_3)$, $r_M = -27b_3^2/160$, $b_3 \ll 1$.

Spatial dynamics and spatial reversibility

Suppose that

$$u_t = g(u, u_x, u_{xx}, \dots),$$

with g real-valued and $g(\mathbf{0}) = 0$. Then $g(u, u_x, u_{xx}, \dots) = 0$ is a dynamical system in space. Necessary conditions for the existence of LS biasymptotic to the homogeneous state $u = 0$ is that $u = 0$ is hyperbolic. The spatial eigenvalues are given by

$$g_u(\mathbf{0}) + g_{u_x}(\mathbf{0})u_x + g_{u_{xx}}(\mathbf{0})u_{xx} + \cdots = 0$$

or, for $u \propto \exp \lambda x$,

$$P(\lambda) = 0. \tag{69}$$

Thus (a) $P(\lambda) = 0 \implies P(\bar{\lambda}) = 0$. If the system is spatially **reversible**, then (b) $P(\lambda) = 0 \implies P(-\lambda) = 0$. Thus generically the spatial eigenvalues of the system come in complex quartets and we need at least a fourth order problem in space to capture this property.

Spatial dynamics and spatial reversibility

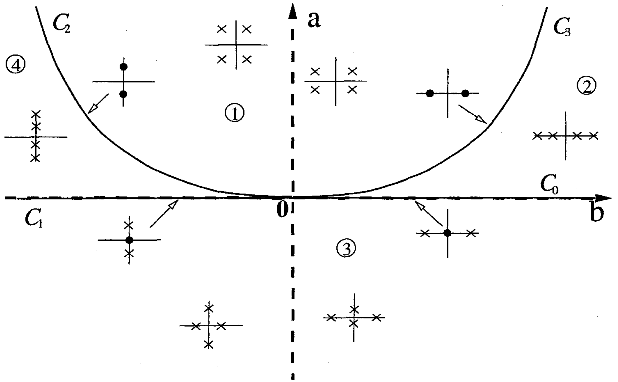

The roots of the equation $\lambda^4 + b\lambda^2 + a = 0$

Stable and unstable manifolds

The eigenvectors of stable (unstable) eigenvalues span the stable (unstable) eigenspace $E^{s,u}$ of the equilibrium O: $u = u_x = \dots = 0$; associated with each eigenspace is an invariant manifold $W^{s,u}$ tangent to $E^{s,u}$ at O. To get localized structures we need to find orbits homoclinic to O, i.e., we need W^u and W^s to intersect. This is more likely if the dimensions of these manifolds are high.

Reversible systems with $n = 4$:

- Suppose $g = 0$ has a hyperbolic fixed point O with $n_{u,s}(O) = 2$. In $n = 4$ the intersection of $W^u(O)$ and $W^s(O)$ is generically of codimension one, i.e., we expect homoclinics $O \to O$ at isolated parameter values only. But in a reversible system the codimension is zero and LS are structurally stable.
- Suppose $g = 0$ has a pair of hyperbolic fixed points O and P with $n_u(O) = 2$ and $n_s(P) = 2$. In $n = 4$ the intersection of $W^u(O)$ and $W^s(P)$ is generically of codimension one, i.e., we expect (stationary!) fronts $O \to P$ at isolated parameter values only.

Stable and unstable manifolds

Reversible systems with $n = 4$:

- Suppose next that $g = 0$ has a symmetric hyperbolic periodic solution $u_P(x)$ satisfying $u_P(-x) = u_P(x)$. Such a solution will have one stable and one unstable Floquet multiplier plus two $+1$ multipliers. Its center-stable eigenspace will therefore be three-dimensional and $W^s(u_P)$ is therefore also three-dimensional. Thus the intersection between $W^u(O)$ and $W^s(u_P)$ is of codimension zero and therefore structurally stable, i.e. fronts $O \to u_P$ are *robust*. Moreover, if this is the case $g = 0$ will have a *robust* heteroclinic *cycle* $O \to u_P \to O$.

It turns out that near such cycles one finds a plethora of homoclinic orbits $O \to O$ and so knowing where such cycles are is of great help in finding different types of LS, particularly in systems that do not have gradient structure.

Snakes-and-ladders structure of the pinning region: SH23

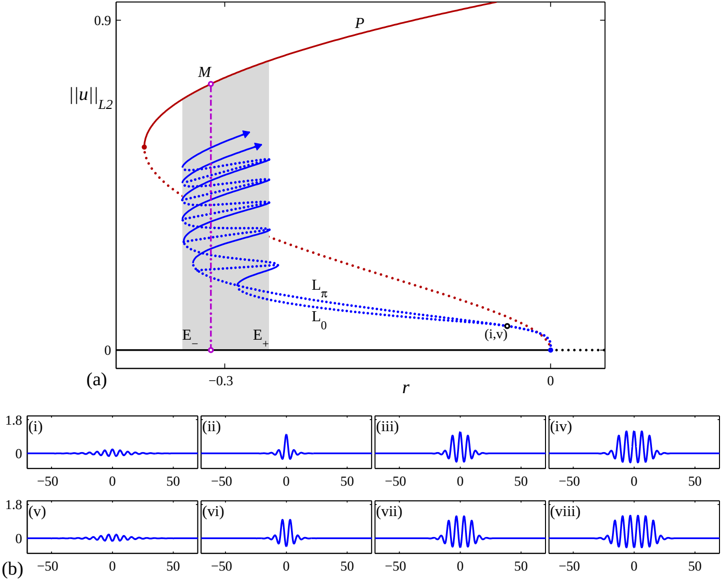

Depinning: SH23

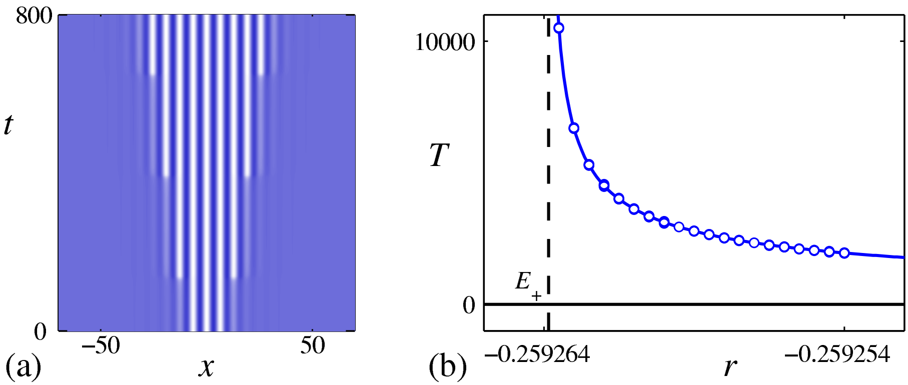

New cells are nucleated symmetrically on either side of the structure

Burke and Knobloch, PRE **73**, 056211 (2006)

Depinning: SH23

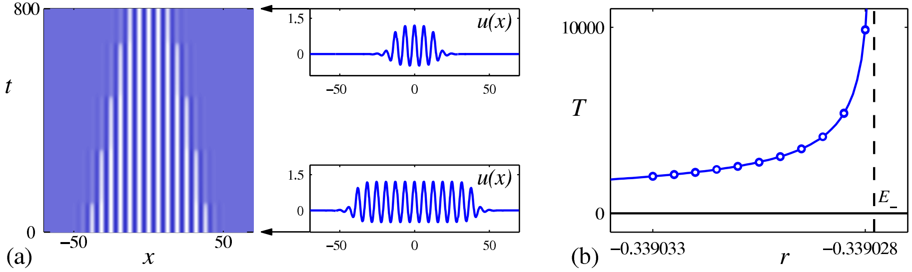

New cells are destroyed symmetrically on either side of the structure

Burke and Knobloch, PRE **73**, 056211 (2006)

Depinning: theory

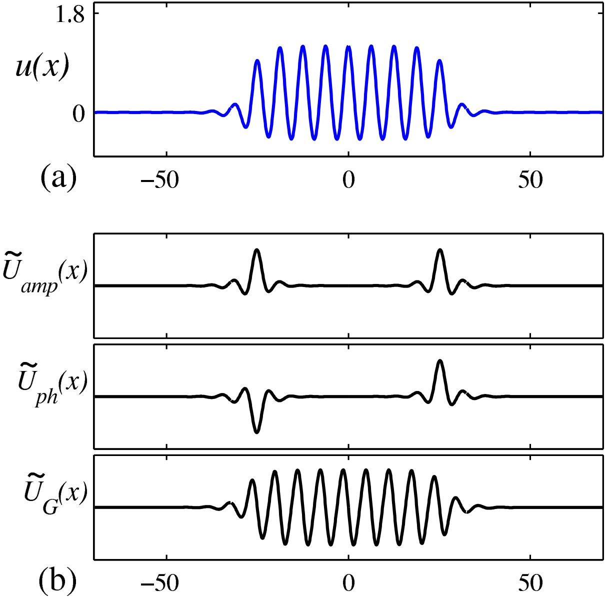

Depinning: theory

When $r = r(E_-) + \delta$, $|\delta| \ll 1$, we have

$$u(x,t) = u_0(x) + |\delta|^{1/2} u_1(x,\tau) + \mathcal{O}(|\delta|), \quad (70)$$

where $\tau = |\delta|^{1/2} t$ and

$$\mathcal{L}[\partial_x, u_0] u_1(x,\tau) = |\delta|^{1/2}(\partial_\tau u_1 - \mathrm{sgn}(\delta) u_0 - b_2 u_1^2 + 3u_0 u_1^2) + \mathcal{O}(|\delta|). \quad (71)$$

Here $\mathcal{L}$ is a differential operator evaluated at $r = r(E_-)$. At leading order

$$\mathcal{L}[\partial_x, u_0] u_1(x,\tau) = 0, \quad (72)$$

so that

$$u_1(x,\tau) = a(\tau)\tilde{U}_{amp} + b(\tau)\tilde{U}_{ph} + c(\tau)\tilde{U}_G. \quad (73)$$

Since the "center of mass" remains fixed $b = c = 0$ and at next order we have a single solvability condition

$$\alpha_1 \partial_\tau a = \alpha_2 \mathrm{sgn}(\delta) + \alpha_3 a^2, \quad (74)$$

where

$$\alpha_1 \equiv \int_{-\infty}^{\infty} \tilde{U}_{amp}^2 dx, \quad \alpha_2 \equiv \int_{-\infty}^{\infty} u_0 \tilde{U}_{amp} dx, \quad \alpha_3 \equiv \int_{-\infty}^{\infty} (b_2 - 3u_0)\tilde{U}_{amp}^3 dx. \quad (75)$$

Depinning: theory

Hence the transition time T_- to pass between successive saddle-nodes is

$$T_- = \frac{\pi\alpha_1}{(\alpha_2\alpha_3\delta)^{1/2}} \approx 4.388|\delta|^{-1/2}, \qquad \delta < 0. \tag{76}$$

For comparison simulation gives

$$T_- \approx (4.57 \pm 0.34)|\delta|^{-0.499\pm0.006}, \qquad \delta < 0. \tag{77}$$

The corresponding results for $r = r(E_+) + \delta$, $\delta \ll 1$, are

$$T_+ = \frac{\pi\alpha_1}{(\alpha_2\alpha_3\delta)^{1/2}} \approx 5.944\delta^{-1/2}, \qquad \delta > 0. \tag{78}$$

For comparison simulation gives

$$T_+ \approx (6.04 \pm 0.18)\delta^{-0.501\pm0.003}, \qquad \delta > 0. \tag{79}$$

Drifting localized states and asymmetric nucleation

The addition of a third order derivative leads to pattern drift:

$$0 = \left(r - \left(1 + \partial_x^2\right)^2\right) u + c\partial_x u + \gamma\partial_x^3 u + b_2 u^2 - u^3$$

Drifting localized states fall of stack of figure-eight isolas

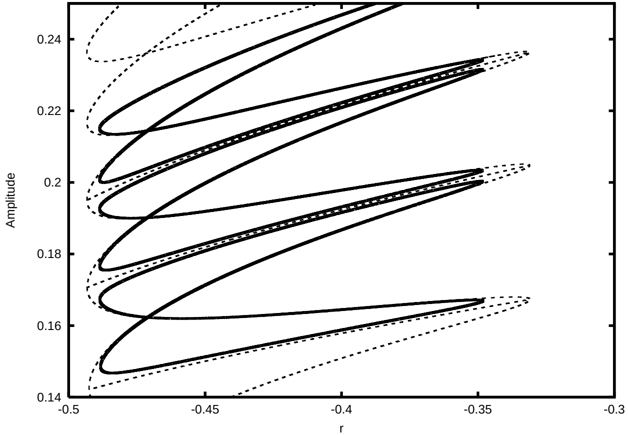

Drift speeds

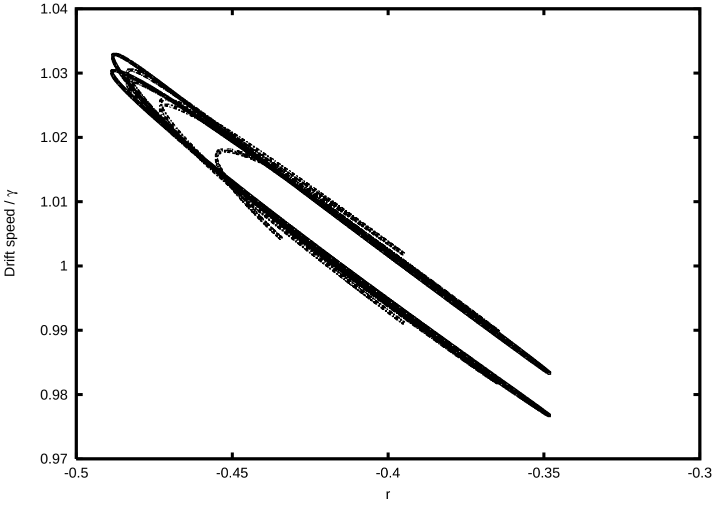

Parameters: $b_2 = 2.0$ and different values of γ

Figure-eight isolas as a function of γ

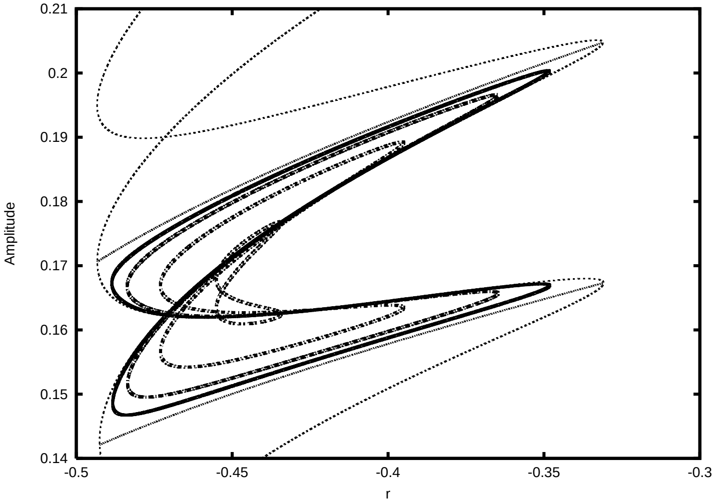

Parameters: $b_2 = 2.0$ and $\gamma = 0.05, 0.10, 0.20, 0.35$

Outside the isolas

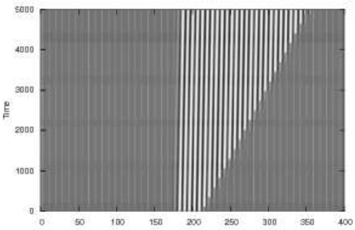

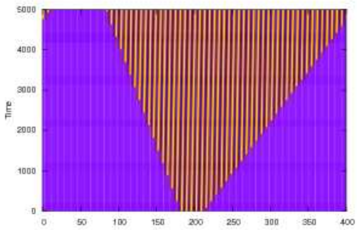

$\gamma = 0.001, r = r(E_+) + 0.00015$ $\quad$ $\gamma = 0.001, r = r(E_+) + 0.00065$

- In both cases the patterns are slowly drifting to the right
- Very close to the saddle-node, the pattern only grows on the right-hand side, i.e., the leading side
- Further from the saddle-node, the pattern grows on both side, but at different rates

Outside the isolas

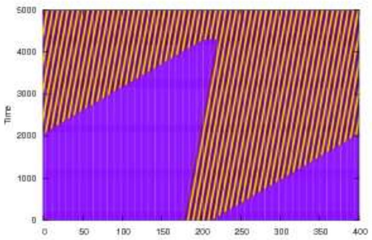

$$\gamma = 0.01, r = r(E_+) + 0.00065$$

- Increasing γ the pattern now only grows at the leading edge
- Therefore, transition is dependent on degree of symmetry breaking
- Drift speed has increased with γ
- When $\gamma = 0$ (symmetric) the pattern grows symmetrically

Theory

When $r = r(E_+) + \delta$ we take $\gamma = \sigma|\delta|$, $\sigma = O(1)$, and write

$$u(x,t) = u_0(x+\theta(T)) + |\delta|^{1/2} u_1(x+\theta(T),\tau) + |\delta| u_2(x+\theta(T),\tau) + \dots$$

where $\tau = |\delta|^{1/2} t$, $T = |\delta| t$ and $\theta(T)$ takes account of the spatial phase of the solution. The leading-order, $O(1)$, terms are

$$r(E_+)u_0 - \left(1+\partial_x^2\right)^2 u_0 + b_2 u_0^2 - u_0^3 = 0.$$

This is the equation for steady solutions of the reversible Swift-Hohenberg equation and has solutions $u_0 = U_0(x+\theta(T))$.

At next order, $O(|\delta|^{1/2})$,

$$\mathcal{L}u_1 \equiv \left(r(E_+) - (1+\partial_x^2)^2 + 2b_2 U_0 - 3U_0^2\right) u_1 = 0,$$

and u_1 is again a superposition of the three (almost) marginal modes.

Solvability conditions

Since the translation has been included by introducing the phase $\theta(T)$ the $\tilde{U}_G$ mode is already included. Thus

$$u_1 = a(\tau)\tilde{U}_{amp}\left(x + \theta(T)\right) + b(\tau)\tilde{U}_{ph}\left(x + \theta(T)\right),$$

where $a(T), b(T)$ and $\theta(T)$ are determined from solvability conditions at next order, $O(|\delta|)$.

At $O(|\delta|)$,

$$U_0'\theta_T + u_{1\tau} = \mathcal{L}u_2 + \mathrm{sgn}\delta\, U_0 + \sigma U_0''' + \left(b_2 - 3U_0\right)u_1^2.$$

Multiplying in turn by $\tilde{U}_G \equiv U_0'$, $\tilde{U}_{amp}$ and $\tilde{U}_{ph}$ and integrating over the real line yields three solvability conditions.

Drift speed

The first solvability condition gives

$$\theta_T = -0.9663\sigma$$

or, equivalently,

$$\theta_t = -0.9663\gamma.$$

The predicted drift speed towards the right when $\gamma = 0.001$ is therefore 0.0009663.

The drift speed measured from numerical simulations is 0.0009589. The prediction is in good agreement.

At leading-order the drift speed depends only on the magnitude of the broken reversibility and not distance from the saddle-node.

Nucleation times

The remaining solvability conditions give a coupled pair of equations

$$\begin{aligned} a_\tau &= \alpha_1 \mathrm{sgn}\delta + \alpha_2 a^2 + \alpha_3 b^2 \\ b_\tau &= -\beta\sigma + 2\alpha_4 ab. \end{aligned}$$

The coefficients in this equation depend on the length $2L$ of the localized state. High up the snaking structure, $2L$ is large and the eigenfunctions $\tilde{U}_{amp}$, $\tilde{U}_{ph}$ consist, up to exponentially small terms, of pairs of non-overlapping neutral modes localized at the bounding fronts. Consequently we may write $\tilde{U}_{amp} = v(x+L) + v(x-L)$, $\tilde{U}_{ph} = v(x+L) - v(x-L)$ for a suitable function $v(x)$. From the expressions for the coefficients it now follows that, up to exponentially small terms, $\alpha_2 = \alpha_3 = \alpha_4$.

Thus

$$(a \pm b)_\tau = \alpha_1 \mathrm{sgn}\delta \mp \beta\sigma + \alpha_3 \left(a \pm b\right)^2 .$$

Nucleation times

We define the time for a new cell to be created at the leading edge to be

$$T_{leading} \equiv \int_{-\infty}^{\infty} \frac{\mathrm{d}\tau}{a-b} = \frac{\pi}{\alpha_3^{1/2}} \frac{1}{(\alpha_1\delta + \beta\gamma)^{1/2}}$$

and the time for a new cell to be created at the trailing edge to be

$$T_{trailing} \equiv \int_{-\infty}^{\infty} \frac{\mathrm{d}\tau}{a+b} = \frac{\pi}{\alpha_3^{1/2}} \frac{1}{(\alpha_1\delta - \beta\gamma)^{1/2}}.$$

This time diverges (i.e., nucleation ceases) when

$$\delta_c^{leading} = -\beta\gamma/\alpha_1 = -0.3543\gamma, \qquad \delta_c^{trailing} = \beta\gamma/\alpha_1 = 0.3543\gamma.$$

Thus when $\gamma = 0.001$ the predicted value of $|r(E_+) - r_{SN}| = 0.0003543$, compared with the measured value 0.000356.

Nucleation times

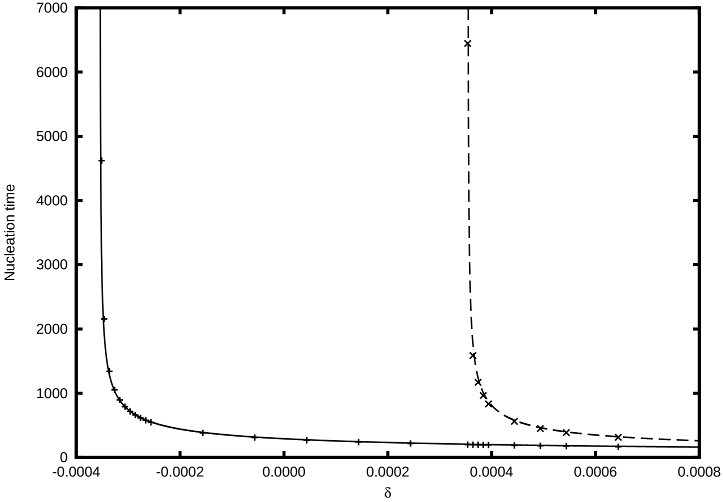

Parameters: $b_2 = 2.0, \gamma = 0.001$

Snakes-and-ladders structure of the pinning region: SH35

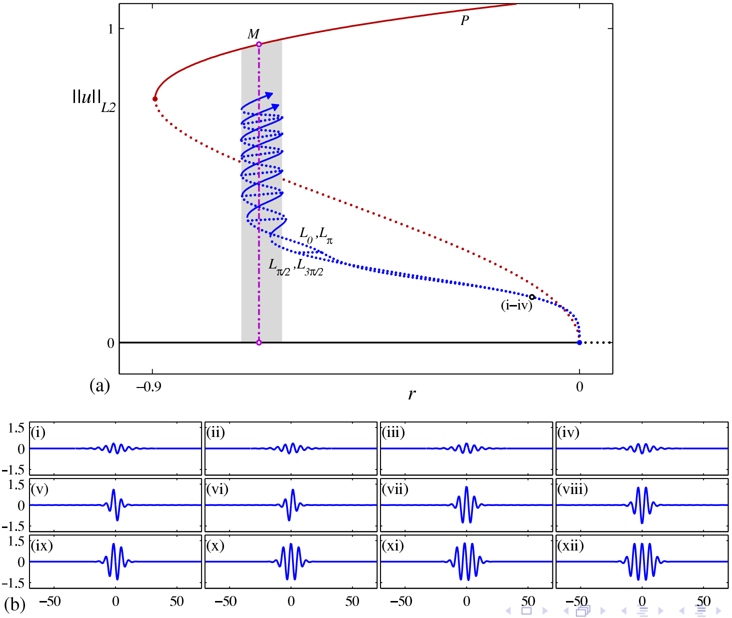

Comparison of SH23 and SH35

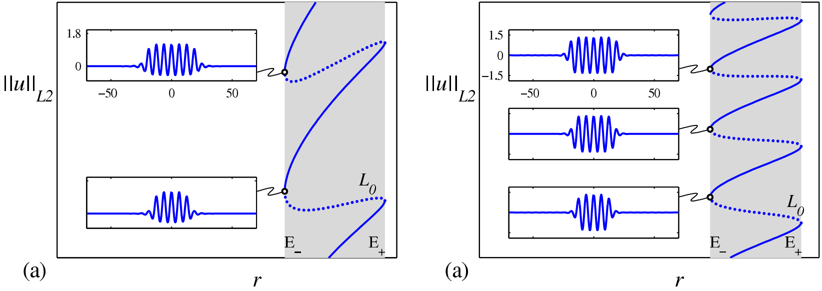

Growth along the L_0 branches in (a) SH23 and (b) SH35

Burke and Knobloch, Chaos **17**, 037102 (2007)

Two spatial dimensions: SH35

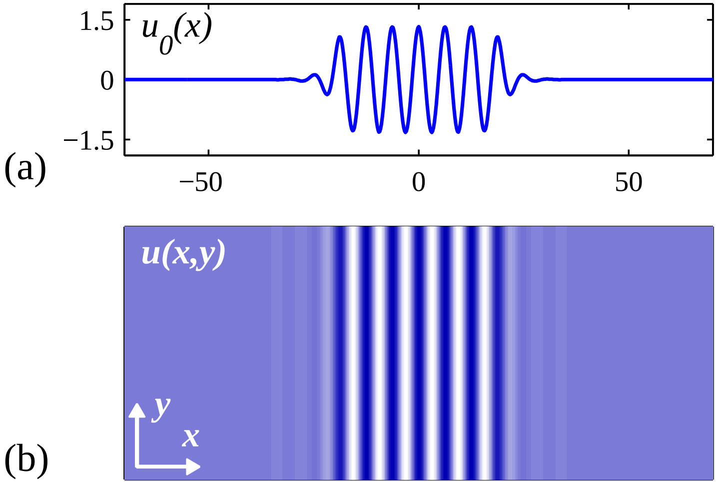

Two spatial dimensions: SH35

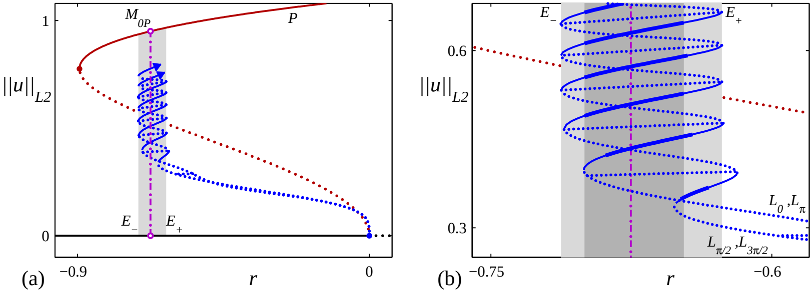

Burke and Knobloch, Chaos **17**, 037102 (2007)

Two spatial dimensions: SH35

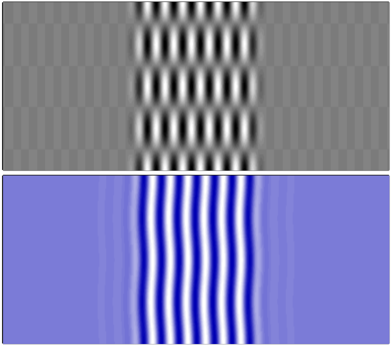

(a)

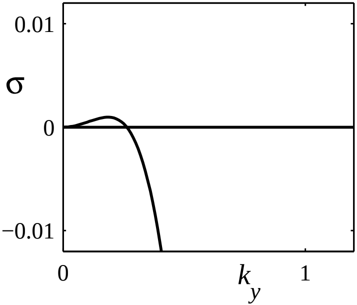

(b)

Burke and Knobloch, Chaos **17**, 037102 (2007)

Two spatial dimensions: SH35

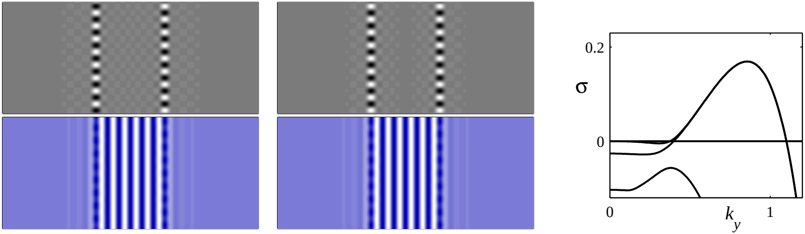

(a) (b) (c)

Burke and Knobloch, Chaos **17**, 037102 (2007)

Two spatial dimensions: SH35

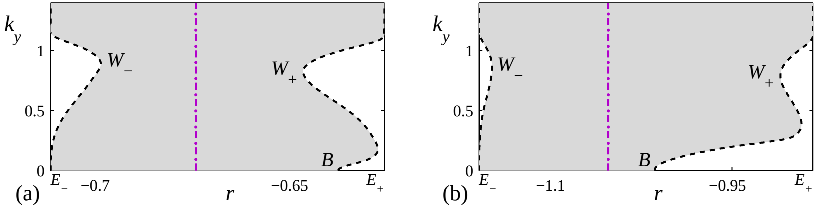

Burke and Knobloch, Chaos **17**, 037102 (2007)

Two spatial dimensions: SH35 and SH23

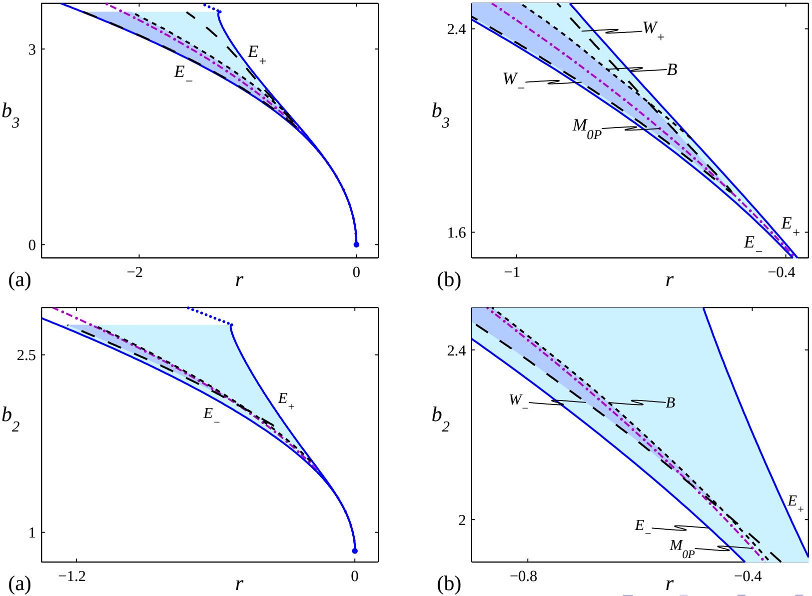

Two spatial dimensions: SH23

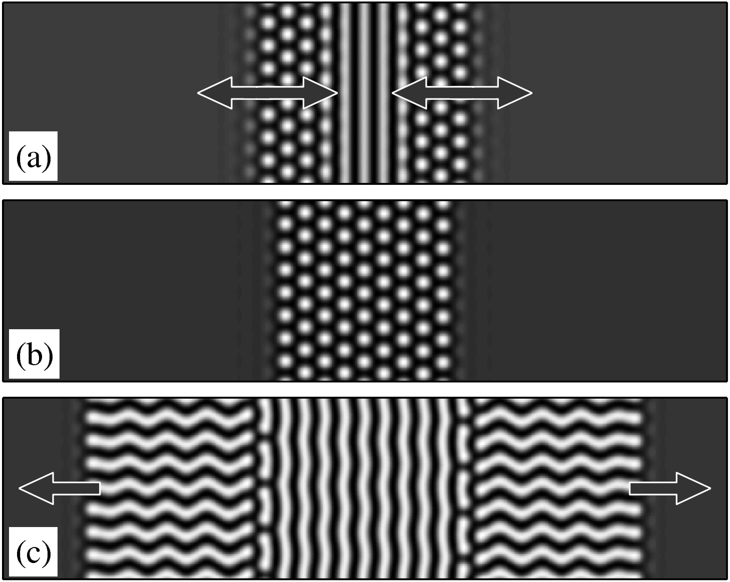

Two spatial dimensions: SH35

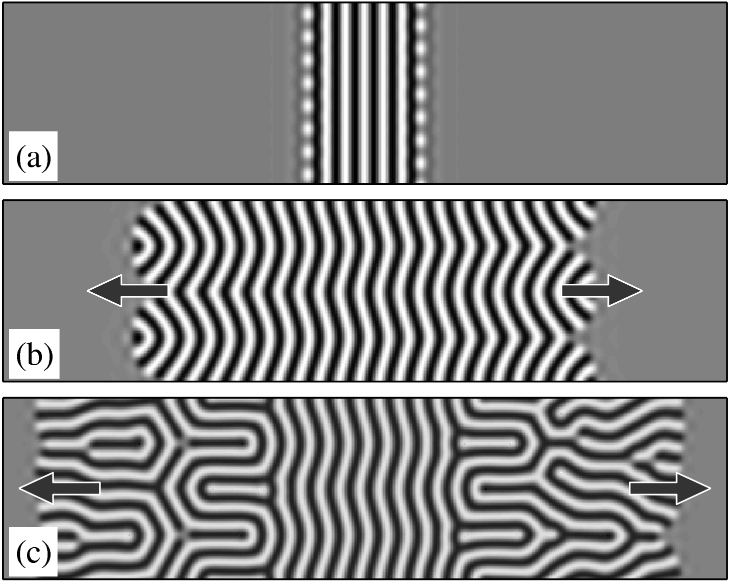

Snaking of stripe-like patterns: SH35

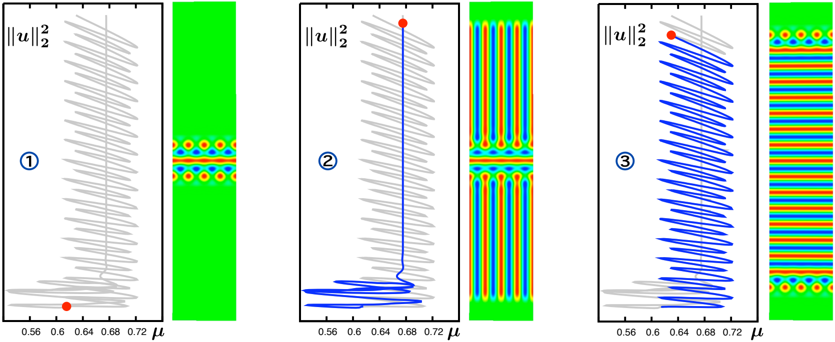

Avitabile et al., SIADS **9**, 704 (2010)

Snaking of stripe-like patterns: SH35

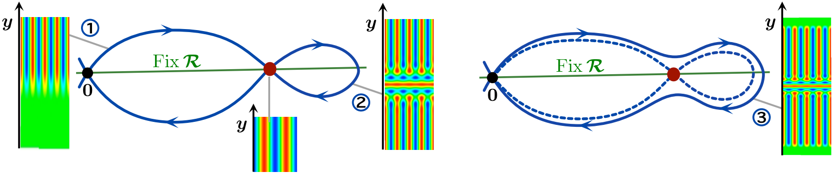

Snaking of stripe-like patterns: SH35

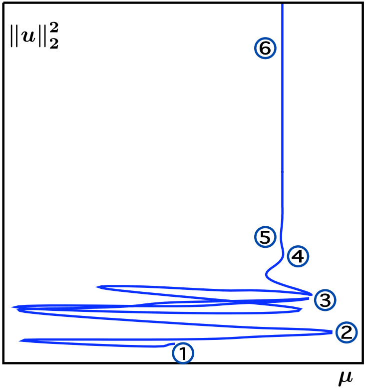

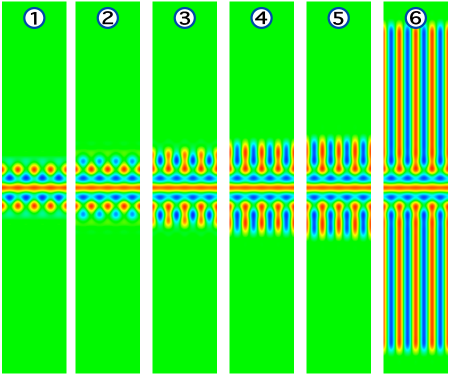

Snaking of stripe-like patterns: SH35

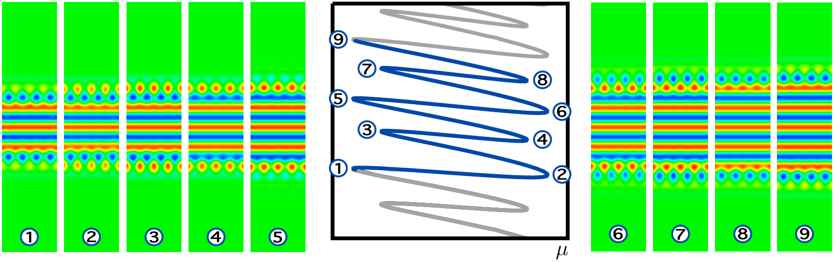

Snaking of stripe-like patterns: SH35

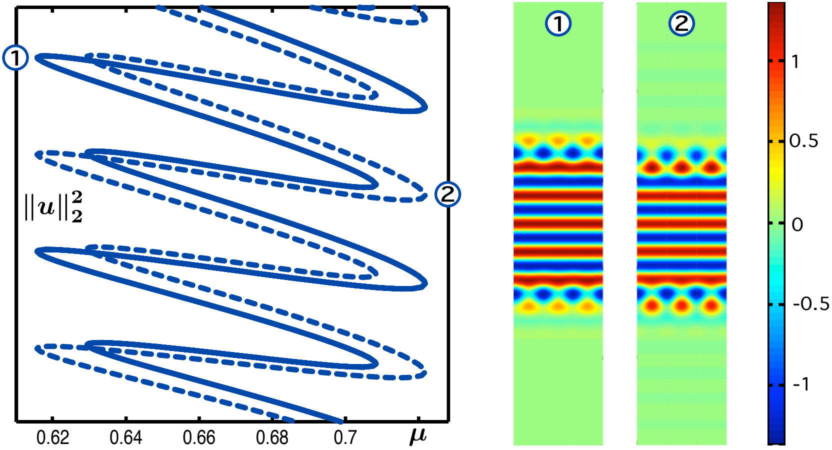

Snakes-and-ladders structure of the pinning region

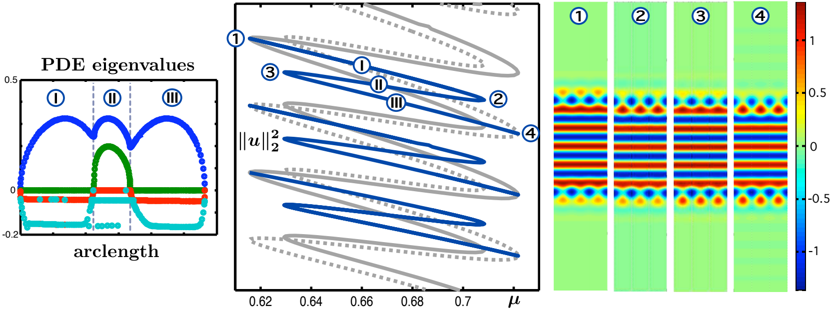

Snakes-and-ladders structure of the pinning region

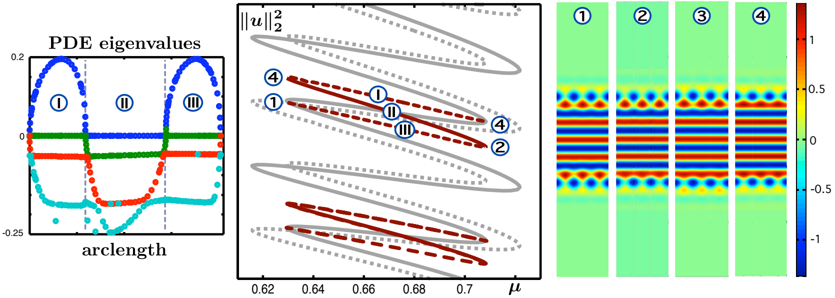

Isolas

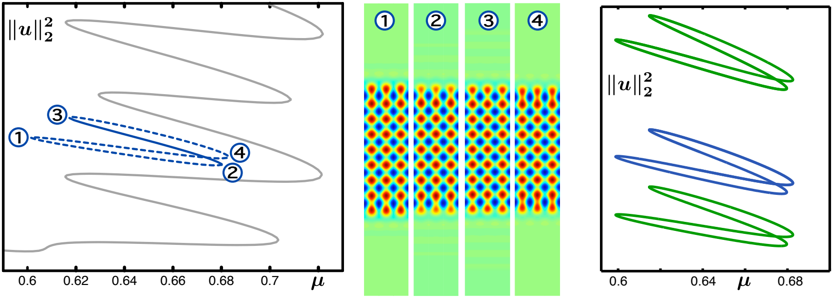

Localized states in two spatial dimensions: SH35

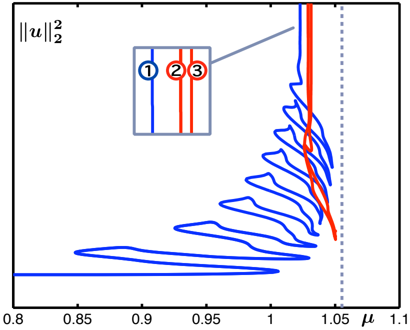

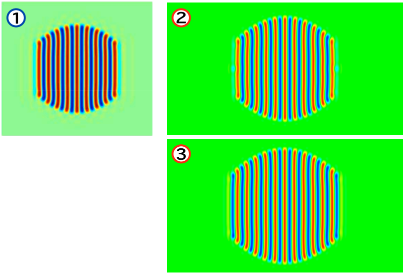

Localized states in two spatial dimensions: SH35

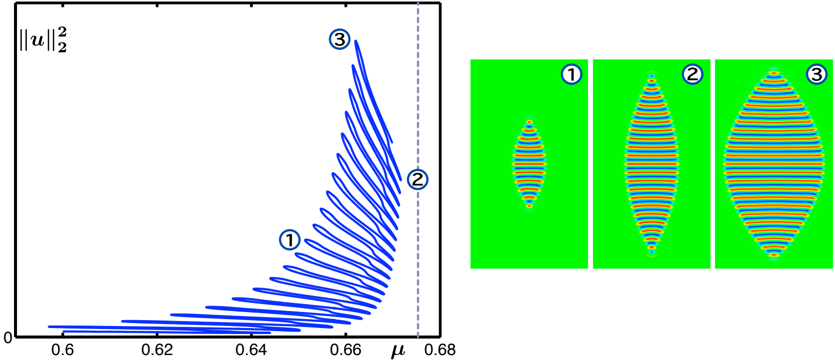

Avitabile et al., SIADS **9**, 704 (2010)

Localized states in two spatial dimensions: SH35

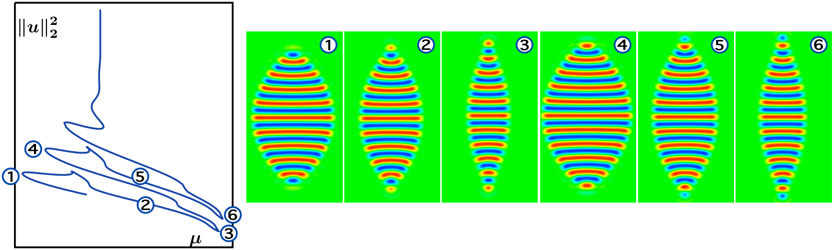

Avitabile et al., SIADS **9**, 704 (2010)

Localized spots and targets in two spatial dimensions: SH23

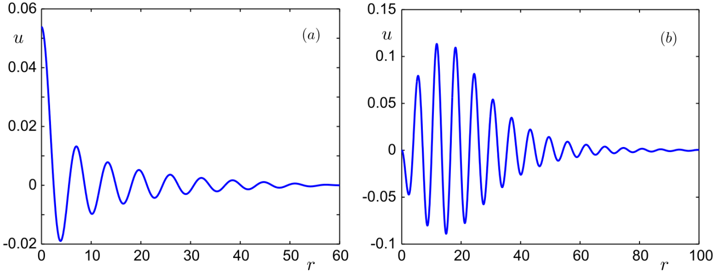

(a) Spots bifurcate from $u = 0$ at $\mu = 0$ even when $b_2 < 0$ with amplitude $\propto (-\mu)^{1/4}$. (b) Rings bifurcate from $u = 0$ at $\mu = 0$ provided $b_2 > \sqrt{27/38}$ and do so subcritically with amplitude $\propto (-\mu)^{3/4}$ (Lloyd and Sandstede, Nonlinearity **22**, 485 (2009)).

Snaking of spots in two spatial dimensions: SH23

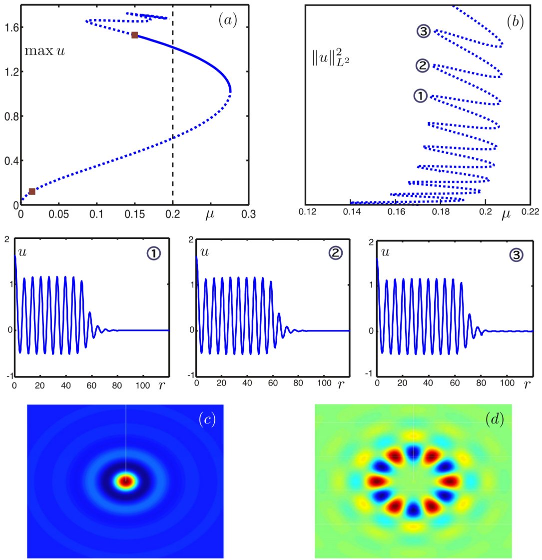

Spots in two spatial dimensions: SH23

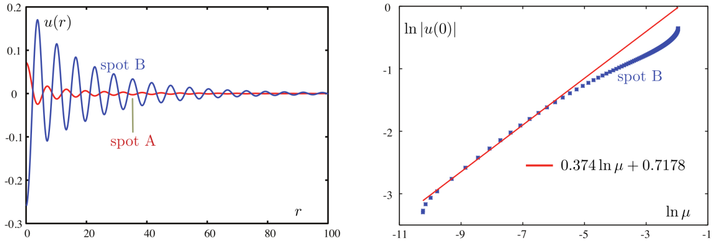

There are in fact two types of axisymmetric spots: spot A with amplitude $\propto \sqrt{-\mu}$ and spot B with amplitude $\propto (-\mu)^{3/8}$ (McCalla and Sandstede, SIADS **12**, 831 (2013)). Spot A bifurcates from $u = 0$ at $\mu = 0$ even if $b_2 < \sqrt{27/38}$.

Snaking in two spatial dimensions: SH23

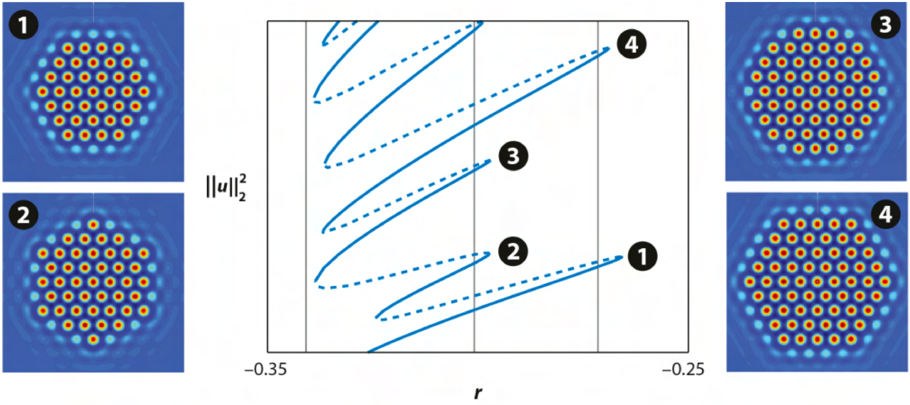

Localized hexagons in SH23: Lloyd et al., SIADS **7**, 1049–1100 (2008)

Snaking in two spatial dimensions: SH23

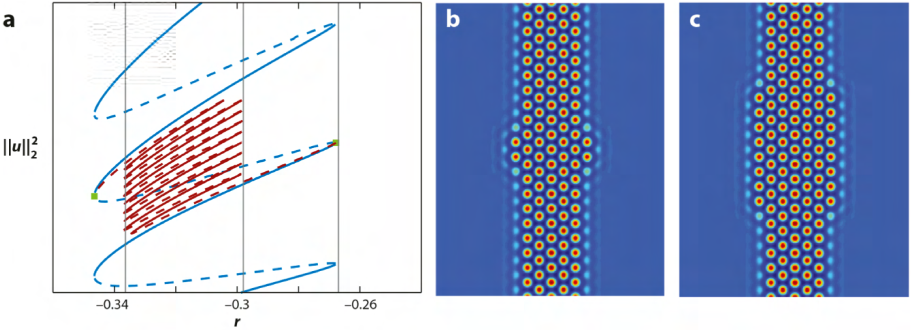

Lloyd et al., SIADS **7**, 1049–1100 (2008)

Localized states in two spatial dimensions: SH23

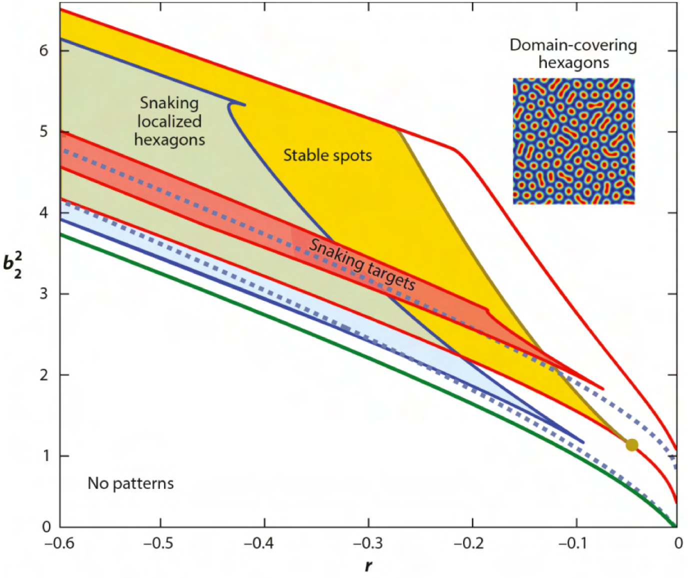

Oscillons

TYPES OF OSCILLATING LOCALIZED STATES

Damped oscillations

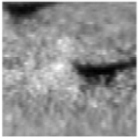

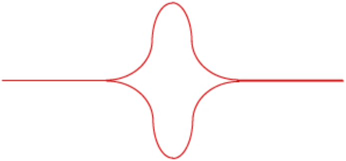

“Standard” oscillons

Self-excited oscillations

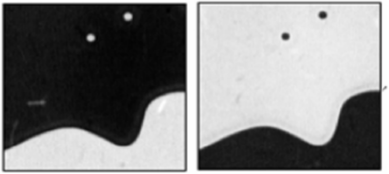

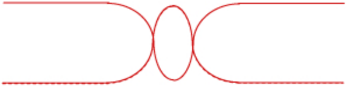

“Reciprocal” oscillons

Forced Ginzburg-Landau equation

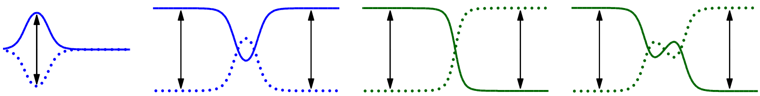

(a) SSO (b) SRO (c) SIF (d) SSF

Different types of localized states in parametrically forced systems

In such systems a dynamical observable w takes the form

$$w = w_0 + Ae^{i\Omega t/2} + c.c. + \cdots, \tag{80}$$

where w_0 represents the equilibrium state and $A(x,t)$ is a complex amplitude. The oscillation amplitude $A(x,t)$ obeys the FCGL equation

$$A_t = (\mu + i\nu)A - (1+i\beta)|A|^2A + (1+i\alpha)A_{xx} + \gamma\bar{A}, \tag{81}$$

where μ represents the distance from onset of the oscillatory instability, ν is the detuning from the unforced frequency, and α, β and γ represent dispersion, nonlinear frequency correction and the forcing amplitude, respectively.

Resonance tongues

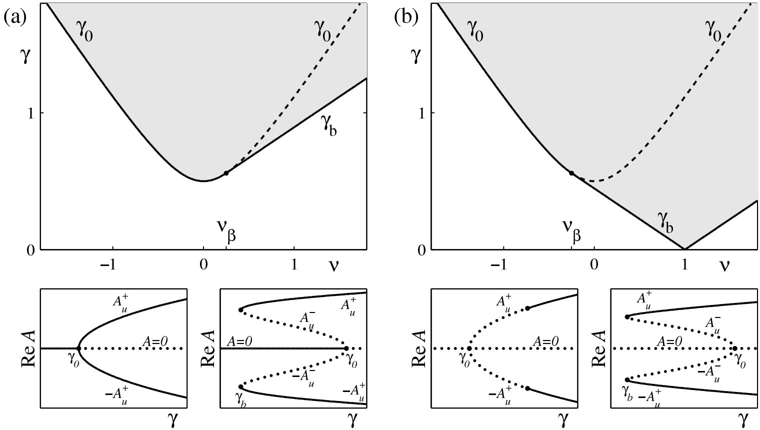

Frequency-locked states when (a) $\mu < 0$, (b) $\mu > 0$

Forced Ginzburg-Landau equation

When $\mu < 0$, $z > 0$ a saddle-node bifurcation involving the uniform phase-locked states A_u^+ and A_u^- occurs at $\gamma = \gamma_b$ whenever $\nu > \nu_\beta$. At this point the uniform state has two zero spatial eigenvalues and two nonzero spatial eigenvalues, and the nonzero eigenvalues are real provided $\nu > \nu_z$. Along the A_u^+ branch the zero eigenvalues split along the real axis and localized states may exist in the form of orbits homoclinic to A_u^+.

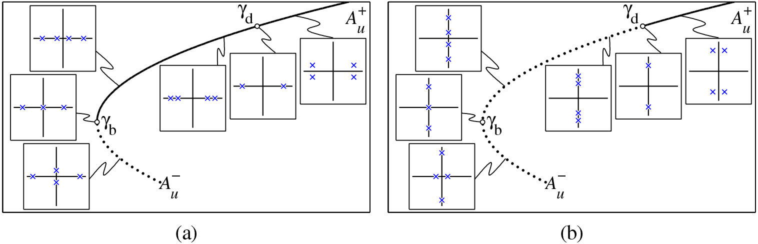

Spatial eigenvalues for (a) $\nu > \nu_z$, (b) $\nu < \nu_z$

Forced Ginzburg-Landau equation

To find these states we write $\gamma = \gamma_b + \epsilon^2\delta$, where $\epsilon \ll 1$ and $\delta > 0$, and solve the time-independent problem

$$(\mathcal{L} + \mathcal{N}) \begin{bmatrix} U \\ V \end{bmatrix} = 0, \tag{82}$$

where $A = U + iV$. Localized states biasymptotic to A_u^+ take the form

$$\begin{bmatrix} U \\ V \end{bmatrix} = \begin{bmatrix} U \\ V \end{bmatrix}^+ + \begin{bmatrix} u \\ v \end{bmatrix}, \tag{83}$$

where the first term is the uniform phase-locked state A_u^+ and the second corresponds to the space-dependent terms that decay to zero as $x \to \pm\infty$. Thus A_u^+ can be approximated by the series

$$\begin{bmatrix} U \\ V \end{bmatrix}^+ = \begin{bmatrix} U_0 \\ V_0 \end{bmatrix} + \epsilon \begin{bmatrix} U_1 \\ V_1 \end{bmatrix} + \epsilon^2 \begin{bmatrix} U_2 \\ V_2 \end{bmatrix} + \dots, \tag{84}$$

where

$$\begin{bmatrix} U_0 \\ V_0 \end{bmatrix} = \begin{bmatrix} \eta_b \\ 1 \end{bmatrix} \Upsilon_0, \qquad \begin{bmatrix} U_1 \\ V_1 \end{bmatrix} = \sqrt{\delta} \begin{bmatrix} \xi_b \\ 1 \end{bmatrix} \Upsilon_1. \tag{85}$$

Here

$$\eta_b = \beta + \rho_\beta \,, \quad \xi_b = \frac{\eta_b \nu + (1 - \beta\eta_b)|A_u(\gamma_b)|^2}{\nu - (\beta + \eta_b)|A_u(\gamma_b)|^2} \,, \tag{86}$$

$$\Upsilon_0 = \frac{|A_u(\gamma_b)|}{\sqrt{1+\eta_b^2}} \,, \quad \Upsilon_1 = \mathrm{sgn}[\xi_b\eta_b + 1]\sqrt{\frac{\eta_b}{(\xi_b\eta_b+1)(\xi_b-\eta_b)}} \,. \tag{87}$$

The second term in Eq. (83) can be expanded as

$$\begin{bmatrix} u \\ v \end{bmatrix} = \epsilon \begin{bmatrix} u_1 \\ v_1 \end{bmatrix} + \epsilon^2 \begin{bmatrix} u_2 \\ v_2 \end{bmatrix} + \dots \,, \tag{88}$$

where all quantities depend on x via the slow spatial scale $X \equiv \epsilon^{1/2}x$. The linear operator in Eq. (82) takes the form $\mathcal{L} = \mathcal{L}_0 + \epsilon\mathcal{L}_1 + \epsilon^2\mathcal{L}_2$, where

$$\mathcal{L}_0 = \begin{bmatrix} \mu + \gamma_b & -\nu \\ \nu & \mu - \gamma_b \end{bmatrix} \,, \quad \mathcal{L}_1 = \begin{bmatrix} 1 & -\alpha \\ \alpha & 1 \end{bmatrix} \partial_{XX} \,, \quad \mathcal{L}_2 = \begin{bmatrix} \delta & 0 \\ 0 & -\delta \end{bmatrix} \,, \tag{89}$$

while the nonlinear terms take the form $\mathcal{N} = \mathcal{N}_0 + \epsilon\mathcal{N}_1 + \epsilon^2\mathcal{N}_2 + \dots$, where

$$\mathcal{N}_0 = -\begin{bmatrix} U_0 & V_0 \end{bmatrix} \begin{bmatrix} U_0 \\ V_0 \end{bmatrix} \begin{bmatrix} 1 & -\beta \\ \beta & 1 \end{bmatrix}, \quad \mathcal{N}_1 = -2\begin{bmatrix} U_0 & V_0 \end{bmatrix} \begin{bmatrix} U_1 + u_1 \\ V_1 + v_1 \end{bmatrix} \begin{bmatrix} 1 & -\beta \\ \beta & 1 \end{bmatrix} \tag{90}$$

$$\mathcal{N}_2 = -\left\{ \begin{bmatrix} U_1 + u_1 & V_1 + v_1 \end{bmatrix} \begin{bmatrix} U_1 + u_1 \\ V_1 + v_1 \end{bmatrix} + 2\begin{bmatrix} U_0 & V_0 \end{bmatrix} \begin{bmatrix} U_2 + u_2 \\ V_2 + v_2 \end{bmatrix} \right\} \begin{bmatrix} 1 & -\beta \\ \beta & 1 \end{bmatrix} \tag{91}$$

At order ϵ^0 stationary solutions to Eq. (82) satisfy

$$\{\mathcal{L}_0 + \mathcal{N}_0\} \begin{bmatrix} U_0 \\ V_0 \end{bmatrix} = \begin{bmatrix} 0 \\ 0 \end{bmatrix}, \tag{92}$$

an equality that holds by virtue of the definition of U_0 and V_0. At order ϵ we obtain

$$\{\mathcal{L}_0 + \mathcal{N}_0\} \begin{bmatrix} U_1 + u_1 \\ V_1 + v_1 \end{bmatrix} = -\{\mathcal{L}_1 + \mathcal{N}_1\} \begin{bmatrix} U_0 \\ V_0 \end{bmatrix}. \tag{93}$$

The X-independent terms in this equation cancel by virtue of the definition of U_1 and V_1, leaving

$$\left\{\mathcal{L}_0+\mathcal{N}_0-2\begin{bmatrix}1 & -\beta\\ \beta & 1\end{bmatrix}\begin{bmatrix}U_0^2 & U_0V_0\\ U_0V_0 & V_0^2\end{bmatrix}\right\}\begin{bmatrix}u_1\\ v_1\end{bmatrix}=\begin{bmatrix}0\\ 0\end{bmatrix}. \tag{94}$$

Thus

$$\begin{bmatrix}u_1\\ v_1\end{bmatrix}=\begin{bmatrix}\xi_b\\ 1\end{bmatrix}B(X), \tag{95}$$

where $B(X)$ is an unknown function of X.

Proceeding to order ϵ^2 we obtain

$$\{\mathcal{L}_0+\mathcal{N}_0\}\begin{bmatrix}U_2+u_2\\ V_2+v_2\end{bmatrix}=-\{\mathcal{L}_1+\mathcal{N}_1\}\begin{bmatrix}U_1+u_1\\ V_1+v_1\end{bmatrix}-\{\mathcal{L}_2+\mathcal{N}_2\}\begin{bmatrix}U_0\\ V_0\end{bmatrix}. \tag{96}$$

Again the X-independent terms cancel. The solvability condition for this equation is obtained by taking the scalar product with

$$\Xi_b=\begin{bmatrix}-\eta_b & 1\end{bmatrix}, \tag{97}$$

to eliminate the u_2, v_2 terms, leaving

$$a_bB_{XX}=b_b\left(2V_1B+B^2\right). \tag{98}$$

Here

$$a_b = 1 + \alpha\xi_b + \alpha\eta_b - \eta_b\xi_b \,, \quad b_b = -\frac{\Upsilon_0(1+\eta_b^2)}{\Upsilon_1^2} \,. \tag{99}$$

The latter quantity is always negative. Equation (98) admits spatially homogeneous solutions $B = -2V_1$, or

$$\begin{bmatrix} U \\ V \end{bmatrix} = \begin{bmatrix} U_0 \\ V_0 \end{bmatrix} - \epsilon \begin{bmatrix} U_1 \\ V_1 \end{bmatrix} + \dots \,, \tag{100}$$

corresponding to the other branch of uniform phase-locked states, A_u^-. In addition, Eq. (98) admits a branch of X-dependent localized states

$$B(X) = -3\Upsilon_1\sqrt{\delta}\,\mathrm{sech}^2\left\{\left(\frac{\Upsilon_1\sqrt{\delta}}{2a_b/b_b}\right)^{1/2} X\right\} \tag{101}$$

corresponding to

$$\begin{bmatrix} U \\ V \end{bmatrix} = \begin{bmatrix} U \\ V \end{bmatrix}^+ - 3\Upsilon_1\sqrt{\gamma-\gamma_b}\begin{bmatrix} \xi_b \\ 1 \end{bmatrix}\mathrm{sech}^2\left\{(\gamma-\gamma_b)^{1/4}\left(\frac{\Upsilon_1}{2a_b/b_b}\right)^{1/2} x\right\} \,. \tag{102}$$

Reciprocal oscillons

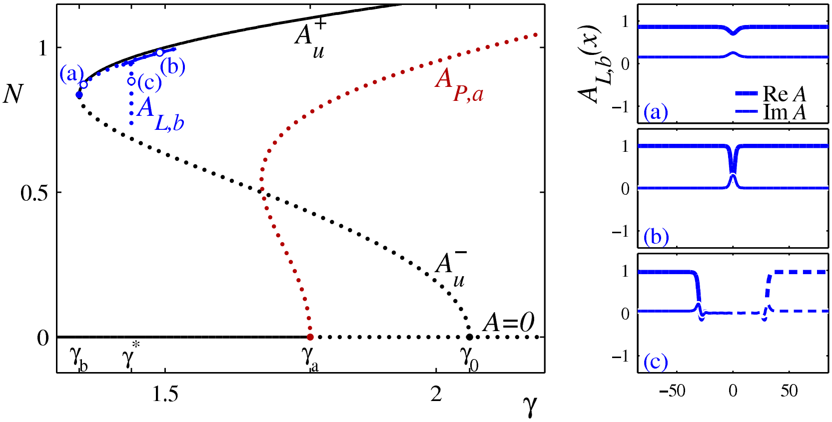

Reciprocal oscillons

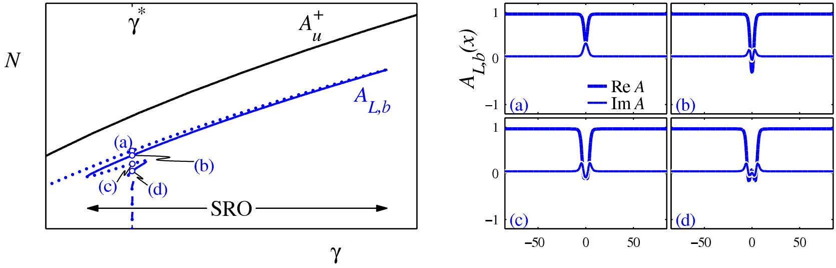

The 2 : 1 resonance: parameter plane for $\mu > 0$

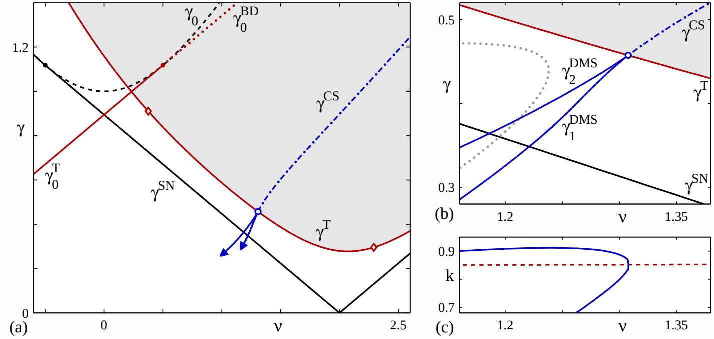

Parameter plane for $\alpha = -2$, $\beta = 2$ and $\mu = 1$ (excitable regime)

Ma et al., Physica D **239**, 1867 (2010)

The 2 : 1 resonance: collapsed snaking for $\nu > \nu^*$

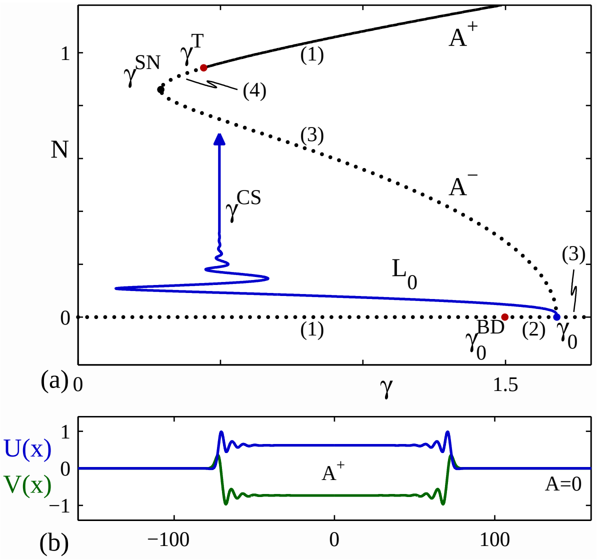

The 2 : 1 resonance: defect-mediated snaking for $\nu < \nu^*$

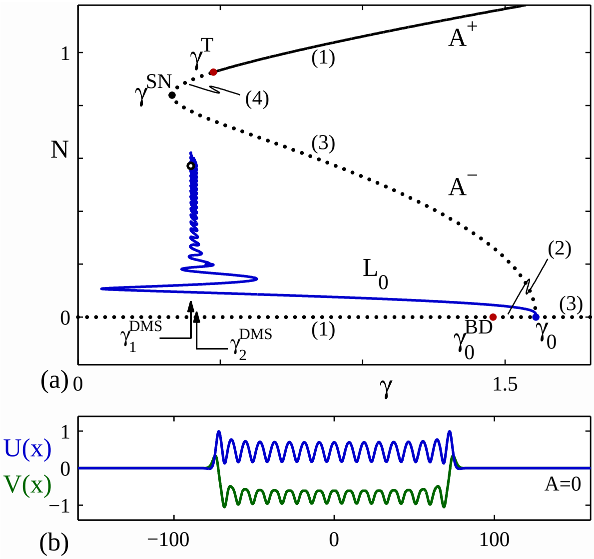

The 2 : 1 resonance: defect-mediated snaking

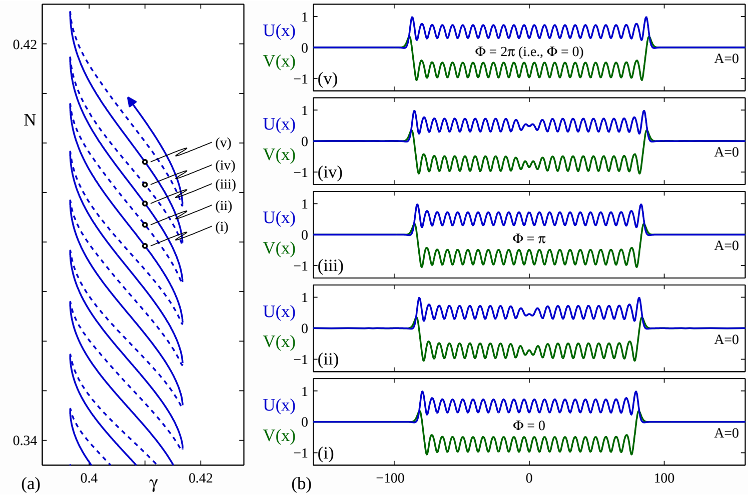

The 2 : 1 resonance: detail of defect-mediated snaking

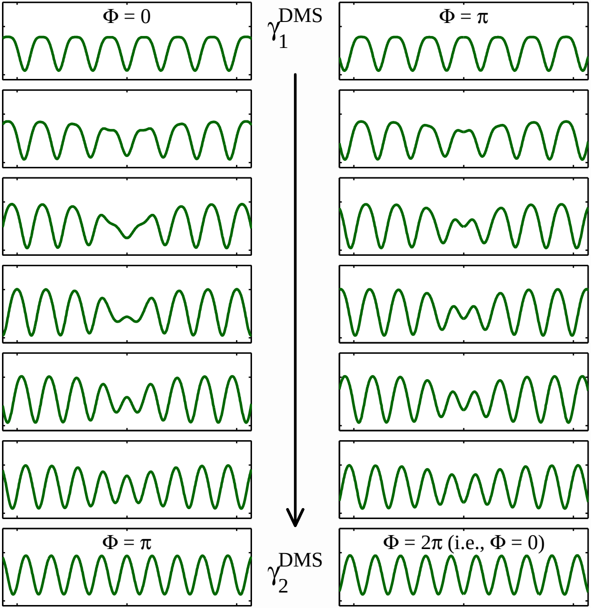

The 2 : 1 resonance: defect-mediated snaking

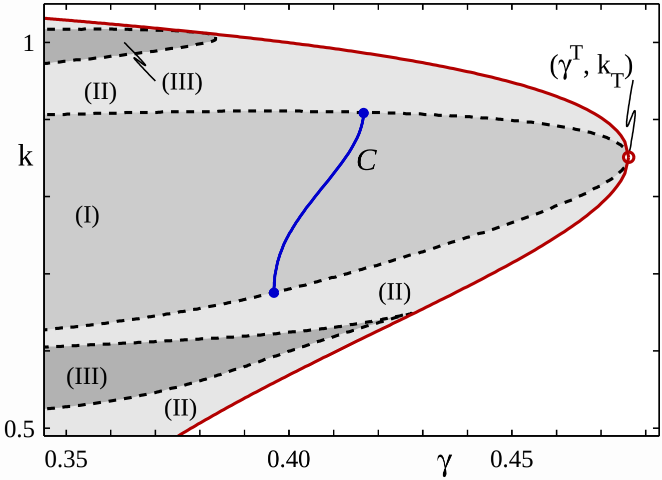

The 2 : 1 resonance: localized breathers

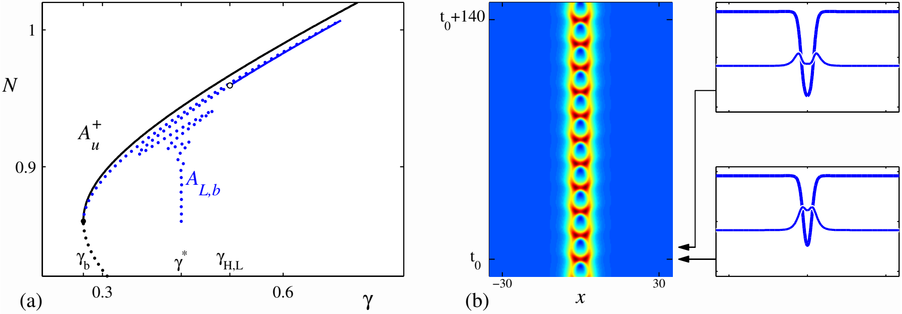

The 2 : 1 resonance: breathing front

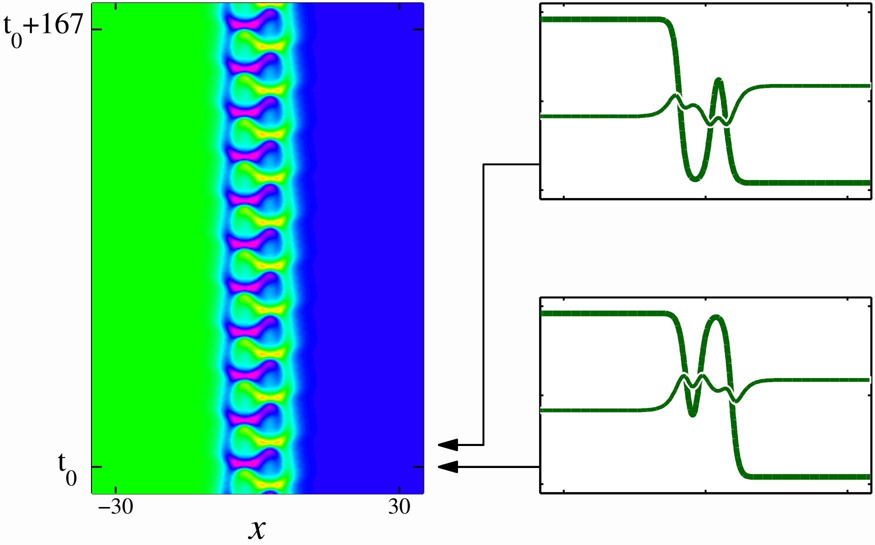

The 1 : 1 resonance

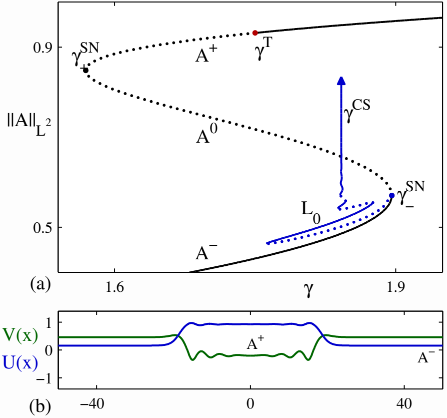

A bound pair of steady 1D fronts between $A^{\pm}$ can be found by following the weakly nonlinear LS near the lower saddle-node in γ. This branch is referred to as the L_0 branch and plotted using the L^2-norm N. The branch undergoes *collapsed snaking* to $\gamma^{CS} = 1.8419$. Temporally stable (unstable) segments are shown in solid (dotted) lines.

The 1 : 1 resonance

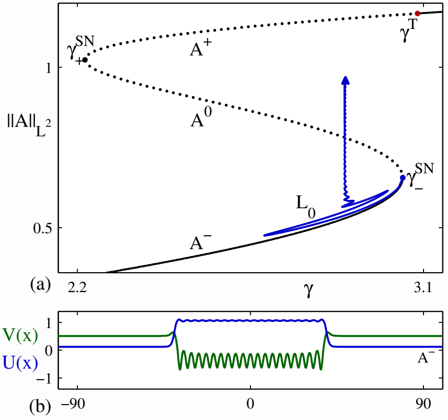

The L_0 branch at $\nu = 7$. The branch undergoes defect-mediated snaking (DMS) between $\gamma_1^{DMS} = 2.8949$ and $\gamma_2^{DMS} = 2.8970$. In the snaking region, the solution profile resembles a Turing pattern bifurcating from A^+ embedded in an A^- background [Ma et al., Physica D **239**, 1867 (2010)].

The 1 : 1 resonance

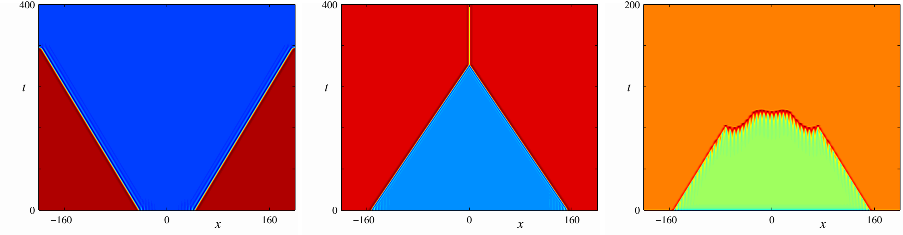

Type-I depinning at (a) $d\gamma = 0.04$; (b) $d\gamma = -0.04$; (c) $d\gamma = -0.24$

Ma and Knobloch, Chaos **22**, 033101 (2012)

The 1 : 1 resonance

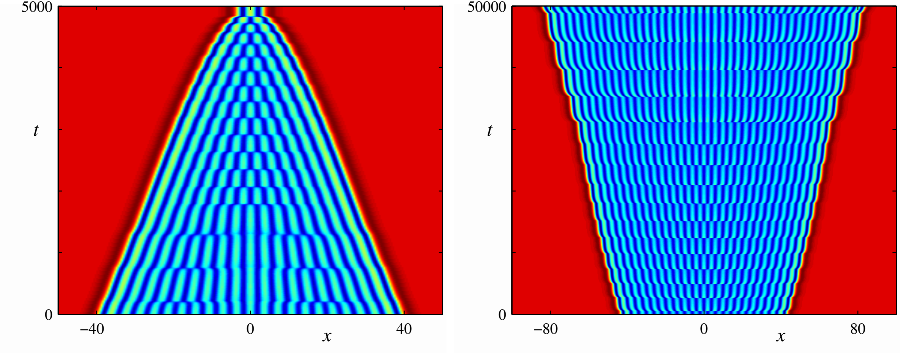

Type-II depinning at (a) $N = 45$, $d\gamma = -1 \times 10^{-3}$; (b) $N = 46$, $d\gamma = 1 \times 10^{-4}$

The 1 : 1 resonance

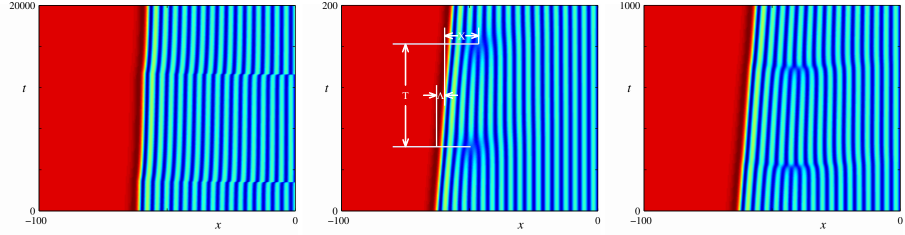

Type-II depinning: (a) Slow depinning ($d\gamma = -2 \times 10^{-5}$): phase slips take place at the center $x = 0$. (b) Fast depinning ($d\gamma = -4 \times 10^{-3}$): phase slips take place at a constant distance from the moving front. (c) Intermediate case ($d\gamma = -1 \times 10^{-3}$): phase slips gradually move towards the front.

Different mechanisms for front propagation

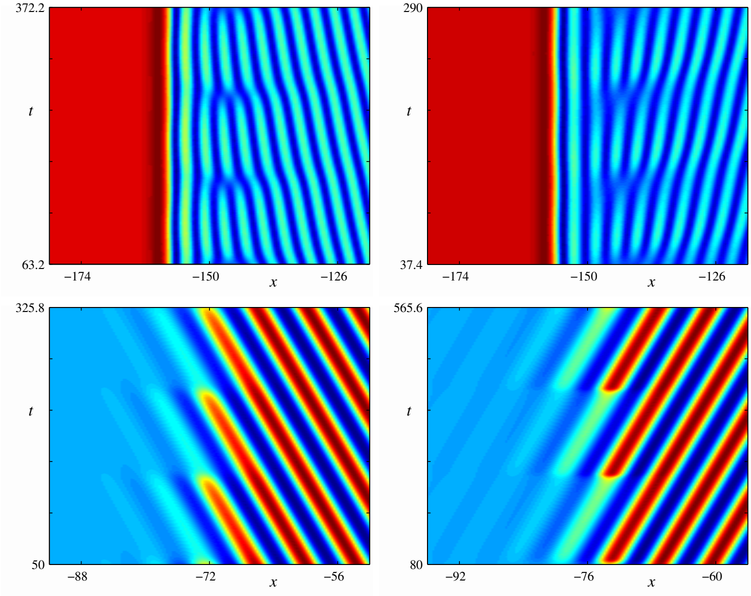

Different mechanisms for front propagation

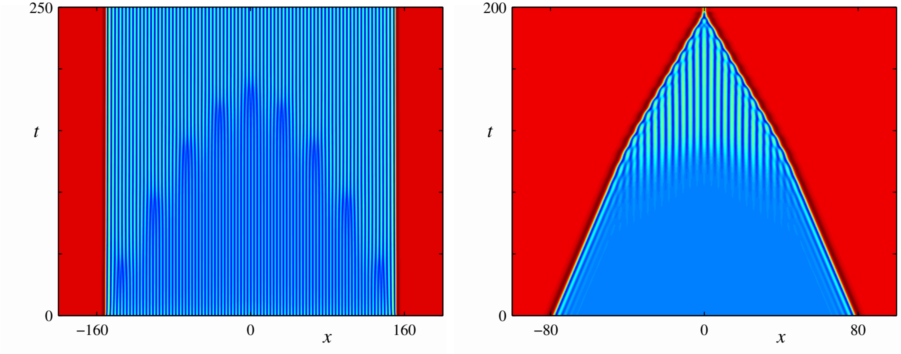

Ma and Knobloch, Chaos **22**, 033101 (2012)

Radially symmetric solutions in 2D ($\nu = 5$)

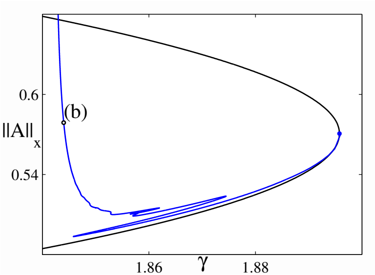

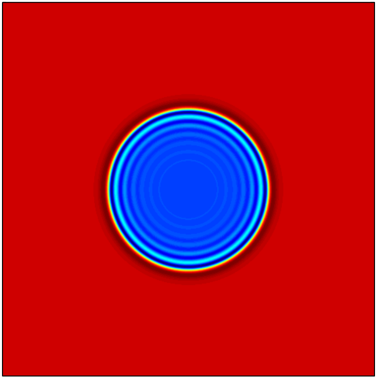

(a) The branch of 2D axisymmetric steady states followed from the lower saddle-node at $\nu = 5$. (b) A sample solution profile $V(x, y)$.

For γ near γ^{CS} and ρ large, the speed c of an *expanding* circular front with radius ρ depends on $d\gamma \equiv \gamma - \gamma^{CS}$ and the front curvature $\kappa \equiv \rho^{-1}$ as

$$c = c_\gamma d\gamma + c_\kappa \kappa, \quad \text{where} \quad c_\gamma > 0, \quad c_\kappa < 0.$$

Expanding circular fronts

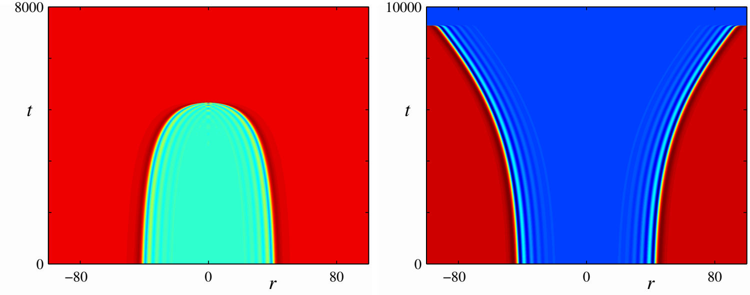

Radial space-time plots of $V(r,t)$ showing traveling circular fronts at $\gamma = 1.844$. The initial condition is the steady circular front at the same γ with radius changed by (a) $dr = -1$; (b) $dr = 1$.

2D radial pinning: localized rings ($\nu = 7$)

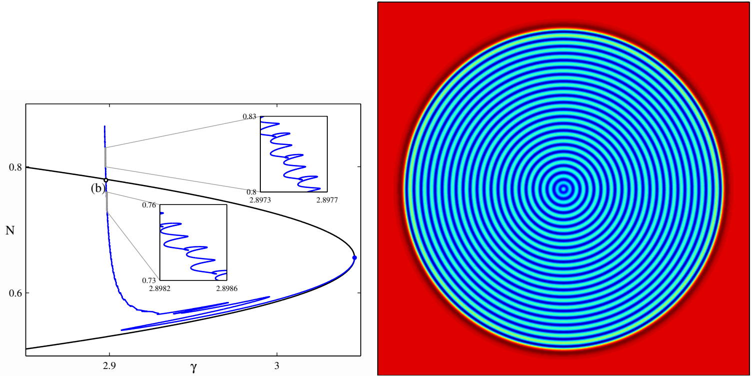

(a) The branch of 2D axisymmetric steady states followed from the lower saddle-node at $\nu = 7$. (b) A sample solution profile $V(x, y)$.

Fully 2D LS: circular localized hexagons

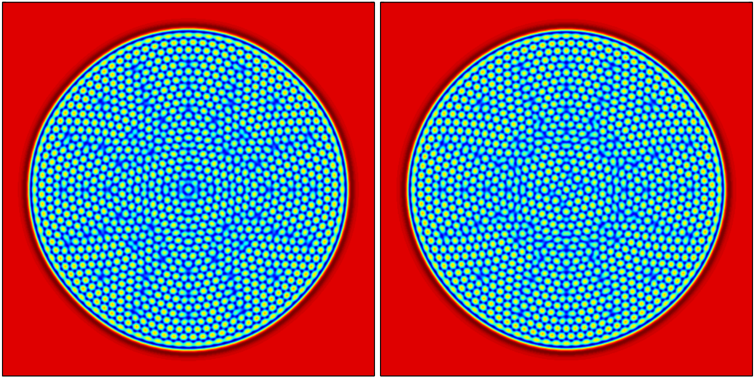

Snapshots of $V(x,y)$ at (a) $t = 300$; and (b) $t = 450$, showing circular localized hexagons. Parameters: $\nu = 7$, $\gamma = 2.8989$.

Planar 2D LS: planar localized hexagons

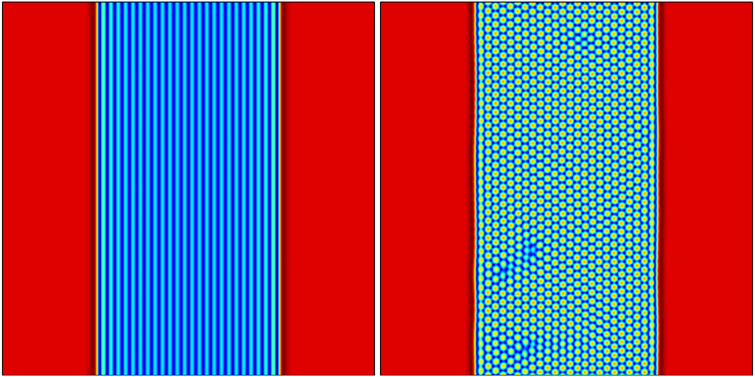

Snapshot of $V(x, y)$ at (b) $t = 100$, starting from a localized stripe pattern at (a) $t = 0$. Parameters: $\nu = 7$, $\gamma = 2.8972$.

2D depinning: shrinking planar localized hexagons

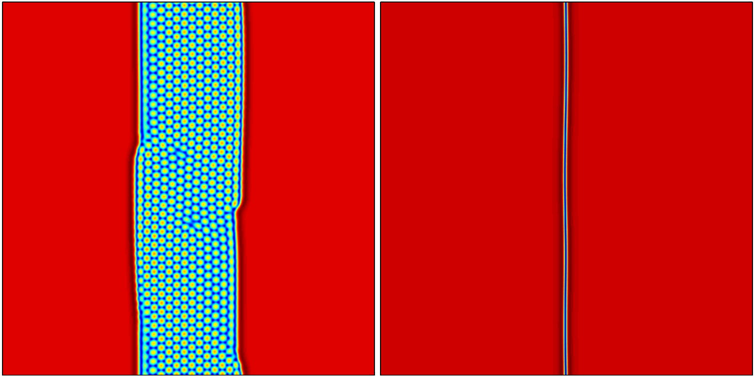

Snapshots of $V(x,y)$ at (a) $t = 400$ and (b) $t = 1000$ showing the shrinkage of planar localized hexagons. Parameters: $\nu = 7$, $\gamma = 2.8955$.
Video:

2D depinning: expanding planar localized hexagons

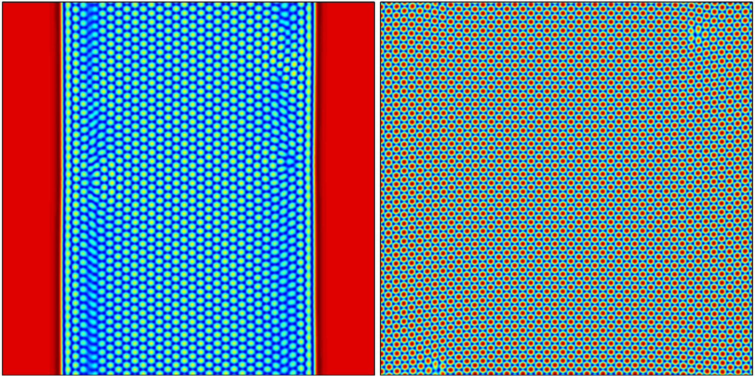

Snapshots of $V(x, y)$ at (a) $t = 1500$ and (b) $t = 4000$ showing the expansion of planar localized hexagons. Parameters: $\nu = 7$, $\gamma = 2.899$.
Video:

2D depinning: pinned planar localized hexagons?

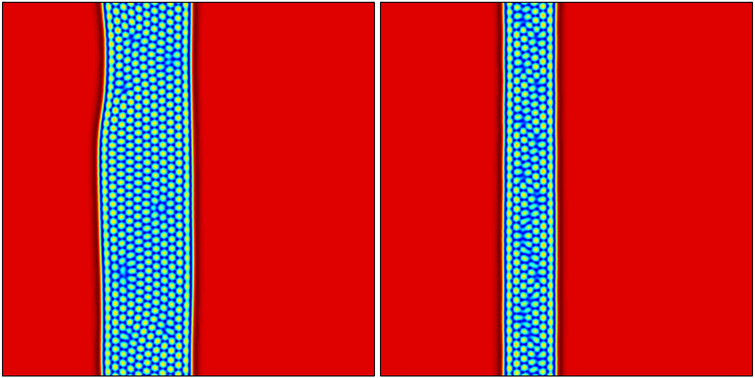

Snapshots of $V(x, y)$ at (a) $t = 10000$ and (b) $t = 30000$ showing the competition between shrinkage and expansion of planar localized hexagons. Parameters: $\nu = 7$, $\gamma = 2.8972$. Video:

Comparison of FCGL results and a nonautonomous PDE

A PDE with time-periodic forcing:

$$U_t = (\mu + i\omega)U + (\alpha + i\beta)U_{xx} + C|U|^2U + i\mathrm{Re}(U)\,F\cos(2t) \qquad (103)$$

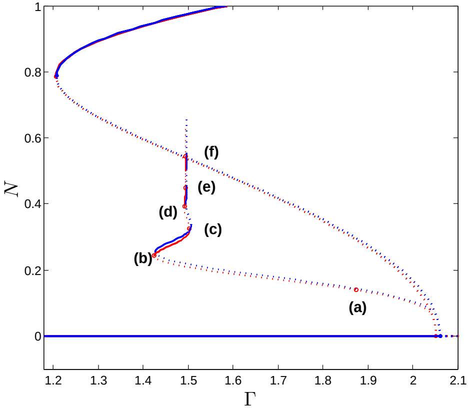

Alnahdi et al, SIADS **13**, 1311-1327 (2014). Blue: FCGL. Red: Eq. (103)

Comparison of FCGL results and a nonautonomous PDE

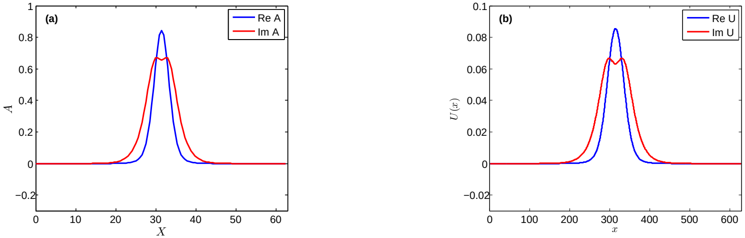

Left: FCGL. Right: Eq. (103)

Alnahdi et al, SIADS **13**, 1311-1327 (2014). Left: FCGL. Right: Eq. (103)

Summary of the first set of lectures

I have described

- Spatially localized steady states of the SH equation
- Homoclinic snaking and associated snakes-and-ladders structure
- Interpreted the behavior in terms of pinning
- Discussed stability and wavelength selection
- Isola structure for (typical) multipulse states
- Termination of homoclinic snaking in finite domains
- Depinning and the calculation of the invasion speed

This behavior appears to be generic in systems with a heteroclinic cycle between a homogeneous and structured state. It requires

- Bistability
- Spatial reversibility
- High enough order

It does not require variational structure, or Hamiltonian structure in space

Convectons

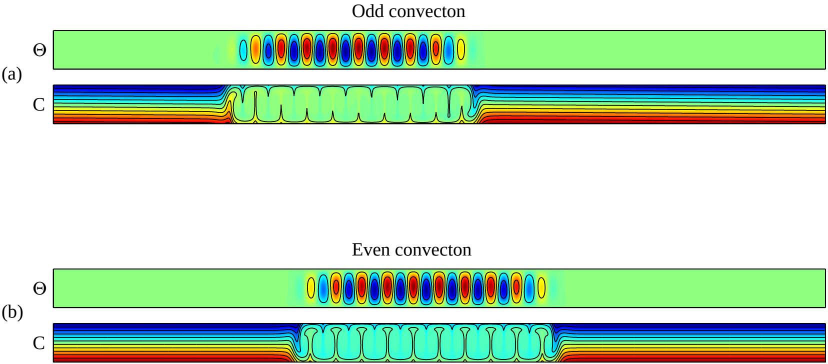

Convectons in binary fluid convection (Batiste et al., J. Fluid Mech. **560**, 149, 2006)

Binary fluid convection

- Binary mixtures with negative separation ratio S.
- Two miscible components with concentration C_1 of the heavier component:

$$\rho = \rho_0(1 - \alpha(T - T_0) + \beta(C_1 - \overline{C}_1)), \qquad \alpha > 0, \quad \beta > 0.$$

- The heavier component migrates towards the hotter boundary:

$$\mathbf{j_1} = -\rho_0 D(S_{Soret}\overline{C}_1(1 - \overline{C}_1)\nabla T + \nabla C_1).$$

- The resulting concentration gradient is stabilizing and competes with the destabilizing thermal gradient that produces it.
- As a result the conduction state loses stability via a Hopf bifurcation and the first state that is observed is time-dependent: dispersive chaos.

Binary fluid convection: Equations and properties

$$
\begin{aligned}
\mathbf{u}_t + (\mathbf{u}\cdot\nabla)\mathbf{u} &= -\nabla P + PrR[(1+S)\theta - S\eta]\hat{\mathbf{z}} + Pr\nabla^2\mathbf{u},\\
\theta_t + (\mathbf{u}\cdot\nabla)\theta &= w + \nabla^2\theta,\\
\eta_t + (\mathbf{u}\cdot\nabla)\eta &= \tau\nabla^2\eta + \nabla^2\theta,
\end{aligned}
$$

where $\mathbf{u} = (u, w)$ in (x, z) coordinates. The Prandtl number Pr, the Lewis number τ, the Rayleigh number R and the separation ratio S are defined by

$$
Pr = \frac{\nu}{\kappa}, \quad \tau = \frac{D}{\kappa}, \quad R = \frac{g|\rho_T|\Delta T \ell^3}{\nu\kappa}, \quad S = \overline{C}_1(1-\overline{C}_1)S_{Soret}\frac{\rho_C}{|\rho_T|}.
$$

The boundary conditions are

$$
\begin{aligned}
&\text{at} \quad z = 1: \quad u = w = T = \eta_z = 0,\\
&\text{at} \quad z = 0: \quad u = w = T - 1 = \eta_z = 0,
\end{aligned}
$$

with either periodic boundary conditions (PBC) with period Γ in x or Neumann boundary conditions (NBC) or no-slip sidewalls (ICCBC) at $x = \pm\Gamma/2$. Thus $\theta \equiv T - 1 + z = 0$ at $z = 0, 1$.

Even and odd convectons

These equations have the symmetries

$R_1 : (u(x,z), w(x,z), \theta(x,z), \eta(x,z)) \to (-u(-x,z), w(-x,z), \theta(-x,z),$
$\eta(-x,z))$

$R_2 : (u(x,z), w(x,z), \theta(x,z), \eta(x,z)) \to (u(x,1-z), -w(x,1-z),$
$-\theta(x,1-z), -\eta(x,1-z))$.

Theory guarantees the existence of solutions with R_1 symmetry (even parity solutions) satisfying

$$(u(x,z), w(x,z), \theta(x,z), \eta(x,z)) = \\ (-u(-x,z), w(-x,z), \theta(-x,z), \eta(-x,z)),$$

relative to a suitable origin in x, and solutions with $R_1 \circ R_2$ symmetry (i.e., point symmetry) satisfying

$$(u(x,z), w(x,z), \theta(x,z), \eta(x,z)) = \\ -(u(-x,1-z), w(-x,1-z), \theta(-x,1-z), \eta(-x,1-z)).$$

Point-symmetric solutions have odd parity in the midplane $z = 1/2$.

Formation of a convecton

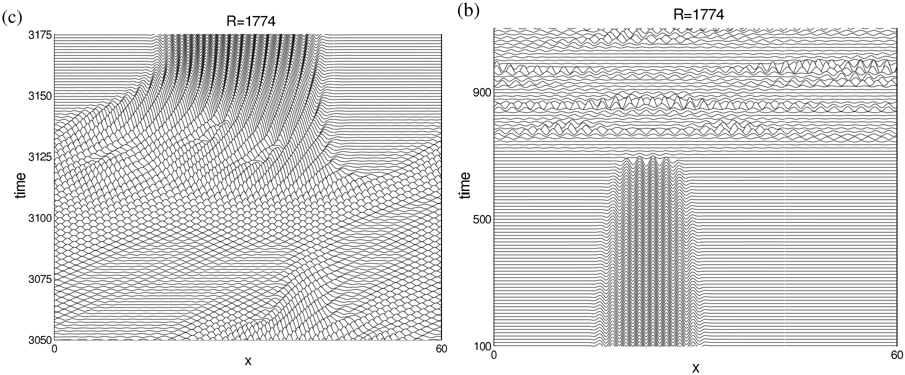

Batiste et al., J. Fluid Mech. **560**, 149 (2006)

Relaxation oscillations at $R = 1774$

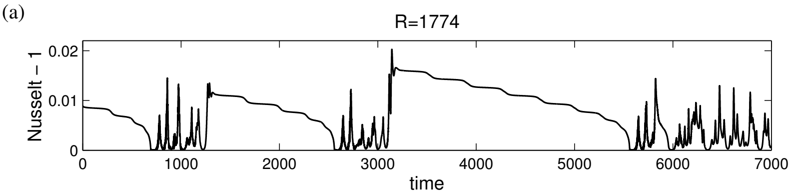

Batiste et al., J. Fluid Mech. **560**, 149 (2006)

Formation of a convecton

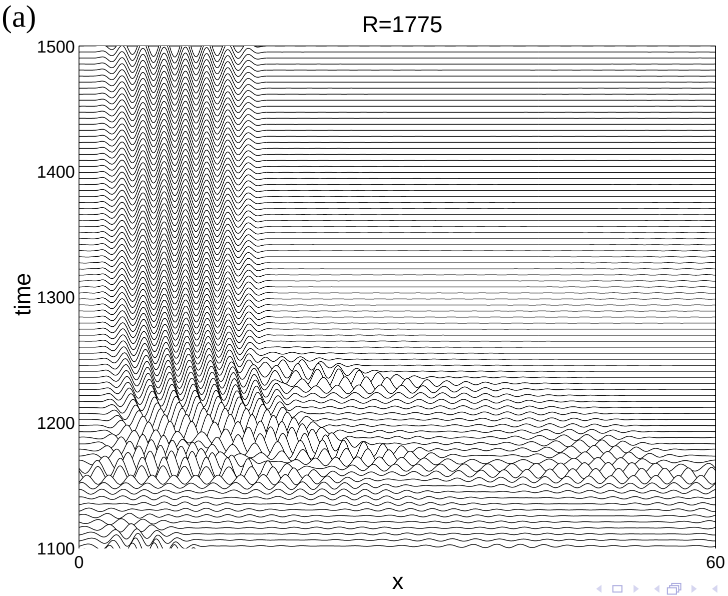

Bifurcation diagram

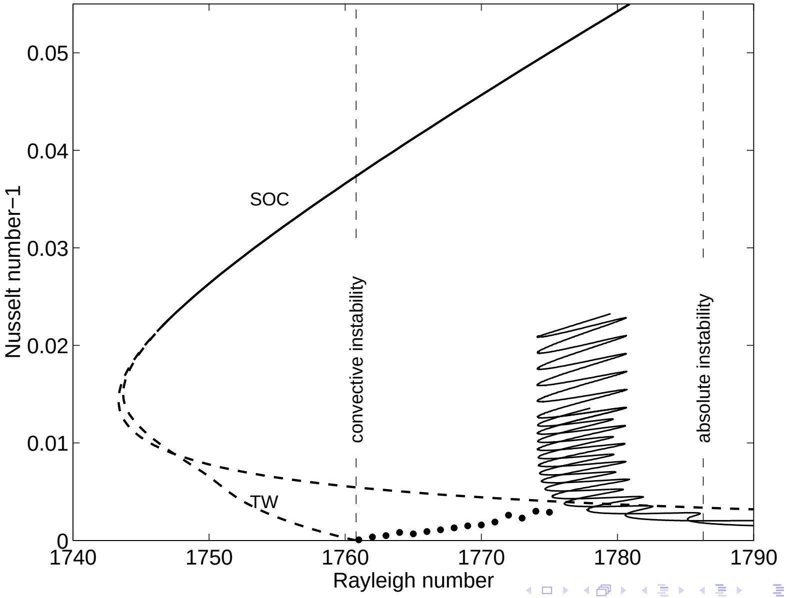

Odd and even convectons

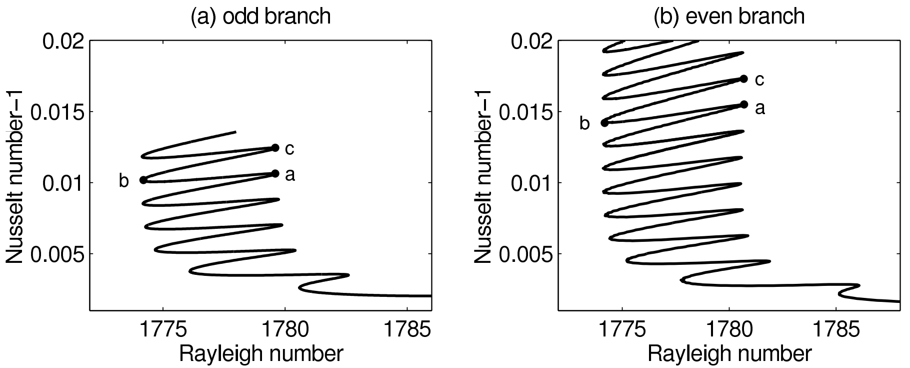

Batiste et al., J. Fluid Mech. **560**, 149 (2006)

Odd and even convectons

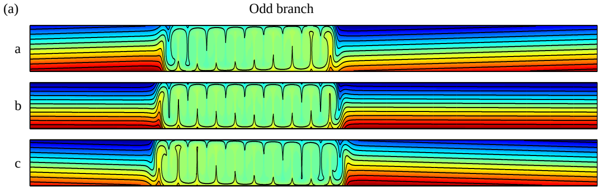

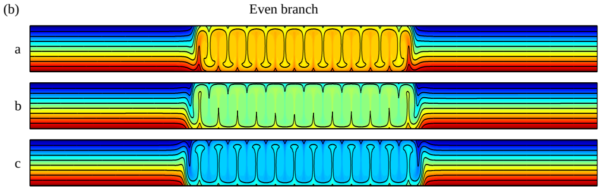

Stability of the convectons

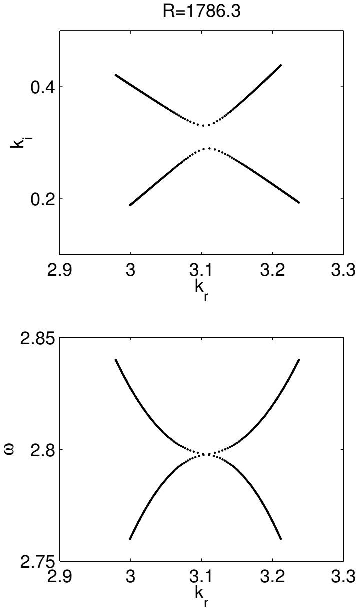

Experiments: $S = -0.20$, $\sigma = 5.97$, $\tau = 0.0085$

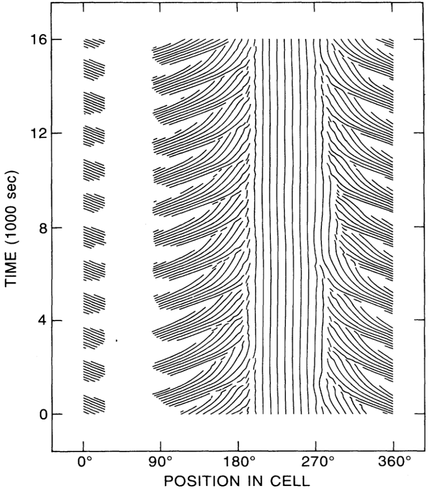

FIG. 1. Coexisting state of TW bursts and steady rolls at ϵ=0.012 12. In this "phase plot," solid curves show the space-time paths of equal-phase points, which correspond to the boundaries of convective rolls in fully developed convection. In this run, persistent steady rolls (SR's) fill the region between angular locations 190° and 280°. Outside the SR region, TW bursts ap-

Experiments: $S = -0.20$, $\sigma = 5.97$, $\tau = 0.0085$

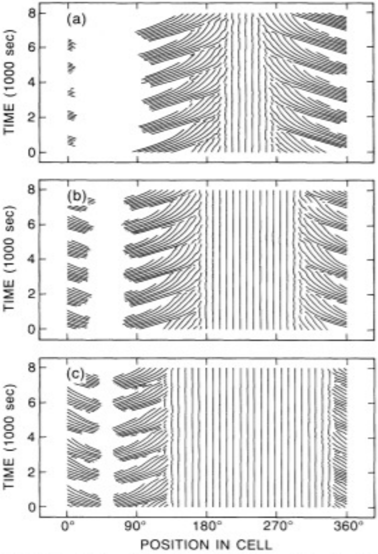

FIG. 2. Evolution of the dynamical state of Fig. 1 with Rayleigh number. (a) ϵ=0.011 31; (b) ϵ=0.012 93; (c) ϵ=0.015 35. With increasing ϵ, the TW region shrinks.

Snaking in periodic and finite domains: binary fluid convection with $\Gamma = 14$: $S = -0.1$, $\sigma = 7$, $\tau = 0.01$

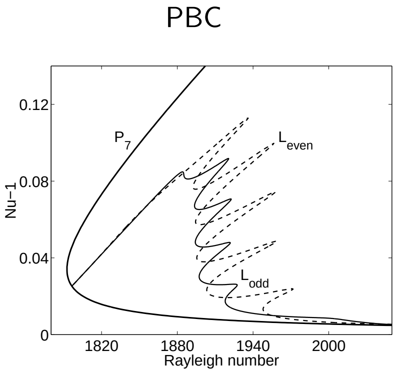

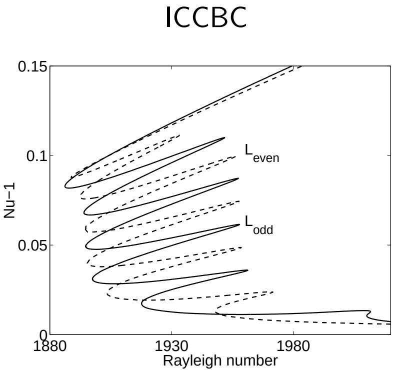

- Convecton branches terminate together on P_7
- Convecton branches turn continuously into mixed modes

Convectons with PBC: $\Gamma = 14$

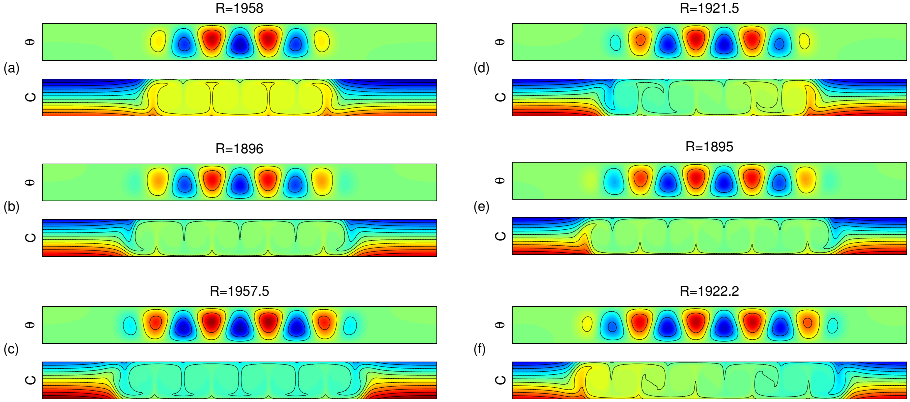

even parity

odd parity

Convectons and holes with PBC: $\Gamma = 14$

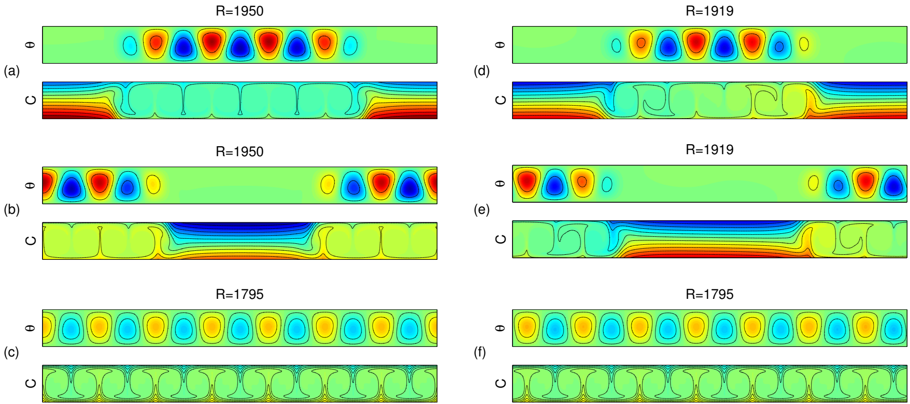

even parity

odd parity

Mixed modes with PBC: $\Gamma = 14$

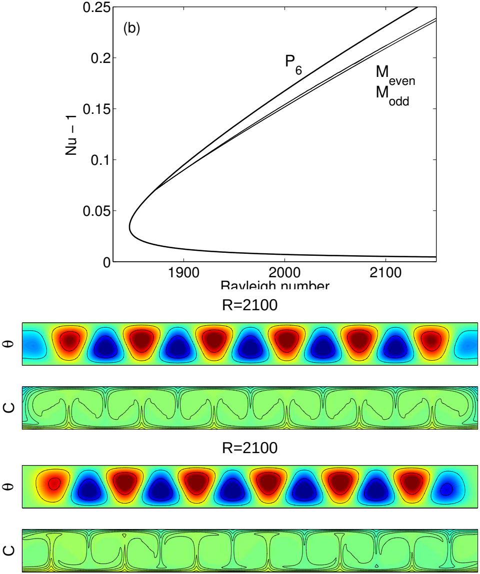

Even parity states with NBC: $\Gamma = 14$

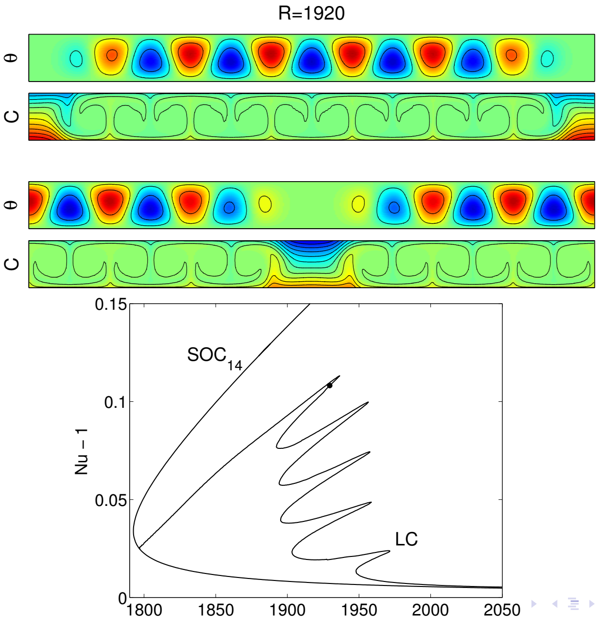

Wall states with NBC: $\Gamma = 14$

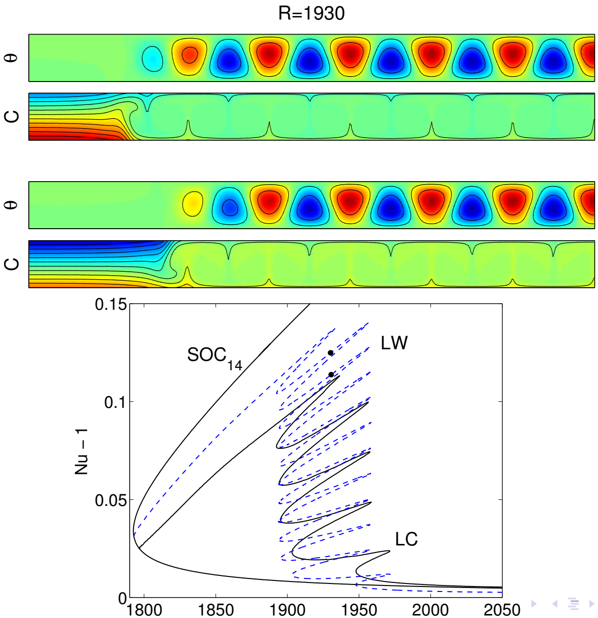

Odd parity convectons with NBC: $\Gamma = 14$

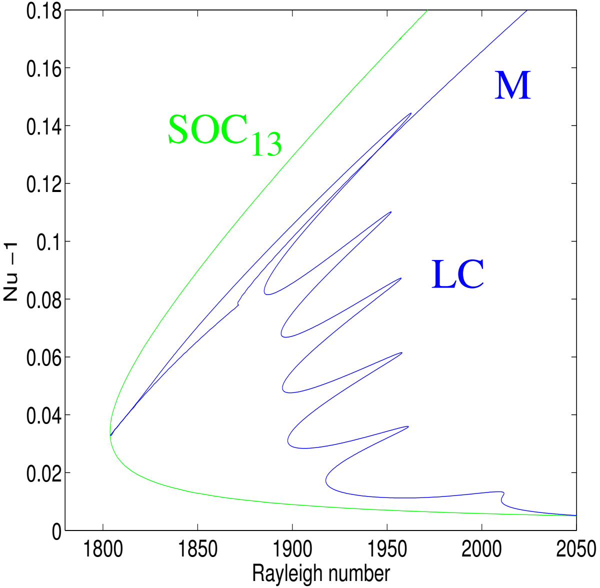

Odd parity holes with NBC: $\Gamma = 14$

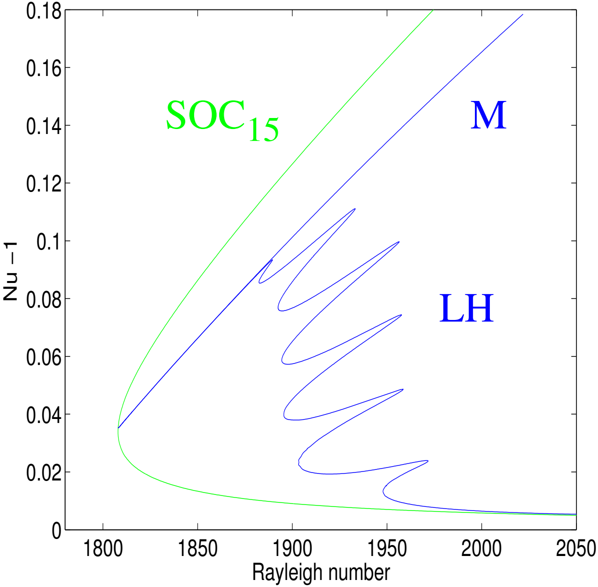

Convectons and holes with NBC: $\Gamma = 14$

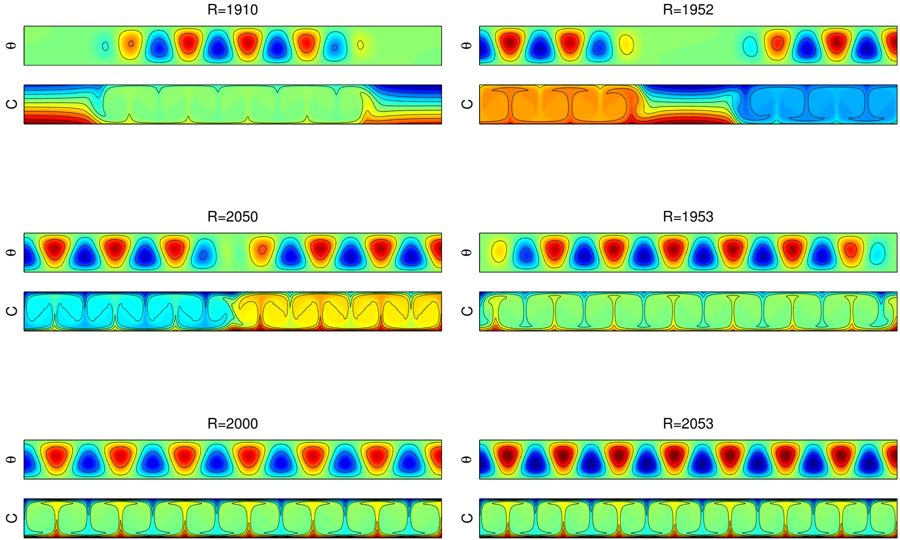

odd parity states: SOC_{13}

odd parity states: SOC_{15}

Even parity convectons with ICCBC: $\Gamma = 14$

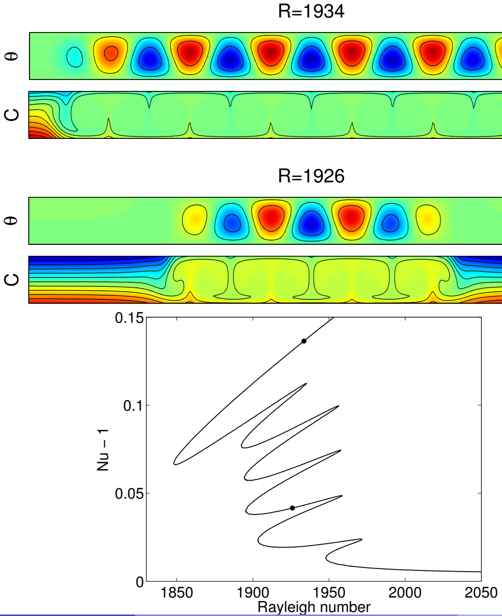

Odd parity convectons with ICCBC: $\Gamma = 14$

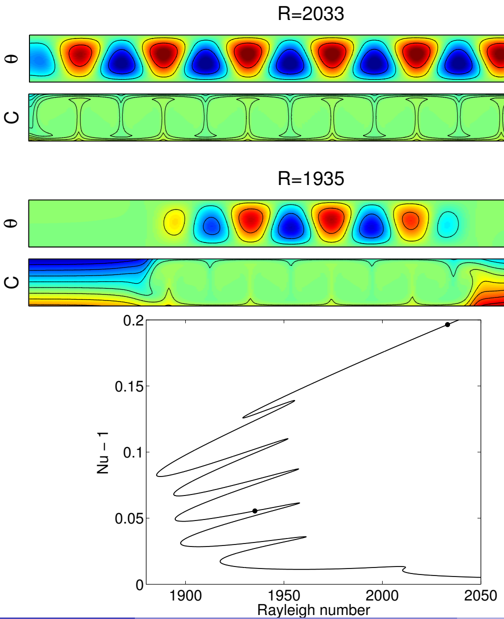

Wall states with ICCBC: $\Gamma = 14$

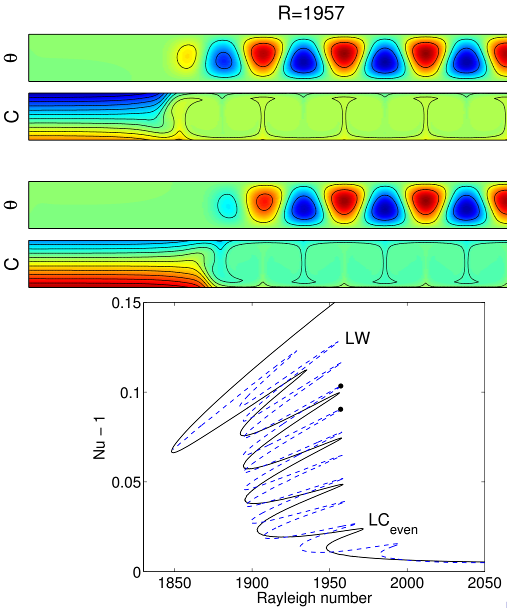

Reflection-symmetric two-pulse states with NBC: $\Gamma = 14$

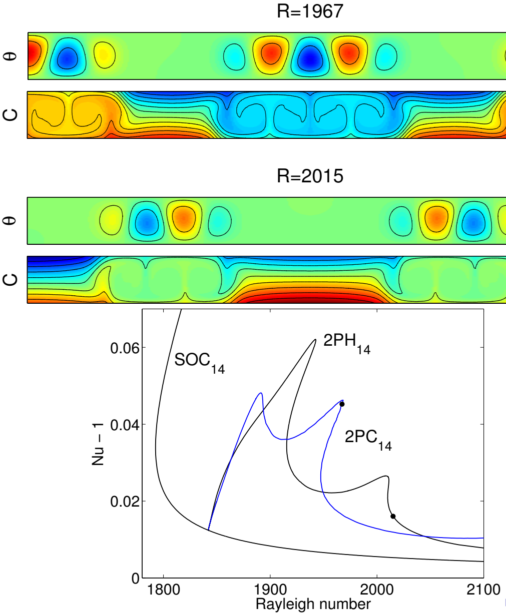

Odd parity two-pulse states with NBC: $\Gamma = 14$

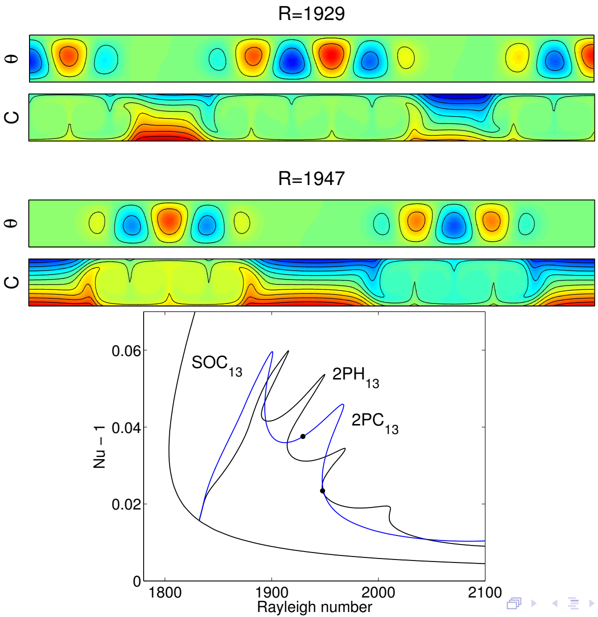

Odd parity two-pulse states with NBC: $\Gamma = 14$

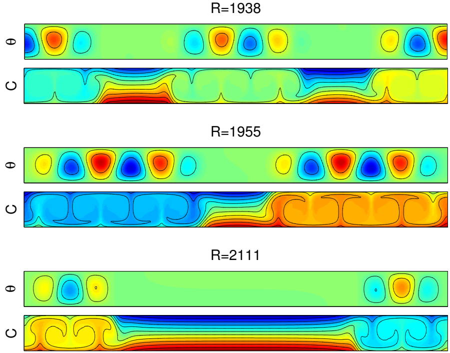

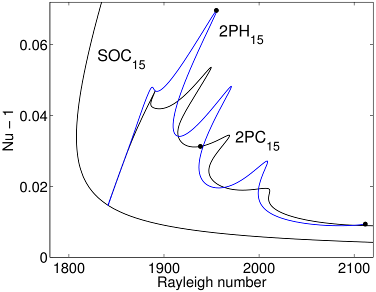

Point-symmetric two-pulse states

Mercader et al., J. Fluid Mech. **667**, 586-606 (2011)

Bound states with ICCBC: $\Gamma = 14$

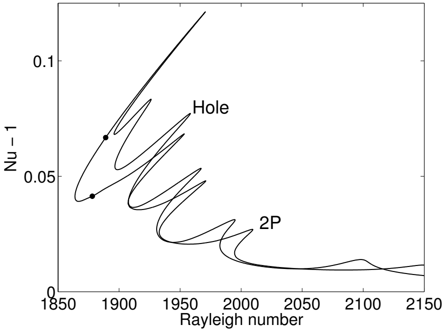

point-symmetric two-pulse states

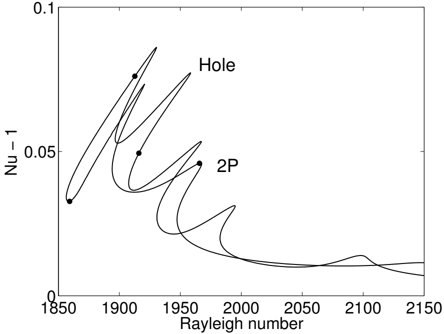

even two-pulse states

Mercader et al., J. Fluid Mech. **667**, 586-606 (2011)

Bound states with ICCBC: $\Gamma = 14$

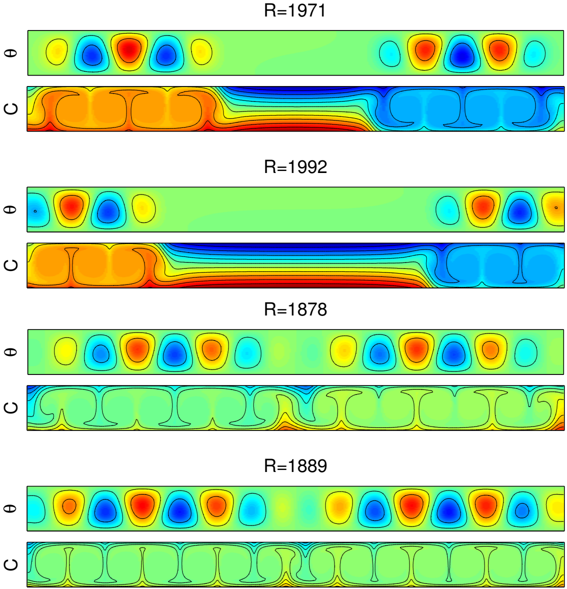

Bound states with ICCBC: $\Gamma = 14$

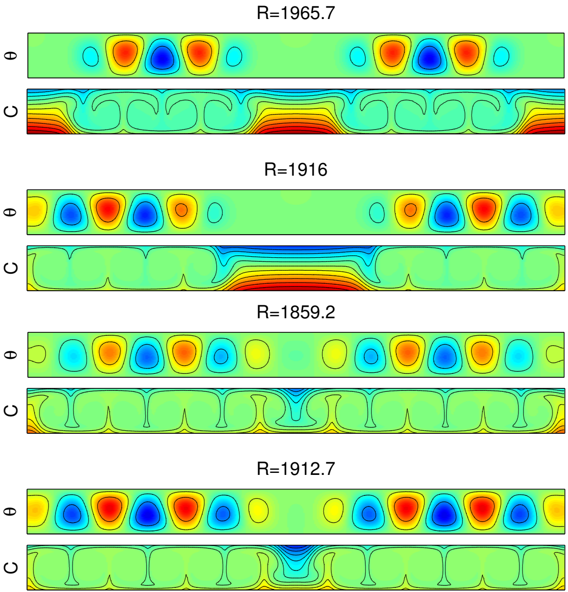

The preceding construction accounts for the states discovered by time-stepping natural doubly diffusive convection:

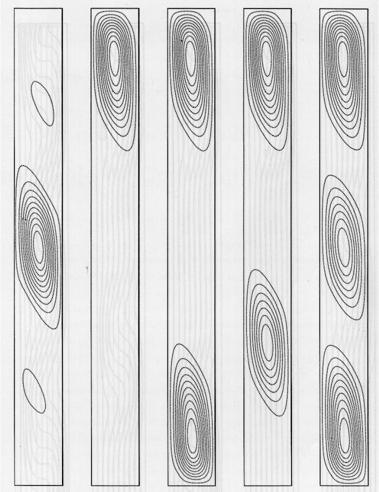

Ghorayeb & Mojtabi, Phys. Fluids **9**, 2339 (1997); Ghorayeb, PhD Thesis, Toulouse, 1997

Homotopic continuation: $\Gamma = 14$

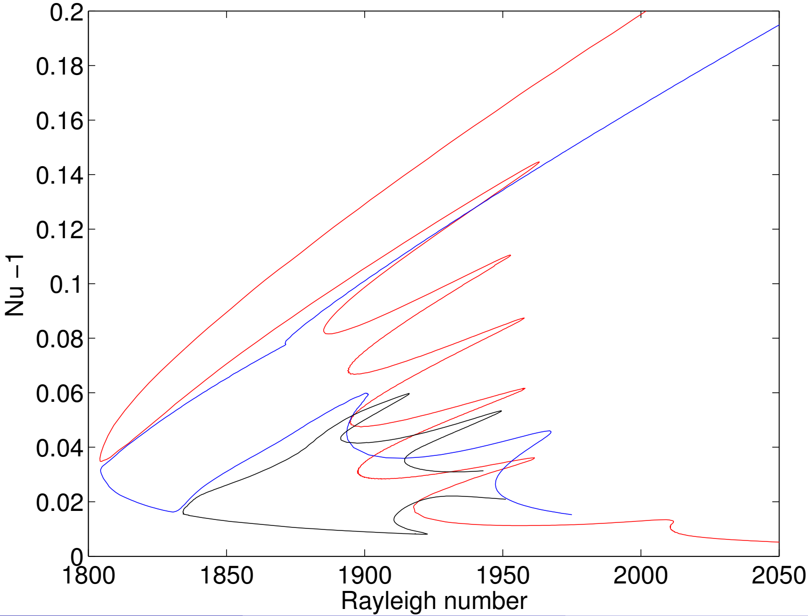

Aspect ratio dependence with PBC

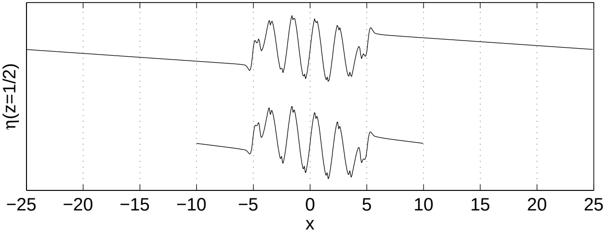

With NBC an odd parity convecton and its image form an even parity bound state. Thus in closed containers the pinning regions for odd and even states have the same width.

Depining: $\Gamma = 60$

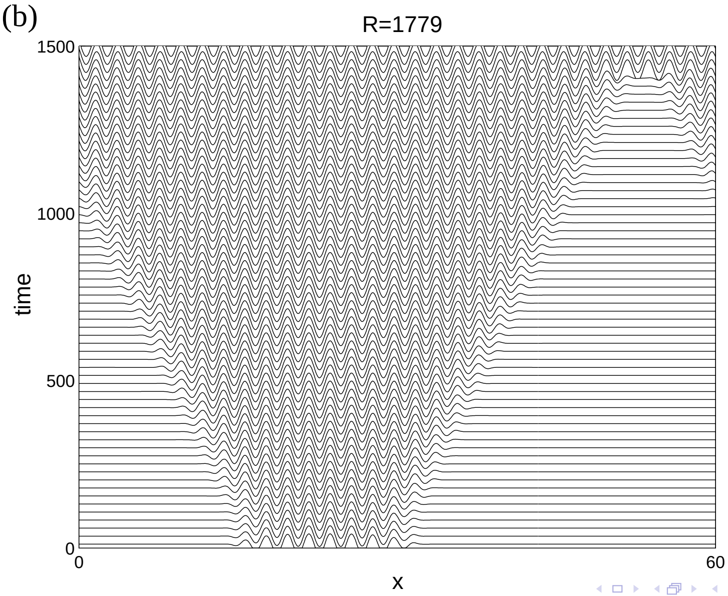

Convectons in three dimensions

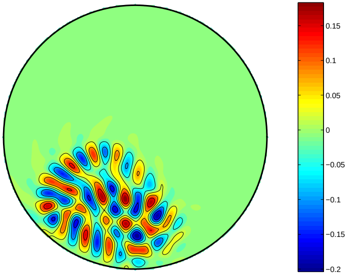

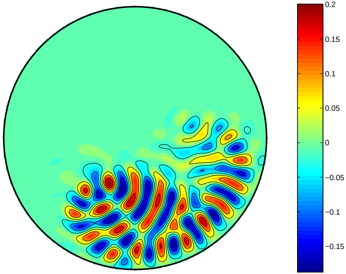

Convecton-like structures in 3D: Mercader et al., Phys. Rev. E **77**, 036313 (2008)

Colliding convectons: Swift-Hohenberg model

Case 1: $f(u) = b_2 u^2 - u^3$ (SH23)

The equation has the symmetries

- $R_1 : x \to -x, \qquad u \to u$
- $T : x \to x + d, \qquad u \to u$

As a result there are two types of localized solutions, those fixed by R_1 (even states L_0, L_π) as well as asymmetric "rung" states with no symmetry.

Case 2: $f(u) = b_3 u^3 - u^5$ (SH35)

The equation has the symmetries

- $R_1 : x \to -x, \qquad u \to u$
- $R_2 : x \to x, \qquad u \to -u$
- $T : x \to x + d, \qquad u \to u$

As a result there are three types of localized solutions, those fixed by R_1 (even states L_0, L_π) and those fixed by $R_1 \circ R_2$ (odd states $L_{\pi/2}$, $L_{3\pi/2}$). In addition, there are also asymmetric "rung" states.

Comparison of SH23 and SH35: symmetries matter

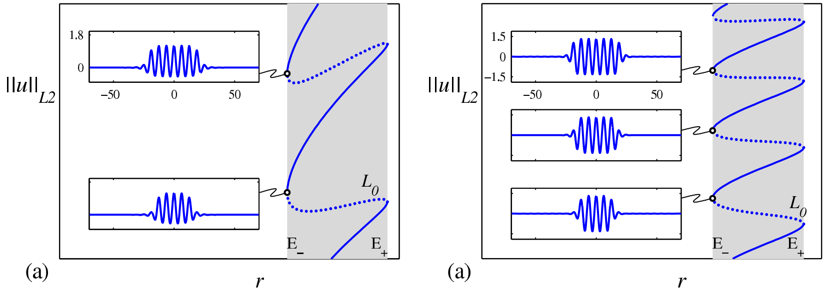

Growth along the L_0 branches in (a) SH23 and (b) SH35

Burke and Knobloch, Chaos **17**, 037102 (2007).

From SH35 to SH23: SH35 with broken R_2 symmetry

Consider the variational equation

$$u_t = ru - \left(1 + \partial_x^2\right)^2 u + b_3 u^3 - u^5 + \epsilon u^2$$

When $\epsilon = 0$ the equation has the symmetries

- $R_1 : x \to -x, \qquad u \to u$
- $R_2 : x \to x, \qquad u \to -u$
- $T : x \to x + d, \qquad u \to u$

When $\epsilon \neq 0$ the equation only has the symmetries R_1 and T and the only symmetric states are L_0, L_π. The odd states become states with no symmetry and reconnect with the rung states forming two types of branches: S branches and Z branches.

From SH35 to SH23: variational case with $\epsilon = 0.03$

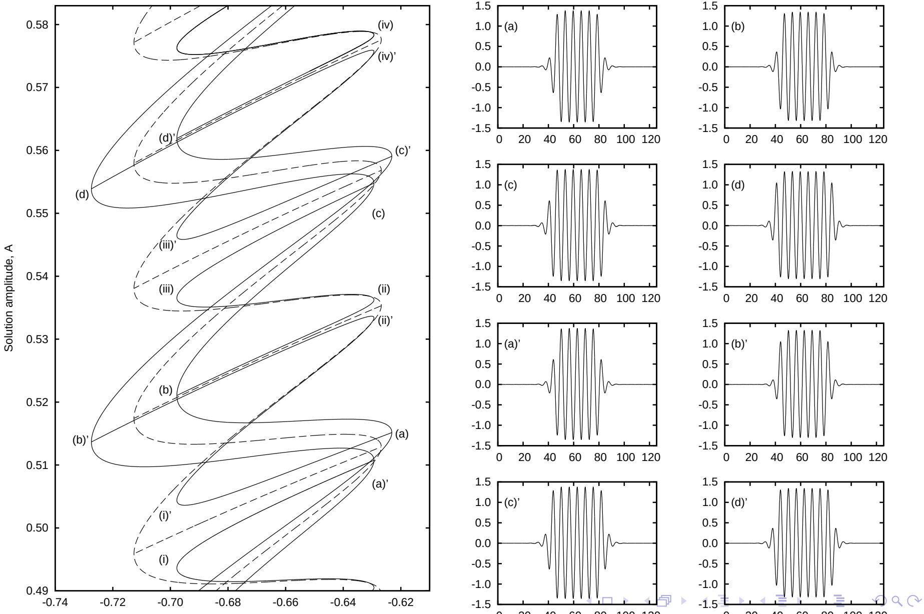

From SH35 to SH23: variational case with $\epsilon = 0.03$

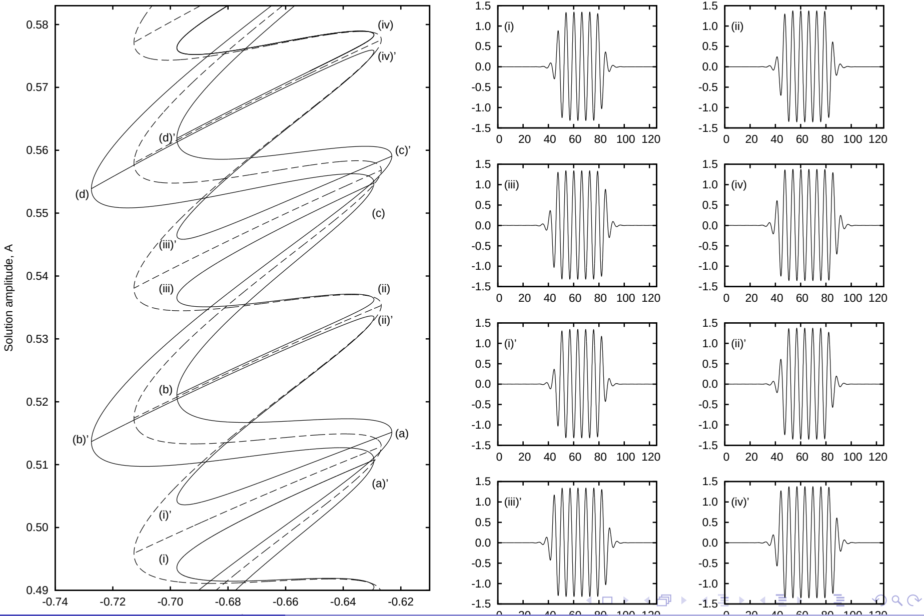

The Swift-Hohenberg equation: the variational case

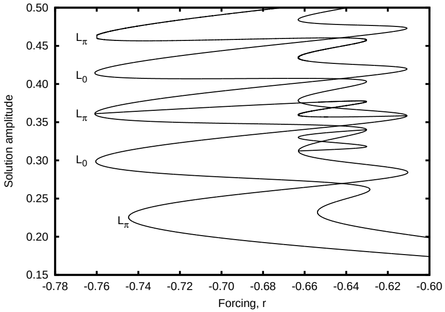

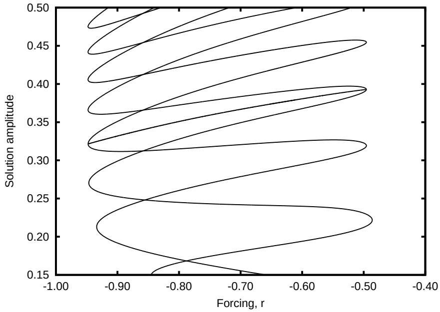

$\epsilon = 0.1$ $\epsilon = 0.5$

Both symmetric and asymmetric states are stationary

The Swift-Hohenberg equation: the nonvariational case

$$u_t = ru - \left(1+\partial_x^2\right)^2 u + 2u^3 - u^5 + \epsilon(\partial_x u)^2$$

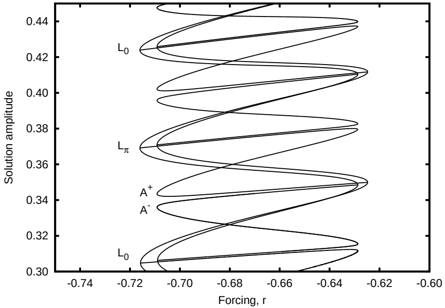

$\epsilon = 0.01$

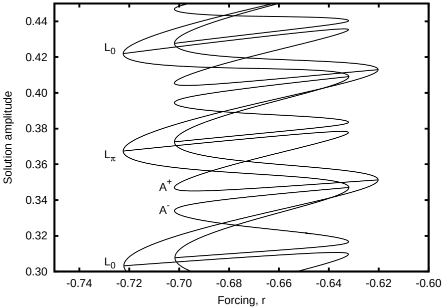

$\epsilon = 0.03$

Asymmetric states are no longer stationary

The Swift-Hohenberg equation: the nonvariational case

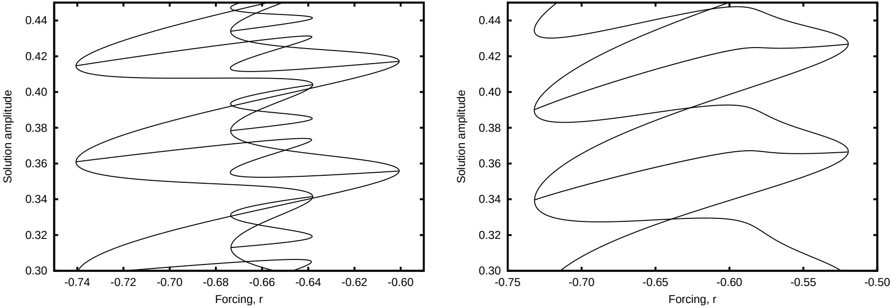

$\epsilon = 0.1$ $\qquad\qquad$ $\epsilon = 0.3$

Asymmetric states are no longer stationary

The S and Z branches for $\epsilon = 0.01$

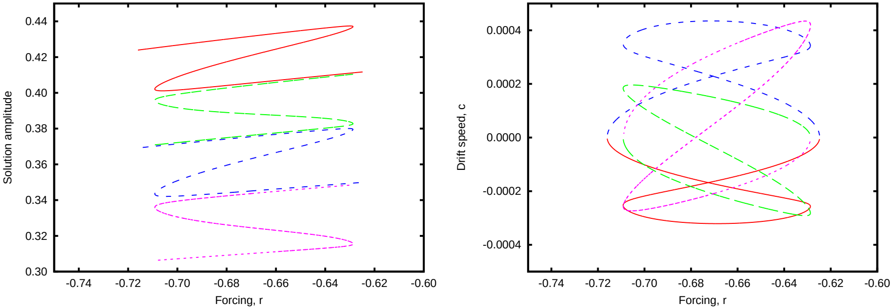

Asymmetric states are no longer stationary

Collision of like pulses for $r = -0.65$, $\epsilon = 0.1$

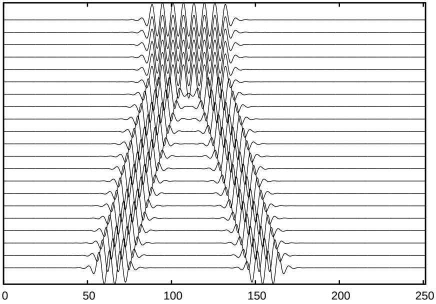

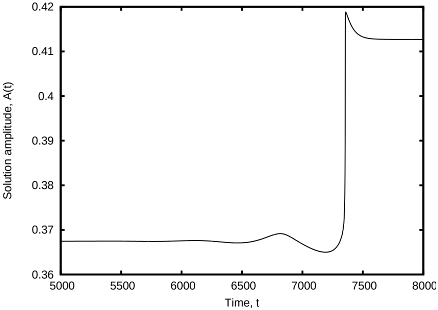

Houghton and Knobloch, PRE **84**, 016204 (2011)

Collision of unlike pulses: $\epsilon = 0.1$, $r = -0.65$

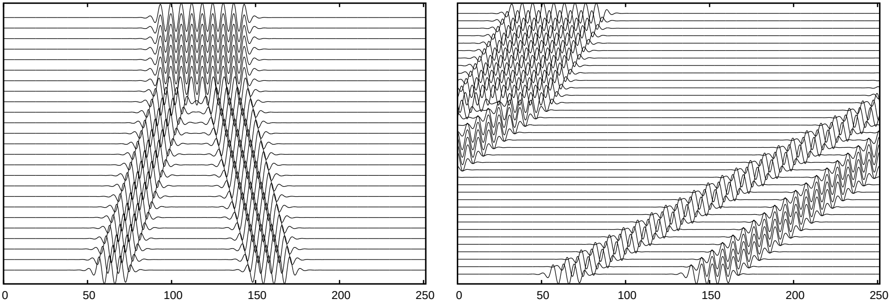

repulsion attraction

Houghton and Knobloch, PRE **84**, 016204 (2011)

Collision of unlike pulses: $\epsilon = 0.1$, $r = -0.65$

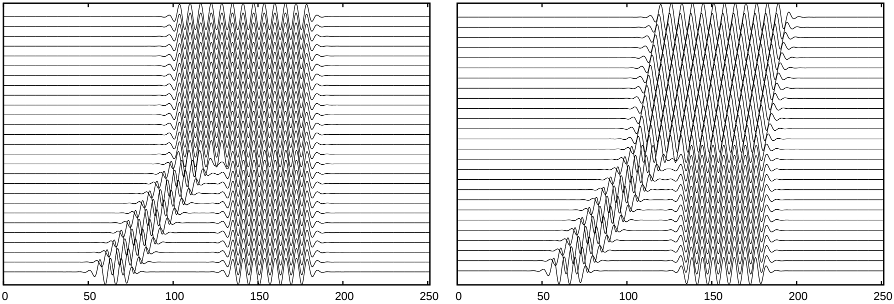

attraction

repulsion

Houghton and Knobloch, PRE **84**, 016204 (2011)

Binary fluid convection – again

$$\begin{aligned}
\mathbf{u}_t + (\mathbf{u}\cdot\nabla)\mathbf{u} &= -\nabla P + \sigma R[(1+S)\theta - S\eta]\hat{\mathbf{z}} + \sigma\nabla^2\mathbf{u},\\
\theta_t + (\mathbf{u}\cdot\nabla)\theta &= w + \nabla^2\theta,\\
\eta_t + (\mathbf{u}\cdot\nabla)\eta &= \tau\nabla^2\eta + \nabla^2\theta,
\end{aligned}$$

where $\mathbf{u} = (u, w)$ in (x, z) coordinates. The Prandtl number σ, the Lewis number τ, the Rayleigh number R and the separation ratio S are

$$\sigma = \frac{\nu}{\kappa}, \quad \tau = \frac{D}{\kappa}, \quad R = \frac{g|\rho_T|\Delta T\ell^3}{\nu\kappa}, \quad S = \overline{C}_1(1-\overline{C}_1)S_{Soret}\frac{\rho_C}{|\rho_T|}.$$

The boundary conditions are

$$\begin{aligned}
&\text{at} \quad z = 1: \quad u = w = (1-\beta)\theta_z + \beta\theta = \eta_z = 0,\\
&\text{at} \quad z = 0: \quad u = w = \theta = \eta_z = 0.
\end{aligned}$$

When $\beta = 1$ the above system has the symmetries R_1 and R_2. When $\beta < 1$ (heat loss from the upper boundary) the symmetry R_2 is lost and only R_1 remains. The change in symmetry is completely analogous to the breaking of the $u \to -u$ symmetry in SH35.

Binary fluid convection with heat loss

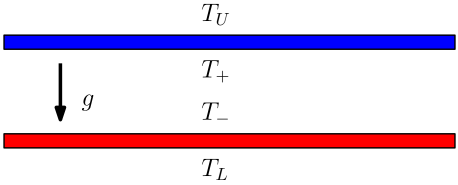

We consider two-dimensional Boussinesq convection between boundaries responsible for the boundary conditions

$$\begin{aligned} \frac{dT_-}{dz} &= -\frac{B_-}{d}(T_L - T_-) \quad \text{at} \quad z = 0, \\ \frac{dT_+}{dz} &= -\frac{B_+}{d}(T_+ - T_U) \quad \text{at} \quad z = d, \end{aligned}$$

where d is the layer depth, and define

$$R = \frac{|\rho_T| g d^3}{\kappa\nu}\Delta T^c, \quad \Delta T^c = (T_L - T_U)\frac{B_+ B_-}{B_+ B_- + B_+ + B_-} \tag{104}$$

so that R is independent of the dynamics in the cell.

Binary fluid convection with $\beta = 1$

Newton's law of cooling:

$$(1-\beta)\theta_z + \beta\theta = 0 \quad \text{on} \quad z = 1, \qquad \theta = 0 \quad \text{on} \quad z = 0.$$

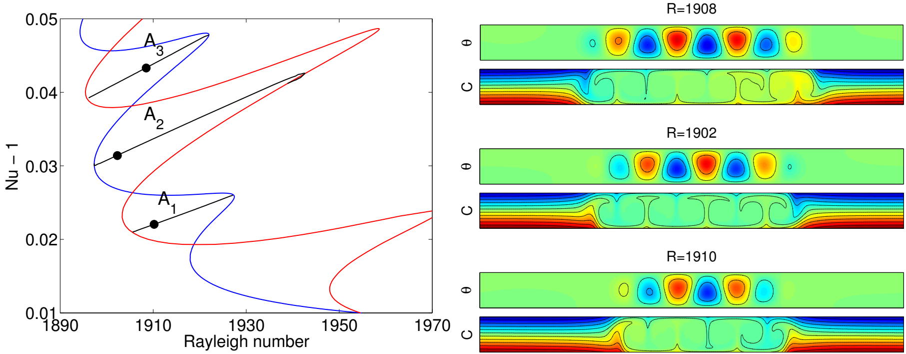

Mercader et al., JFM **722**, 240 (2013)

Binary fluid convection with $\beta = 1$

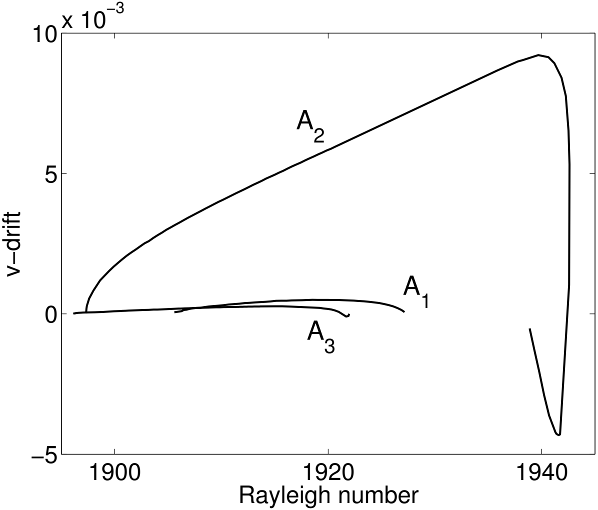

Mercader et al., JFM **722**, 240 (2013)

Binary fluid convection with $\beta = 1$

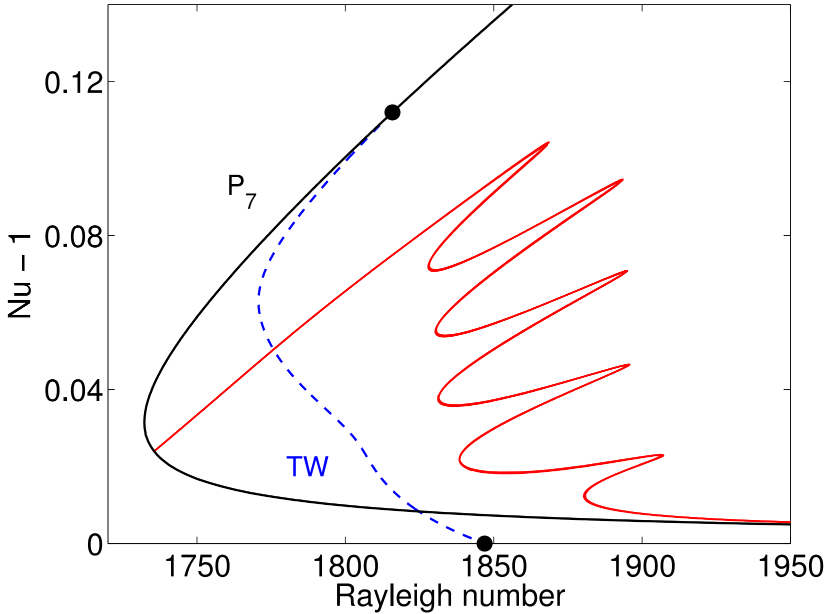

Binary fluid convection with heat loss: $\beta = 0.95$

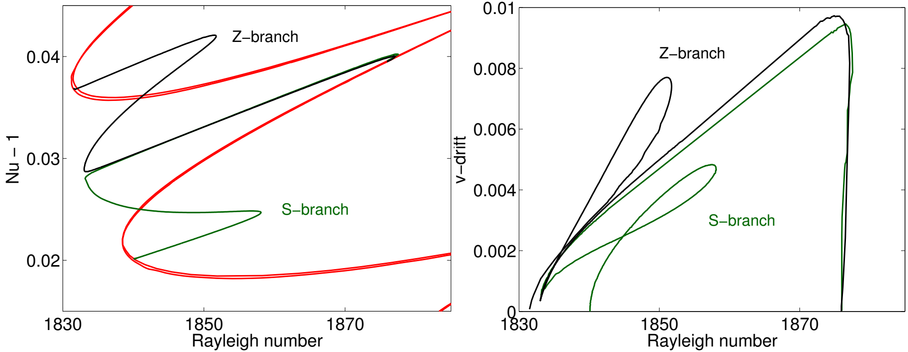

Mercader et al., JFM **722**, 240 (2013)

Binary fluid convection with heat loss: $\beta = 0.50$

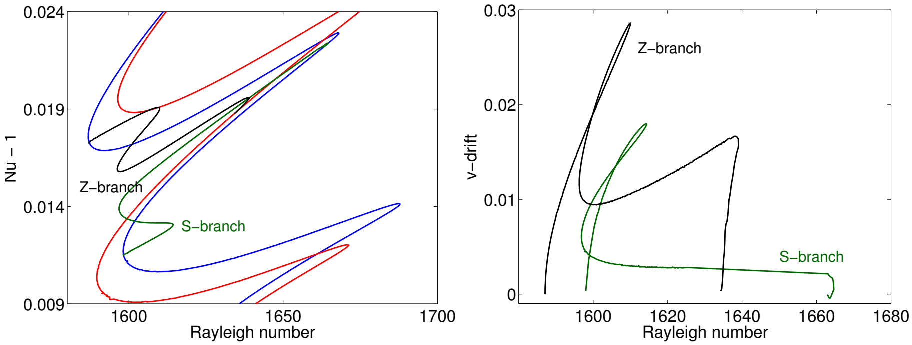

Mercader et al., JFM **722**, 240 (2013)

Binary fluid convection with heat loss: $\beta = 0.30$

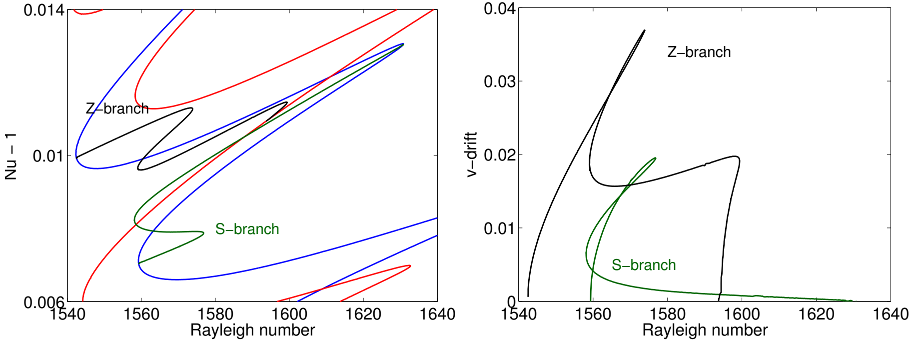

Mercader et al., JFM **722**, 240 (2013)

Binary fluid convection with heat loss: $\beta = 0$

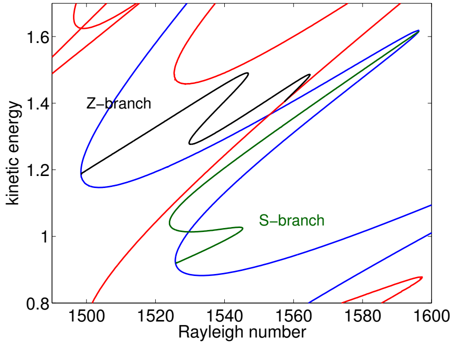

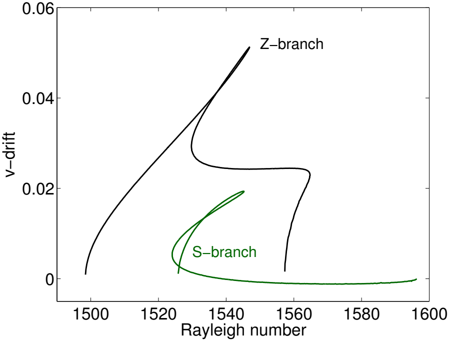

Mercader et al., JFM **722**, 240 (2013)

Binary fluid convection with heat loss: $\beta = 0$

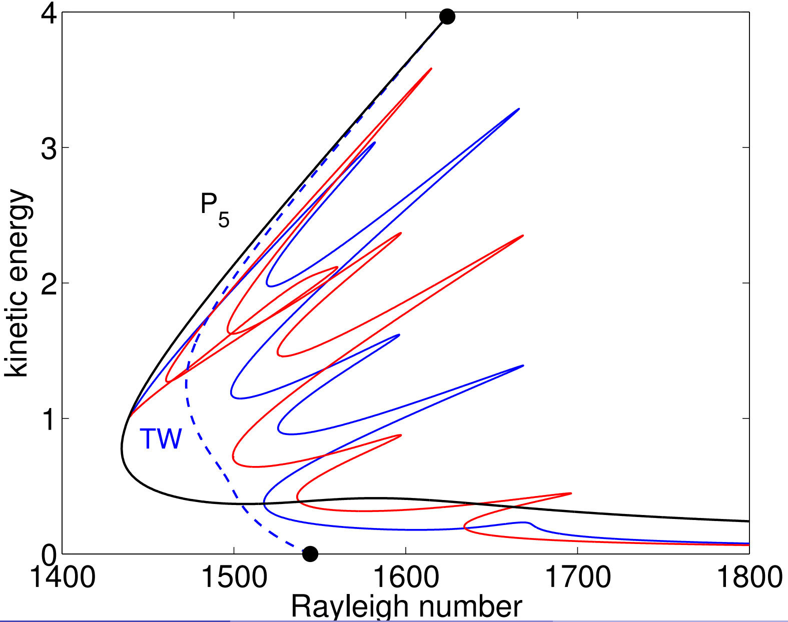

He^3-He^4 mixture: $S = -0.5$, $\sigma = 0.6$, $\tau = 0.03$, $R = 2750$

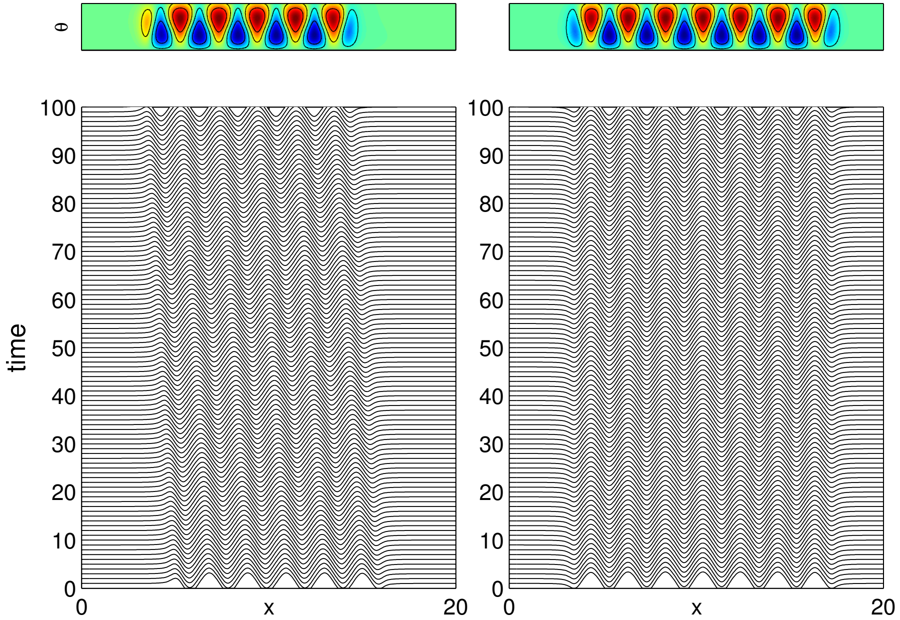

Binary fluid convection with heat loss: $\beta = 0.9$

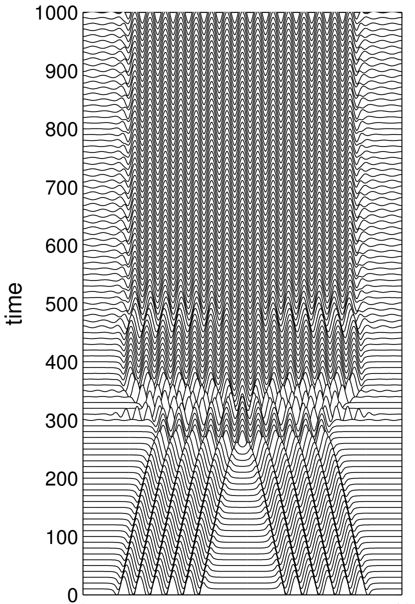

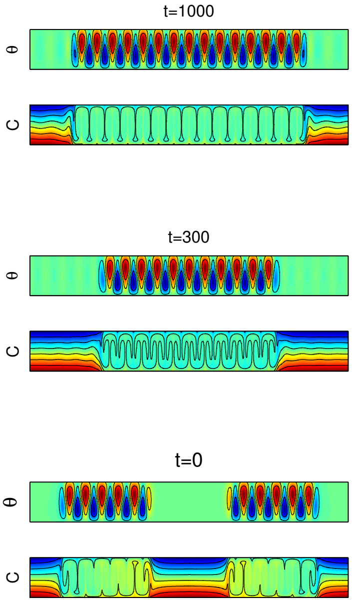

Binary fluid convection with heat loss: $\beta = 0.9$

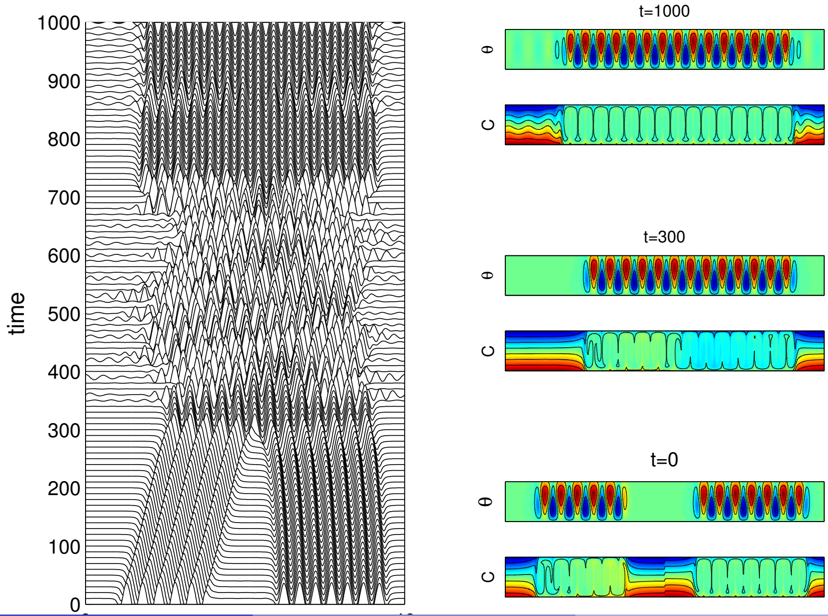

Binary fluid convection with heat loss: $\beta = 0.9$

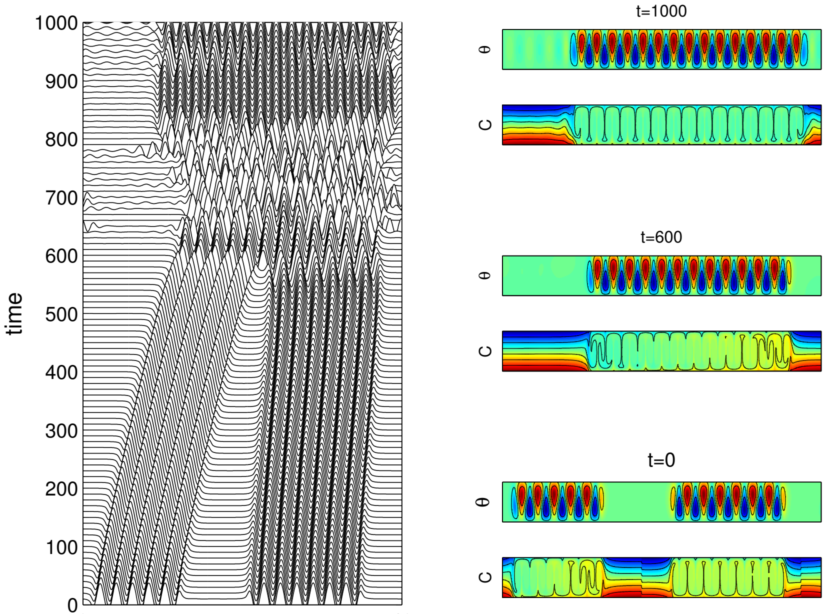

Binary fluid convection with heat loss: $\beta = 0.9$

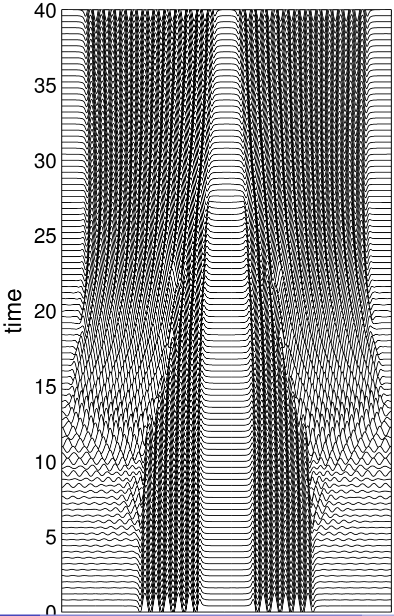

Binary fluid convection with heat loss: $\beta = 0.9$

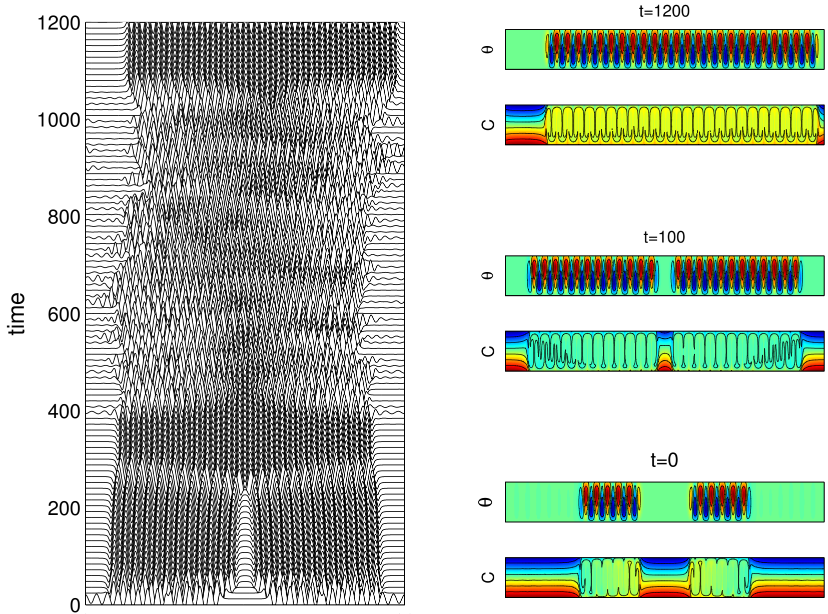

Conclusions

We have see that

- odd parity spatially localized convectons move in the absence of midplane reflection symmetry
- their collisions are sticky but are accompanied by complex dynamics
- convectons interact nonlocally via the background concentration distribution

In addition

- I have described the expected breakup of the snakes-and-ladders structure of the pinning region due to the loss of the midplane reflection symmetry
- I have shown that the interactions of convectons in binary fluid convection behaves in a very similar manner to SH35 with broken R_2 symmetry
- the Swift-Hohenberg equation passes another test!

Porous media convection

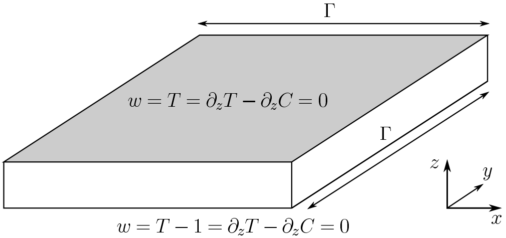

Binary fluid convection in a saturated porous medium

$$
\begin{aligned}
\partial_t T &= -(\mathbf{u}\cdot\nabla)\,T + \nabla^2 T \\
\epsilon\partial_t C &= -(\mathbf{u}\cdot\nabla)\,C + \tau\left(\nabla^2 C - \nabla^2 T\right) \\
\mathbf{u} &= -\nabla p + \mathrm{Ra}\,(T + SC)\,\mathbf{e}_z, \quad \nabla\cdot\mathbf{u} = 0
\end{aligned}
$$

- Periodic lateral boundary conditions
- Parameters:

$$
\tau = \frac{D}{\kappa}, \qquad Ra = \frac{g\alpha\Delta T\ell}{\lambda\kappa}, \qquad S = S_{Soret}\frac{\beta}{\alpha} < 0.
$$

Porous media convection: 2D

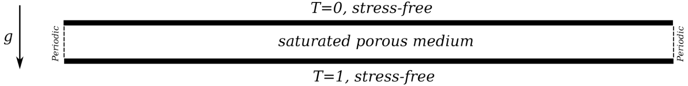

Basic state: $T = 1 - z$, $C = 1 - z$, $\mathbf{u} = 0$

Equations for the departure $(\Theta, \Sigma, \mathbf{u})$ have important symmetry properties

- Invariance under translations in x
- Invariance under reflection with respect to $x = 0$:
  $R_1 : (x, z) \to (-x, z), \ (u, w, \Theta, \Sigma) \to (-u, w, \Theta, \Sigma)$
- Invariance under reflection with respect to $z = 1/2$:
  $R_2 : (x, z) \to (x, 1 - z), \ (u, w, \Theta, \Sigma) \to (u, -w, -\Theta, -\Sigma)$

These operations generate the symmetry group $O(2) \times Z_2$

Consequence: Two solutions bifurcate from the conduction state:

- Even solutions : R_1 invariant
- Odd solutions : $R_2 \circ R_1$ invariant

Parameters: $\Gamma = 20\lambda_c$, $\tau = 0.5$, $S = -0.1$, $\epsilon = 1$.

Porous media convection

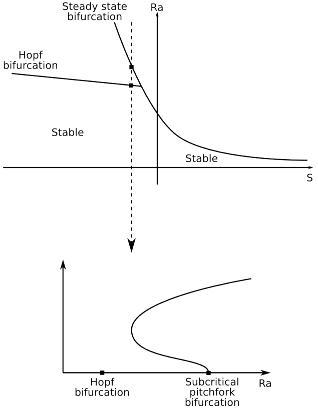

Bifurcation to steady states: linear stability in space: $(\Theta, C) = (\tilde{\Theta}, \tilde{C})(z)\ \exp(qx)$ with $q = q_r + iq_i$

- $Ra \equiv Ra_c = 47.71$; $q = \pm iq_c$, $q_c = 3.40\ (S = -0.01, \tau = 0.1)$
- $Ra < Ra_c$: $q = \pm iq_c \pm \mathcal{O}(\sqrt{Ra_c - Ra})$
- $Ra > Ra_c$: $q = \pm iq_c \pm i\mathcal{O}(\sqrt{Ra - Ra_c})$

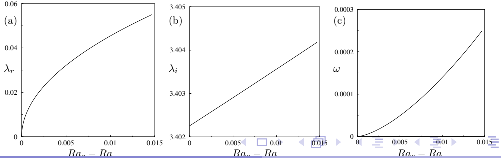

Convectons

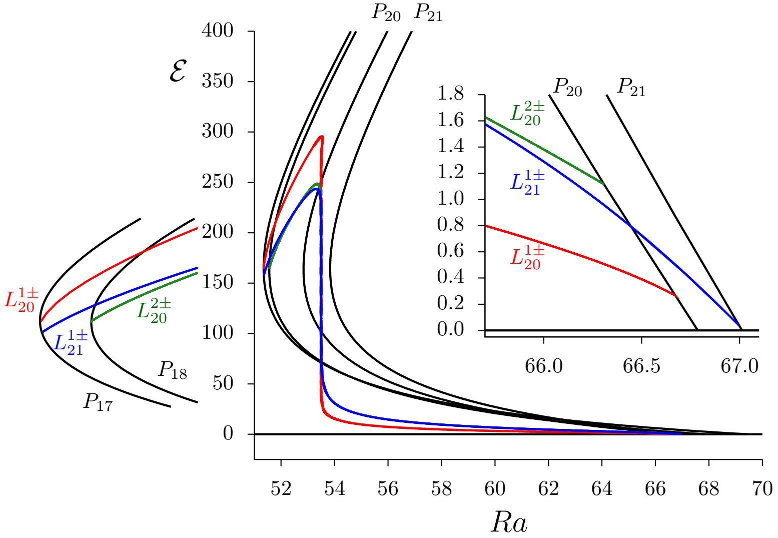

Bifurcation diagram for periodic and spatially localized states in 2D when $\Gamma = 20\lambda_c$ (Lo Jacono et al., PF **22**, 073601, 2010)

Convectons

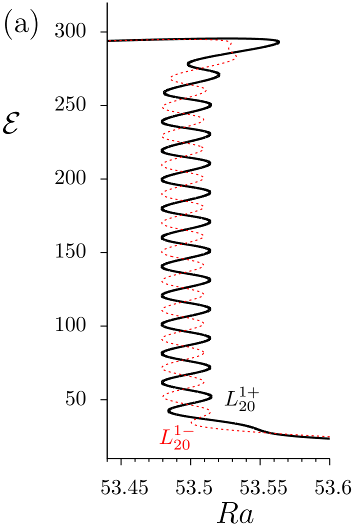

1-pulse states

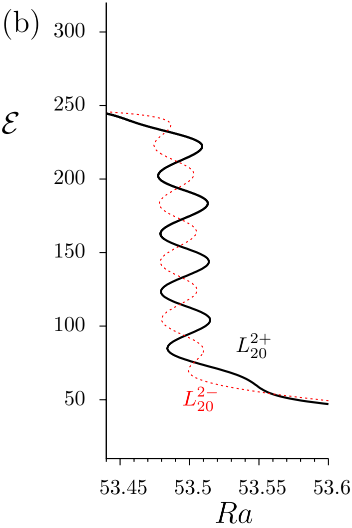

2-pulse states

even parity states

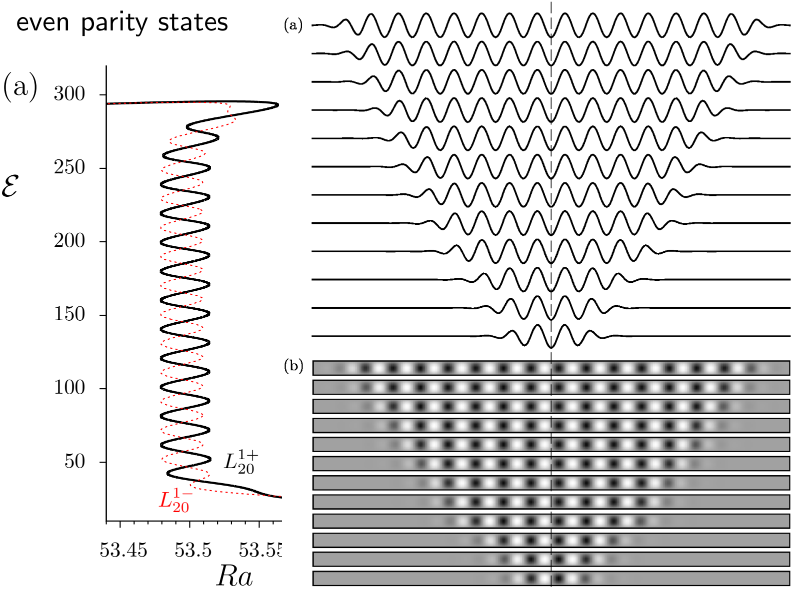

odd parity states

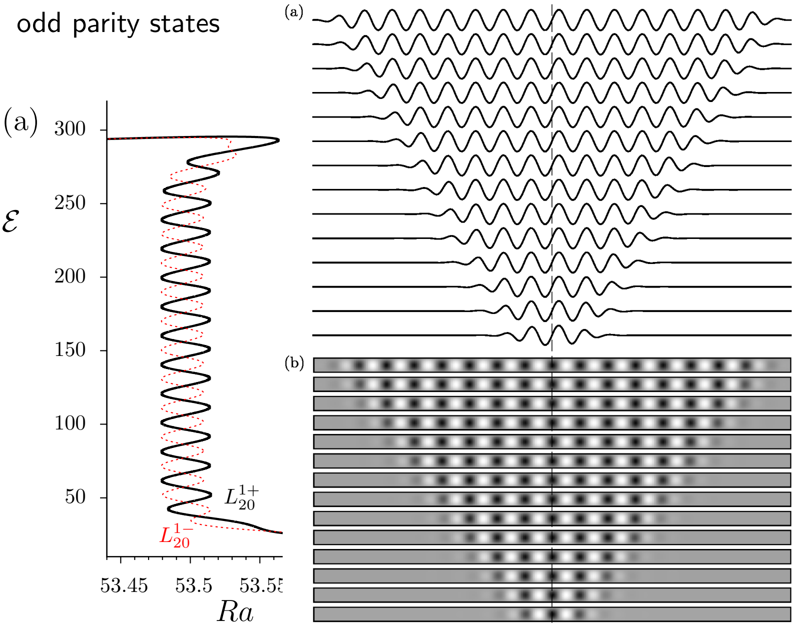

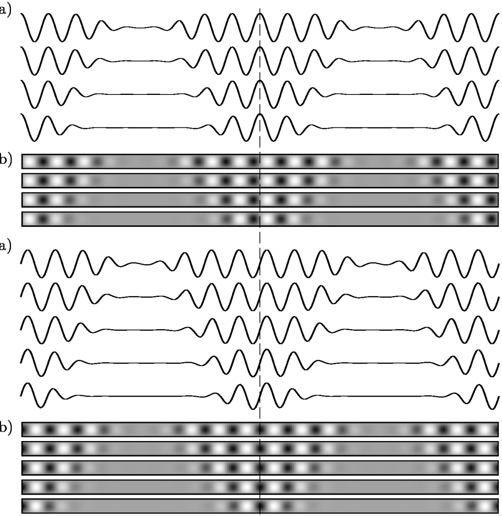

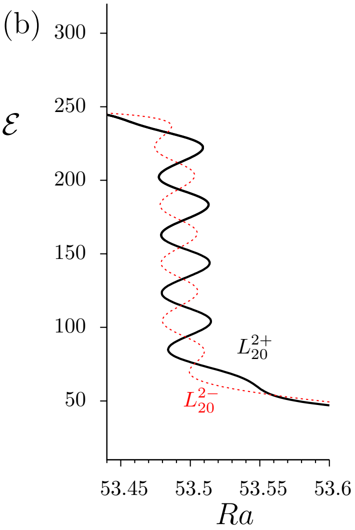

Bound states of two convectons (Lo Jacono et al., PF **22**, 073601, 2010)

Porous media convection: 3D

Basic state: $T = 1 - z$, $C = 1 - z$, $\mathbf{u} = 0$
Equations for the departure $(\Theta, \Sigma, \mathbf{u})$ have important symmetry properties:

Symmetries

- Equivariance under translations in (x, y) modulo Γ
- Equivariance under the reflection $(x, y) \to (-x, y)$
- Equivariance under the $\pi/2$ rotation $(x, y) \to (y, -x)$

These three operations generate the symmetry group $D_4 \dot{+} T^2$.

- Equivariance under reflection in the horizontal midplane $z \to -z$.

Parameters

$\Gamma = 6\lambda_c$, $12\lambda_c$, $18\lambda_c$, for $\tau = 0.5$, $S = -0.1$, $\epsilon = 1$.

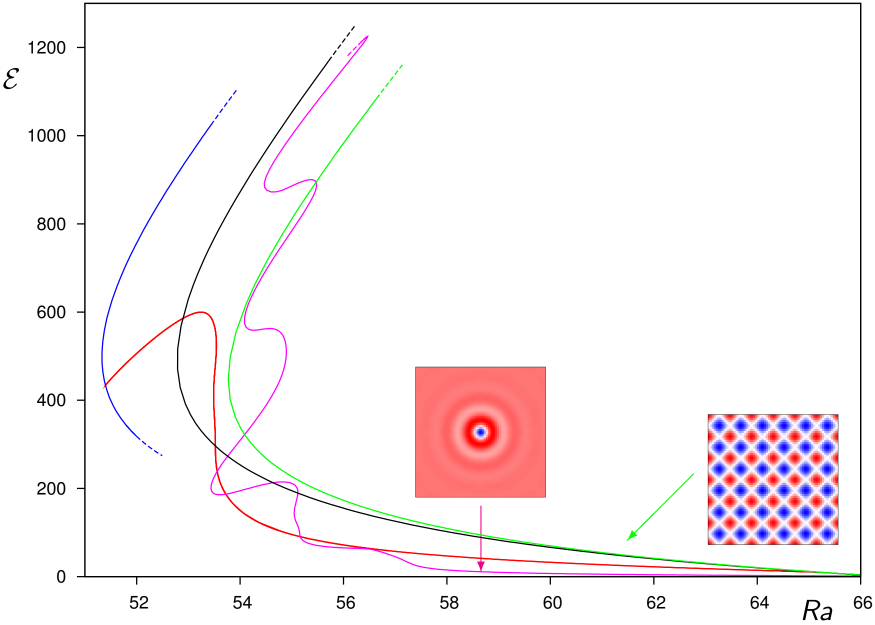

$\Gamma = 6\lambda_c,\ \tau = 0.5,\ S = -0.1,\ \epsilon = 1$

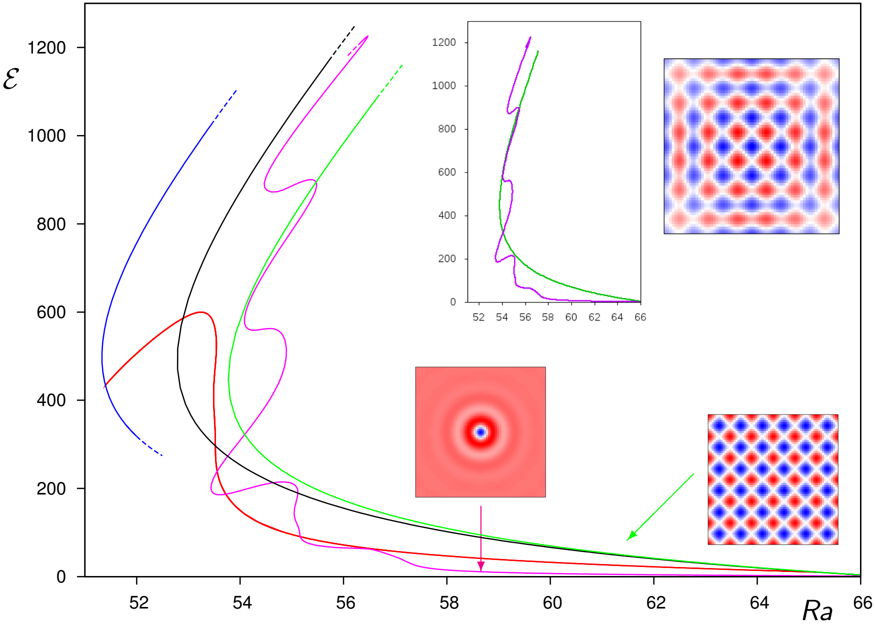

$\Gamma = 6\lambda_c, \ \tau = 0.5, \ S = -0.1, \ \epsilon = 1$

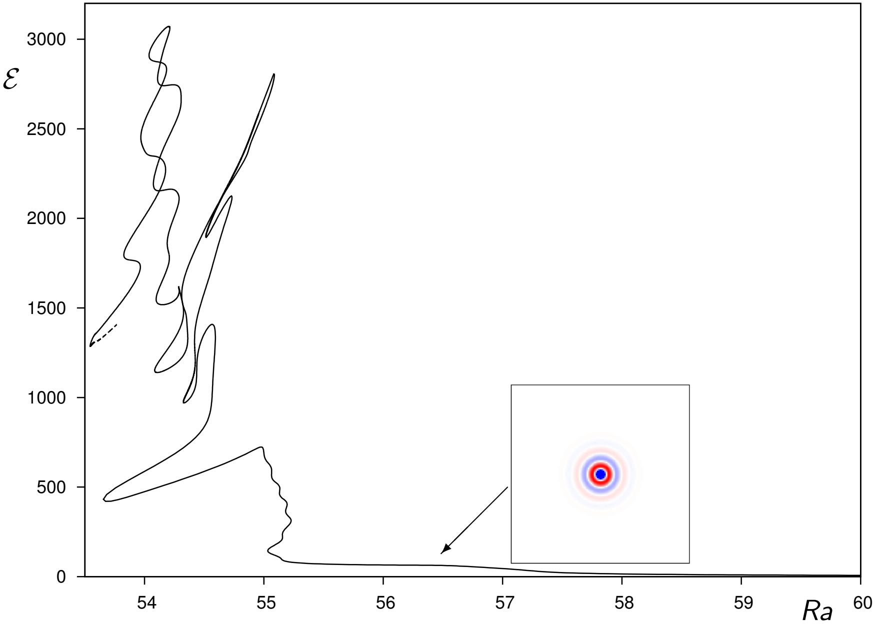

$\Gamma = 12\lambda_c,\ \tau = 0.5,\ S = -0.1,\ \epsilon = 1$

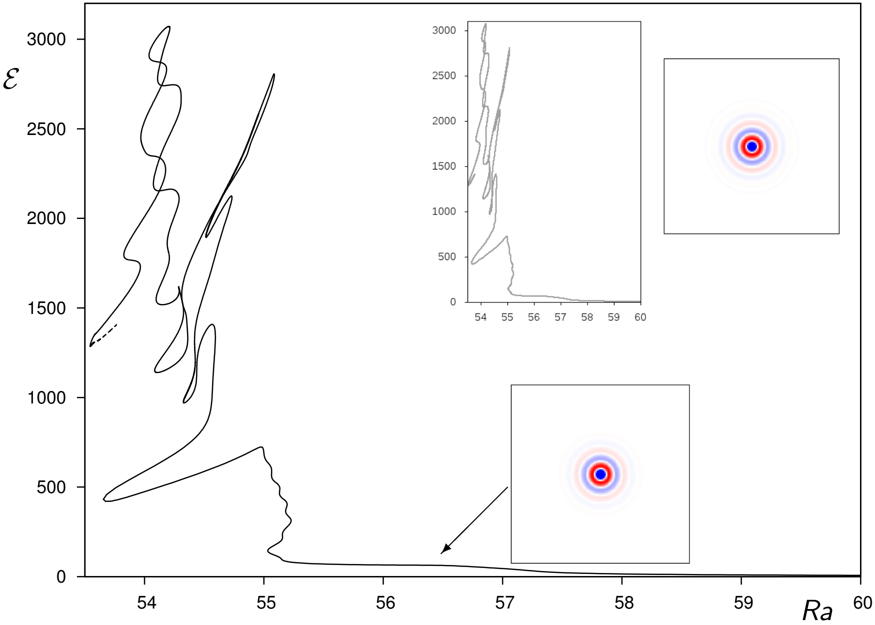

$\Gamma = 12\lambda_c,\ \tau = 0.5,\ S = -0.1,\ \epsilon = 1$

Porous media convection: $\Gamma = 18\lambda_c$

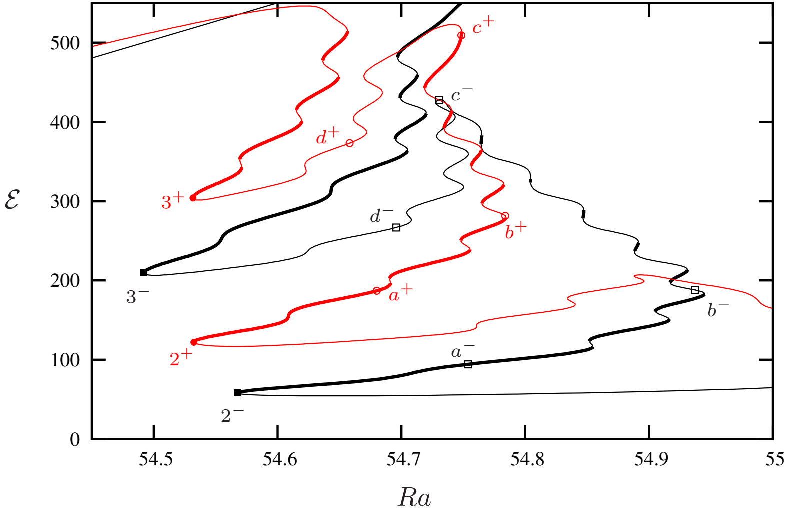

Branches of D_4 and D_2 symmetric states: Lo Jacono et al., JFM **730**, R2 (2013)

Porous media convection: $\Gamma = 18\lambda_c$

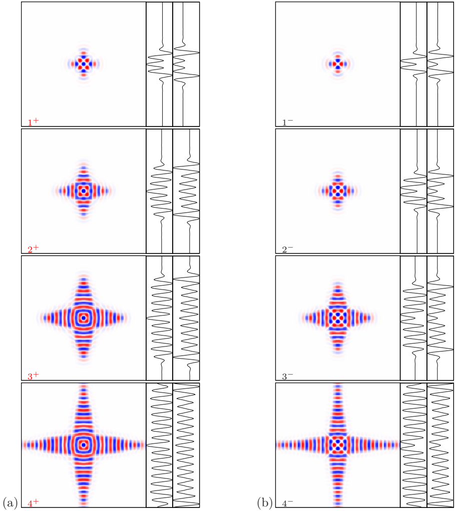

D_4 and D_2 symmetric states at successive folds: Lo Jacono et al., JFM **730**, R2 (2013)

Porous media convection: $\Gamma = 18\lambda_c$

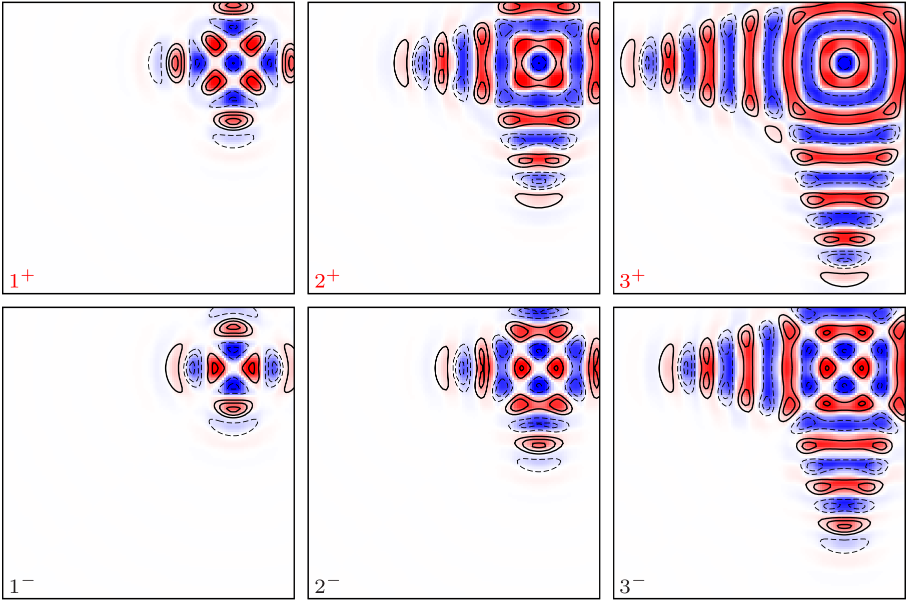

Transition to shear flow turbulence: turbulent puffs

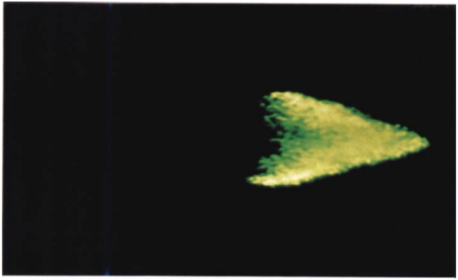

a)

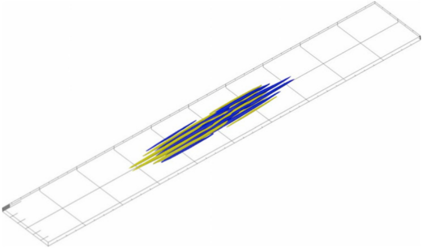

Turbulent stripes in plane Couette flow

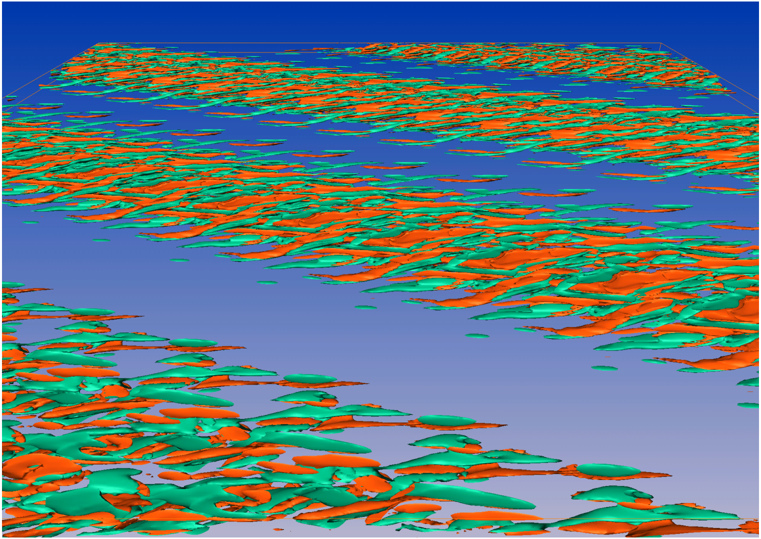

Barkley and Tuckerman, J. Fluid Mech. **576**, 109 (2007)

Plane Couette flow

The problem:

$$\frac{\partial \mathbf{u}}{\partial t} + \mathbf{u} \cdot \nabla \mathbf{u} = -\nabla p + \frac{1}{Re}\nabla^2 \mathbf{u}, \qquad \nabla \cdot \mathbf{u} = 0$$

subject to the boundary conditions $u = \pm 1$, $v = w = 0$ on $y = \pm 1$. Here $Re \equiv UL/\nu$ is the Reynolds number. The base flow the plane Couette flow

$$u = y, \quad v = 0, \quad w = 0.$$

This flow is linearly stable for all values of Re, but is unstable to finite amplitude perturbations for sufficiently large Re, and consequently falls within the class of systems that may exhibit localization. Since the equations for the perturbations are equivariant with respect to R_1 : $(x, y, z) \to (x, y, -z)$, $(\delta u, v, w) \to (\delta u, v, -w)$ and $R_2 : (x, y, z) \to (-x, -y, z)$, $(\delta u, v, w) \to (-\delta u, -v, w)$ the solutions behave like those of SH35. We measure the amplitude of the departure from Couette flow using the dissipation $D \equiv (L_x L_y L_x)^{-1} \int_\Omega |\nabla \times \mathbf{u}|^2 dx\, dy\, dz$, where $\Omega = 4\pi \times 2 \times 16\pi$ is the domain and look for solutions localized in the cross-stream direction. These exhibit snaking, with $\mathrm{LS}_{0,\pi}$ corresponding to TW in the streamwise direction and $\mathrm{LS}_{\pm\pi/2}$ stationary.

Plane Couette flow: Schneider et al., PRL **104**, 104501 (2010) plus a long awaited longer paper

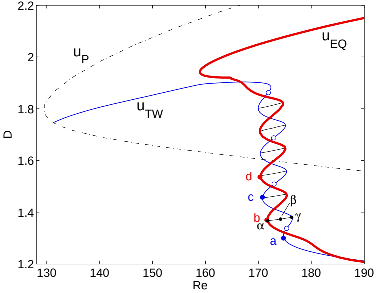

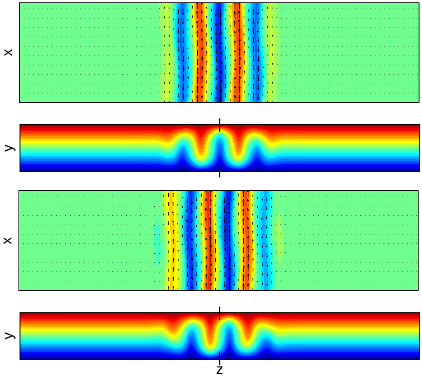

Plane Couette flow: Schneider et al., PRL **104**, 104501 (2010)

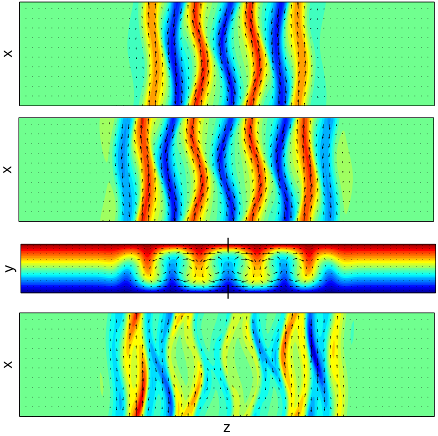

localized TW ($\mathrm{LS}_{\pm\pi/2}$)

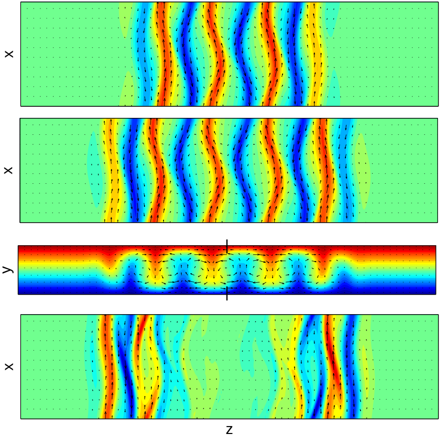

localized steady states (LS_{π})

Plane Couette flow: Schneider et al., PRL **104**, 104501 (2010)

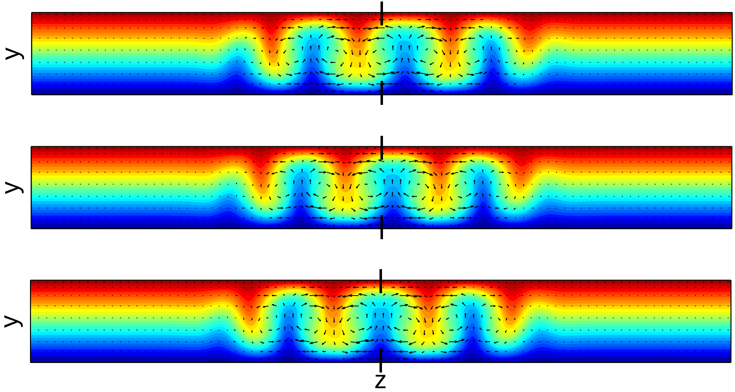

(α)

(β)

(γ)